APOLLO

GUIDANCE, NAVIGATION AND CONTROL

CR-123804

MIT CHARLES STARK DRAPER LABORATORY

MASSACHUSETTS INSTITUTE OF TECHNOLOGY

APOLLO

GUIDANCE, NAVIGATION AND CONTROL

Approved: _____ Date: Dec 30, 71
J. P. CHMORE, DIRECTOR, INERTIAL SUBSYSTEMS
APOLLO GUIDANCE AND NAVIGATION PROGRAM

Approved: _____ Date: 1-3-72
N. E. SEARS, DIRECTOR, G&N SYSTEMS
APOLLO GUIDANCE AND NAVIGATION PROGRAM

Approved: _____ Date: 3 Jan 72
D. G. HOAG, DIRECTOR
APOLLO GUIDANCE AND NAVIGATION PROGRAM

Approved: _____ Date: 3 Jan '72
R. R. RAGAN, DEPUTY DIRECTOR
CHARLES STARK DRAPER LABORATORY

E-2618

DYNAMIC TESTING OF A SINGLE-DEGREE-OF-FREEDOM STRAPDOWN GYROSCOPE

by

Charles B. Lory
Julius Feldman
John S. Sinkiewicz, Jr.

October 1971

MIT CHARLES STARK DRAPER LABORATORY

CAMBRIDGE, MASSACHUSETTS, 02139

ACKNOWLEDGMENTS

The work reported here was originally sponsored by the NASA Electronics Research Center. The work performed and the opportunity for the MIT Draper Laboratory to participate are due mainly to the imagination and perseverence of Dr. Herbert Weinstock. We are also greatly indebted to our present sponsor, the Marshall Space Flight Center, for the continued sponsorship of this program. Mr. B. J. Doran and Mr. B. J. Gaines had the imagination and foresight to broaden the variety of phenomena included, giving it more potential to support error estimation of strapdown system applications. They have implemented more intensive analytic efforts, thus providing a fertile balance between theory and testing.

We can only thank in general the many people in this laboratory who contributed to this report and the work it represents. Some, however, deserve specific citation. First, Duncan Sprague contributed immeasurably by conceiving the idea to use an Apollo inertial measurement unit as an angular vibrator. His elegant implementation of the gyro lag compensation, the pulse-torque electronics, and the variable-interrogation-rate clock is also appreciated. Stephen Helfant helped greatly in preparing figures and coordinating the publication process. The entire staff of our Publication Department has helped, especially those who typed the computer input and controlled the automatic composition of the final draft. Jerold Gilmore has technical responsibility for this contract. His supervisory support of all the work is greatfully acknowledged.

This report was prepared under our Project No. 55-34010, sponsored by the George C. Marshall Space Flight Center of the National Aeronautics and Space Administration through contract No. NAS 12-2033. Its publication does not constitute approval by the National Aeronautics and Space Administration of the findings or the conclusions contained therein. It is published only for the exchange and stimulation of ideas.

E-2618

DYNAMIC TESTING OF A SINGLE-DEGREE-OF-FREEDOM STRAPDOWN GYROSCOPE

ABSTRACT

Test methods and results are presented for the equivalent average input rate of a single-degree-of-freedom gyroscope operated both open loop and with a ternary-logic pulse-torque-to-balance loop during multiaxis angular oscillation. For the open-loop tests, good agreement was obtained with theoretical results. Two-axis testing was performed for oscillations about the Input-Output axes, the Input-Spin axes, and the Spin-Output axes. These tests run in the torque-to-balance mode revealed significant departures from open-loop results in the induced drift rate. An analysis is developed explaining much of the closed-loop data presented.

Test data for the gyroscope in a ternary torque-to-balance loop with constant input rates is presented. The tests demonstrate that the instrument rate linearity does not change with interrogation frequency from 3,600 to 14,400 Hz if the torque coil is tuned to offer a resistive load to the current switch. Analysis cited shows that gyroscope lag compensation eliminates multiple pulsing and other equivalent forms of degraded resolution in a wide variety of quantizing loops. This result is test verified for the ternary delta-modulator loop.

Background information describing permanent magnet non-linearities such as ac sensitivity and eddy current effects is also reviewed.

by Charles B. Lory
Julius Feldman
John S. Sinkiewicz

October 1971

PRECEDING PAGE BLANK NOT FILMED

TABLE OF CONTENTS

LIST OF ILLUSTRATIONS

LIST OF ILLUSTRATIONS (Cont)

LIST OF TABLES

DEFINITION OF SYMBOLS

Gyroscope

H_S	angular momentum of the wheel about its spin axis (dyne cm sec)
I_{SA}, I_{IA}, I_{OA}	moment of inertia of the wheel and float about each of the respective axes SA, IA, OA ($gm\ cm^2$)
$I_{W,SA}$, $I_{W,IA}$, $I_{W,OA}$	moment of inertia of the wheel about each of its respective axes SA, IA, OA ($gm\ cm^2$)
$I_{F,SA}$, $I_{F,IA}$, $I_{F,OA}$	moment of inertia of the float about each of its respective axes SA, IA, OA ($gm\ cm^2$)
C_{OA}	viscous damping coefficient between the float and the case about the output axis $\left(\frac{\text{dyne cm}}{\text{rad/sec}}\right)$
$\tau = \frac{I_{OA}}{C_{OA}}$	gyro first order time constant for motion of float with respect to case about the output axis (sec)
A_{OA}	angle about OA of the float with respect to the case (radian)
A_{IA}	angle about IA of the float with respect to the case (radian)
A_{SA}	angle about SA of the float with respect to the case (radian)
A_{SRA}, A_{IRA}, A_{ORA}	gyro case motion with respect to inertial space (angular displacement of the shaking device) about each of the respective axes SRA, IRA, ORA (radian)
$\dot{A}$	angular velocity (rad/sec)
W	angular velocity (rad/sec)
$\ddot{A}$	angular acceleration (rad/sec^2)

DEFINITION OF SYMBOLS (Cont)

$W_D = \frac{C_{OA}}{H_S} \dot{A}_{OA}$	equivalent input rate (rad/sec)

Environment

a, b, c	amplitude of sinusoidal input displacement about SRA, ORA, and IRA respectively (radian)
ϵ	phase angle between two input vibrations (radian, degree)
f	frequence of vibration inputs (Hz)
$\omega = 2\pi f$	circular frequency of vibration inputs (rad/sec)

Rebalance Loop

W_{MAX}	maximum case rate about IRA that the torque loop can rebalance (rad/sec)
T	interrogate, or sample, period (sec)

SECTION 1.0
INTRODUCTION AND BACKGROUND

1.1 INTRODUCTION

This report describes a study of the strapdown gyroscope and the interaction with its dynamic environment. When used in a gimbal system, a gyroscope is isolated at most frequencies from the vehicle angular motion. In a strapdown system, however, the instrument experiences the full spectrum of vehicle angular rate except for the high-frequency attenuation from vibration isolating mountings. To fully determine the expected strapdown system performance, the gyro and its torque-to-balance loop should be evaluated in the corresponding angular dynamic environment. Although body-mounted gyroscopes are now being used in systems, little data describing the gyro and loop behavior under a dynamic environment is currently available to aid the strapdown system designer. This program was initiated to increase knowledge of the instrument, the torque-to-balance loop, and their interaction in a dynamic environment. It is hoped that the test program will place present theory in proper prospective, stimulate initiative where theory is lacking, and supply empirical data where theoretical analysis cannot yet be achieved.

This interim report serves as a first step in a continuing study program intended to achieve the goals above. The analysis and tests covered by this report consist of single-axis, constant and oscillatory inputs and two-axis oscillatory inputs to a single-degree-of freedom gyro. These effects are evaluated using a new loop technique.

The report is divided into three sections. Section 1 presents a description of the instrument tested and background theory on permanent magnets and their non-linearity characteristics. Section 2 describes the ternary torque-to-balance loop, the gyro lag compensator, and the single-axis test facility. It also presents and discusses the single-axis test results. Section 3 describes the angular oscillatory tests, first by presenting background theory, next by describing the test equipment and procedures, and finally by presenting and discussing the test results.

1.2 BACKGROUND

Initially, component-level, inertial reference (servo) and analog torque-to-balance testing of the GG334A gyro was conducted to establish a base line of the instrument's performance capabilities. These results provide a comparative basis for evaluating the instrument's performance with the ternary torque-to-balance loop. Detailed testing of this nature can help evaluate both the gyro and its critical electronics for system applications. It should be noted that the gyro in this program is a typical single-degree-of-freedom, floated instrument. Test findings are generally applicable to many similar gyros. Performance problems presented provide insight for further gyro and electronic design improvement.

1.2.1 Important Features of the Gyroscope Used

The Honeywell GG334A gyro was used for all testing in this program. Some understanding of the characteristics of this instrument is necessary to interpret the data and discussion in this report. This instrument is specifically designed for a strapdown application. The torque generator, for example, is capable of input rates greater than 2 rad/sec. (However, in this program rates did not exceed 1.05 rad/sec.) A cutaway view of the GG334A gyro is shown in Fig. 1. Figure 2 shows its dimensions and electrical schematic, and Tables 1 and 2 list a number of its operational and control parameters. Its gas-bearing wheel rotates at 24,000 rpm, developing an angular momentum of 200,000 gm-cm^2/sec. A four-pole, 800-Hz, two-phase synchronous motor drives the wheel. The wheel and motor structure are mounted in a hermetically sealed cylindrical float surrounded by a high-density damping fluid. At operating temperature, the float is near neutral buoyancy. A bellows assembly allows for fluid thermal expansion. Pivots and jewels maintain the alignment of the output axis. Ring jewels mount in a piezoelectric ceramic disk polarized in the axial direction. When ac voltage is applied across the disk, it flexes parallel to the gimbal output axis at the excitation frequency. This dithering action reduces pivot-to-jewel static friction to improve gyro torque repeatability. The ceramic disk and spin motor are excited from a common source. At one end of the case is a signal generator whose output is proportional in magnitude and phase to the angular position of the float about the output axis. The signal generator (SG) can be operated across a wide frequency range. For the testing of this program, it was excited with five volts at 28.8 kHz.

A permanent-magnet torque generator is at the opposite end of the case. This consists of a six-pole Alnico V permanent magnet mounted to the gyro case and two independent coils molded into an epoxy coil cup mounted on the gyro float.

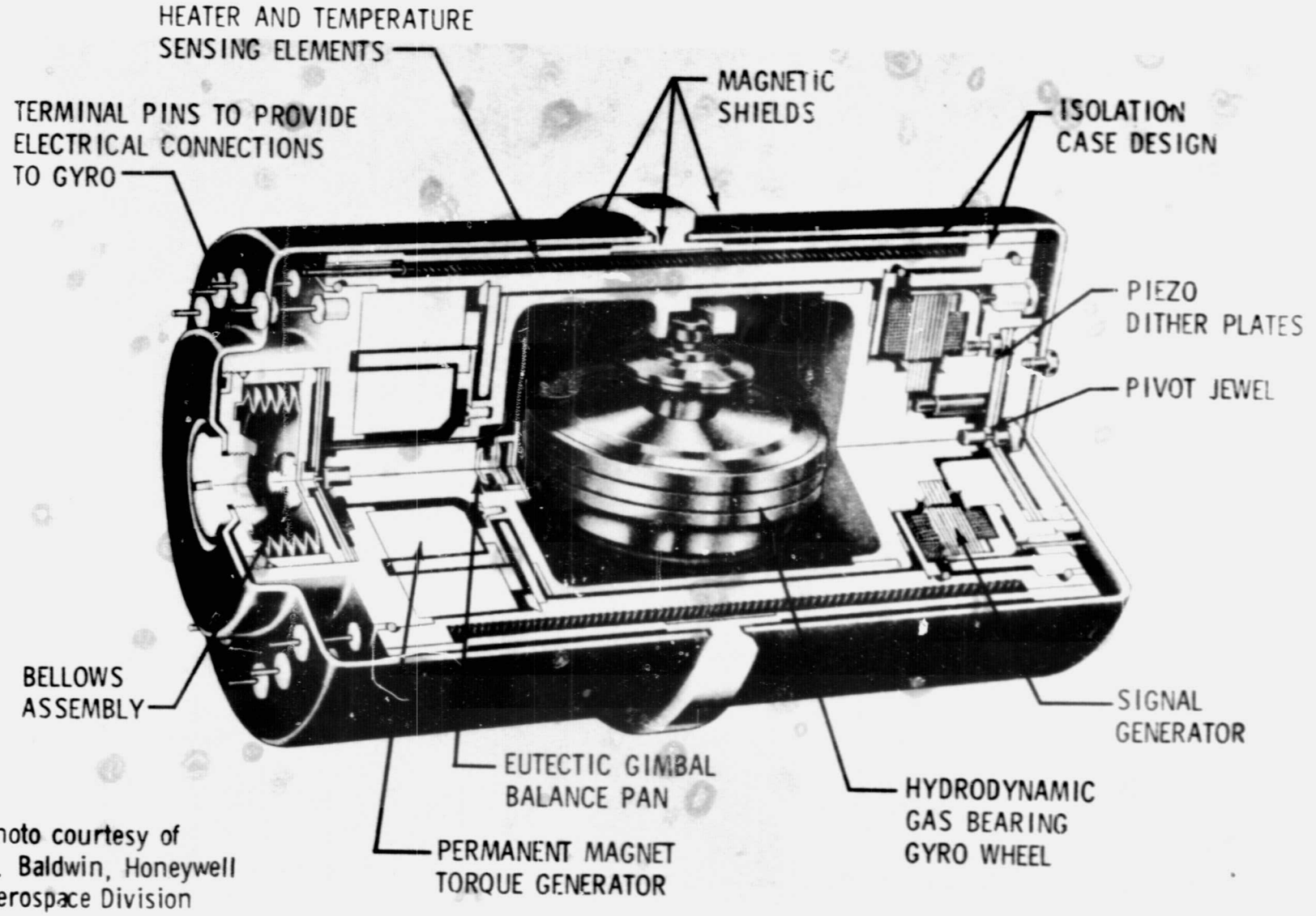

photo courtesy of
R. Baldwin, Honeywell
Aerospace Division

Figure 1. GG334A Gyro Cutaway.

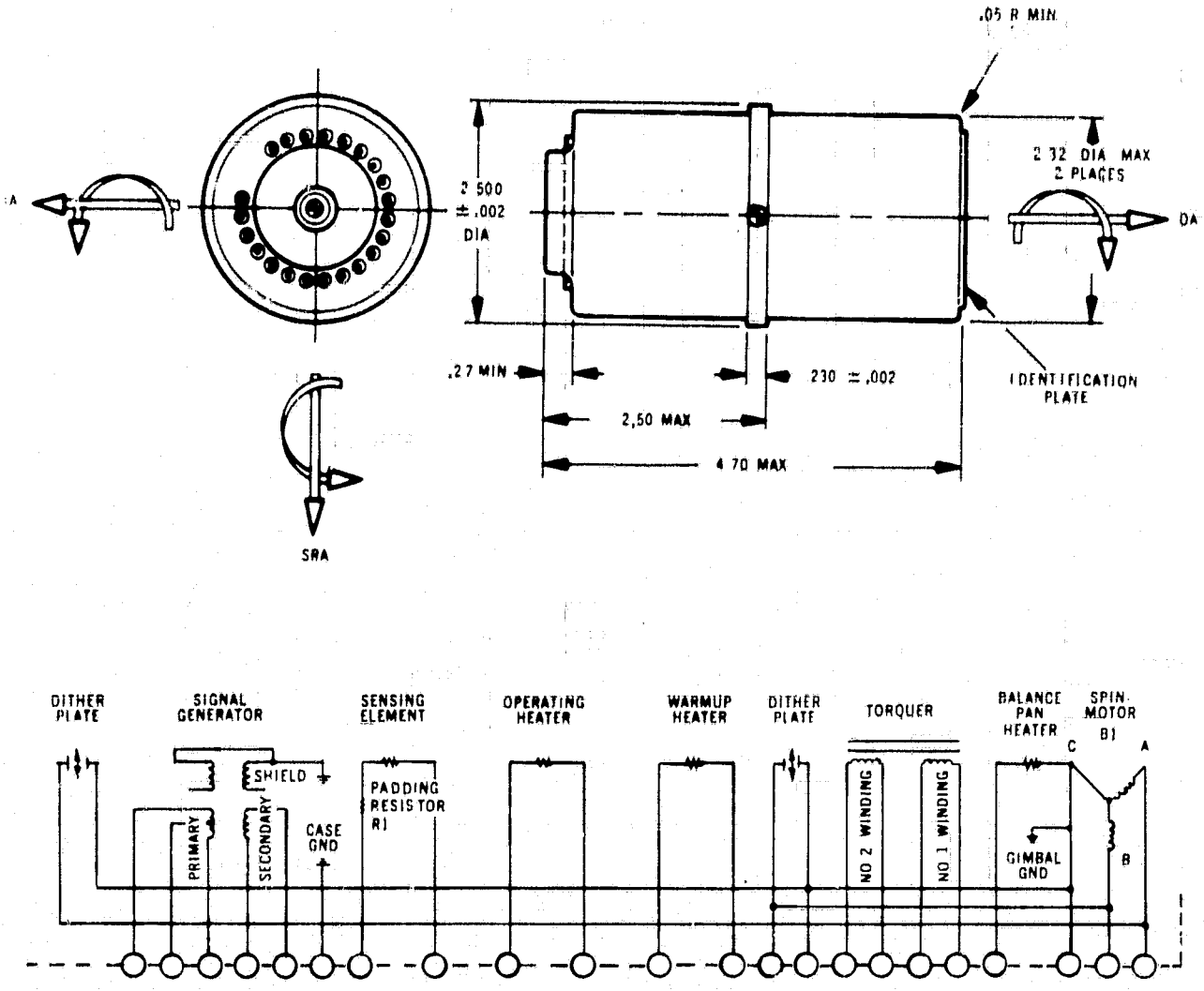

from Ref 2, pp. 1-4

Fig. 2 GG33 . . - Outline Dimensions and Schematic Diagram

Table 1 GG334 Mechanical and Dynamic Nominal Characteristics

PARAMETER	GG334A
Angular Momentum (H)	2×10^5 g-cm^2/sec
Output Axis Damping (C)	5×10^5 d-cm-sec
Gimbal Output Axis Inertia (J)	250 g-cm^2
Characteristic Time (J/C)	0.0005 sec
Gimbal Freedom	±4 degrees
Input Angular Freedom	±10 degrees
Gyro Transfer Function	9.6 volts/radian
Operating Temperature	180°F
Size	2.32-inch diameter 4.7 inches long
Weight	1.4 pounds
Spin Motor Power	3.5 watts
Torque Generator	
Scale Factor	1200 deg/hr/ma
Maximum Torquing Rate (Continuous)	2 rad/sec
Auxiliary Torque Generator	
Scale Factor	120 deg/hr/ma
Piezoelectric Dither Power	0.02 watts
Heaters	
Warm Up	100 v, 140 watts
Control	28 v, 10 watts
Temperature Sensor	
Resistance at Operating Temp.	780 ohms
Slope	1.3 ohm/°F
Signal Generator Sensitivity	24 volts/radian

From Ref 2, pp. 1-7

Table 2 GG334 Performance and Environmental Nominal Characteristics

PARAMETER	GG334A
Fixed Torque	
Magnitude (Nominal)	0.5 deg/hr
Trim Capability	0.1 deg/hr
Stability	
With ± 0°F Cooldowns	0.03 deg/hr rms
30-Day Stability	0.10 deg/hr
Random Drift	0.005 deg/hr
G-Sensitive Torque	
Magnitude (Nominal)	1.0 deg/hr/g
Trim Capability on Request	0.2 deg/hr/g
Stability	
With ±0°F Cooldowns	0.04 deg/hr/g rms
30-Day Stability	0.15 deg/hr/g
Random Drift	0.007 deg/hr/g
G^2-Sensitive Drift	
Anisoelastic (20-1000 Hz)	0.04 deg/hr/g^2
Attitude Angle (20-1000 Hz)	0.04 deg/hr/g^2
Environmental Capability	
Storage Temperature	-65°F
Vibration	25 g's
Acceleration	30 g's
Shock (10 ms)	50 g's
Rate	3 rad/sec

From Ref 2, pp. 1-8

The winding with a high scale factor and low time constant is used in the pulse rebalance loop. The winding with a low scale factor can be used for earth-rate or drift correction.

1.2.2 Background Information on Permanent Magnet Torque Generators

High-performance strapdown systems have almost exclusively used permanent-magnet torque generators in the inertial components because rebalance torque is then a straight-line function of coil current. In a pulse rebalance loop, this current is applied in precision pulses to oppose precession or pendulous torque. Any variation in the area of a pulse or the response to it will result in an error in indicated vehicle rotation. Several torque-generator characteristics which effect the weight of a pulse will be presented prior to discussion of single-axis testing.

1.2.2.1 Rotational Float-Angle Sensitivity. In an actual instrument, the torque generated differs when the same magnitude of current is applied in opposite directions through the torque coil. The torque difference may be explained by noting that the torque coil may be operating at an angle rotated from the radially symmetric axis of the salient poles. This causes armature reaction, an effect familiar in rotating dc machinery. Figure 3 illustrates this: a single coil and a two-pole, permanent magnet are shown with an angle, θ, between them. For the direction of current shown, the magnetomotive force of the permanent magnet, F_m, is decreased by the component of the coil mmf of magnitude $F_c \sin \theta$. If the coil current is reversed, the component of torque-coil mmf $F_c \sin \theta$ adds to the mmf of the permanent magnet. This results in a torque difference between positive and negative pulses even though they have the same magnitude of current. The weight or value of any pulse is conventionally called scale factor and expressed as indicated input-axis rotation per pulse. If the difference between either the positive or negative scale factor and the nominal, normalized to the nominal, is defined as ΔSF, it can be expressed for small θ as

$$\Delta SF = \frac{N_c I_c \theta}{F_m} \qquad (1.1)$$

where

N_c = the number of torque-coil turns
I_c = torque-coil current in amperes
F_m = permanent-magnet mmf in ampere turns
θ = angular misalignment between torque coil and permanent-magnet pole in radians

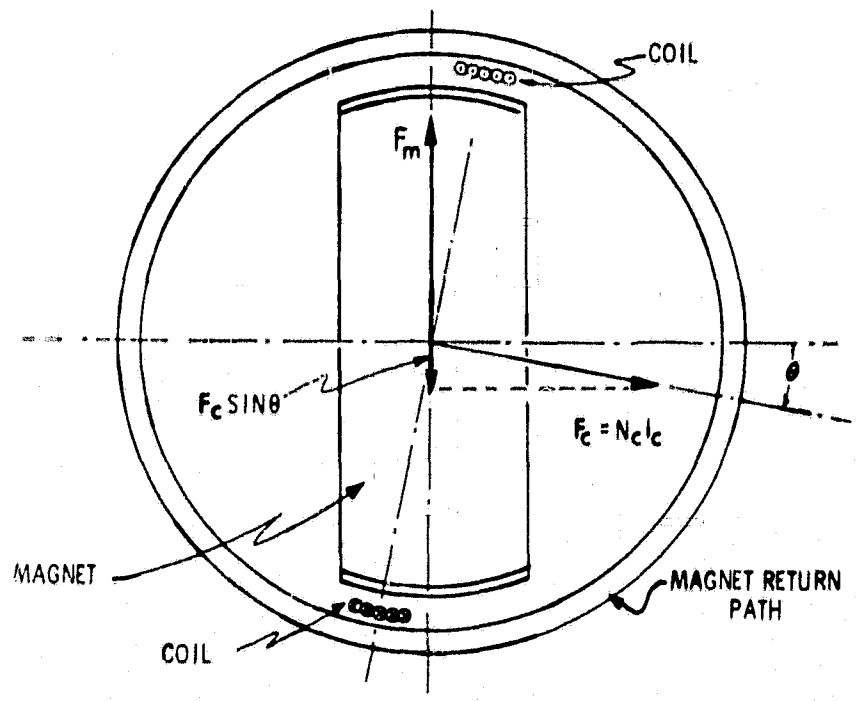

Fig. 3 - Torque-Coil Reaction Effect for 2 Pole PM Torque Generator

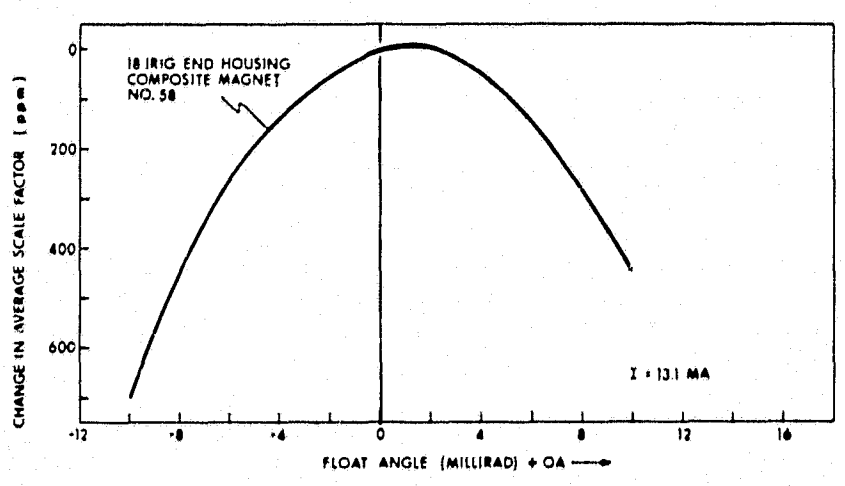

Fig. 4 - TG Scale Factor Sensitivity vs Float Angle

A difference in positive and negative scale factor results in a net bias at null if the gyro is used in a binary torque-to-balance mode. Similarly, if conventional ac is fed to the coil, an output torque will result that is proportional to the angle θ and to the square of the current magnitude. If, during assembly of the instrument, the torque coil is aligned to the SG null until there is no ac torque sensitivity, the plus-to-minus scale-factor difference can be effectively minimized.

From Eq. (1.1) one sees that ΔSF (due to armature reaction) is proportional to float angle as well as coil current. ΔSF also varies with float angle due to non-uniformity (or fringing) at the pole tips. The net active flux decreases as the coil is displaced in either direction, giving an even function with a maximum when the coil is symmetrically aligned with the pole. Since the angular variation due to armature reaction is linear, i.e., odd function of angle, the maximum resultant scale factor is displaced slightly from the alignment point discussed in the paragraph above. The total effect is illustrated in the experimental data shown in Fig. 4. Operation about the maximum point of this curve usually results in minimum variation in scale factor with float motion, but does not correspond with the constant-angle, zero ac sensitivity point.

1.2.2.2 Torque-Generator Frequency Effects. Early in the development of a strapdown gyroscope by MIT, several effects varying with frequency were found in the torque generator. The most easily observed phenomenon was a sharp drop in coil inductance with rising measurement frequency, occurring between one and ten Hertz. This drop was qualitatively associated with the conductivity of the beryllium coil support used. It should be noted that beryllium is commonly used for gyro floats because of its high structural stability and low density. Therefore, its selection for a coil holder that mounts to the float was evolutionary in nature since it simplified balancing and material thermal-gradient. The normalized inductance of this structure vs. frequency is shown in Fig. 5. Also shown is the inductance measured using an experimental potted-plastic coil support similar to that used in Honeywell's GG334A. The explanation of these data as effects of eddy currents in the conductive portions of the magnetic path has since been substantiated analytically by Salamin.[3] The other evidence, presumably from the same cause, is shown in Fig. 6. There one sees that the slope of ac torque sensitivity vs. float angle is a function of frequency for a conductive, beryllium coil support. In similar tests with a nonconductive coil holder, the slope was observed to be constant over the same range of frequencies.

The principal importance established so far for these frequency dependent effects is their influence on matching of the coil to the electronic current switch and on holding the torque scale factor constant with input rate. Fast, accurate

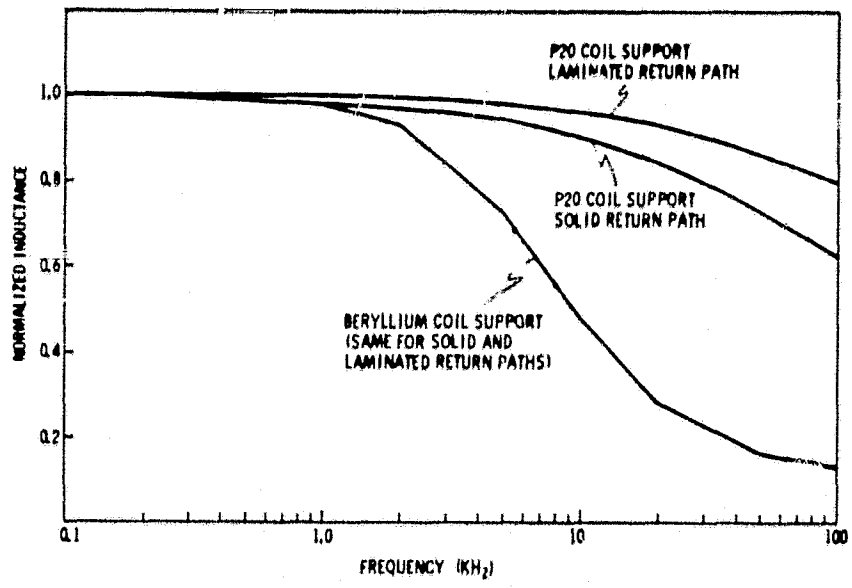

Fig. 5 - Normalized Frequency Sensitivity Plastic vs Beryllium Coil Holder

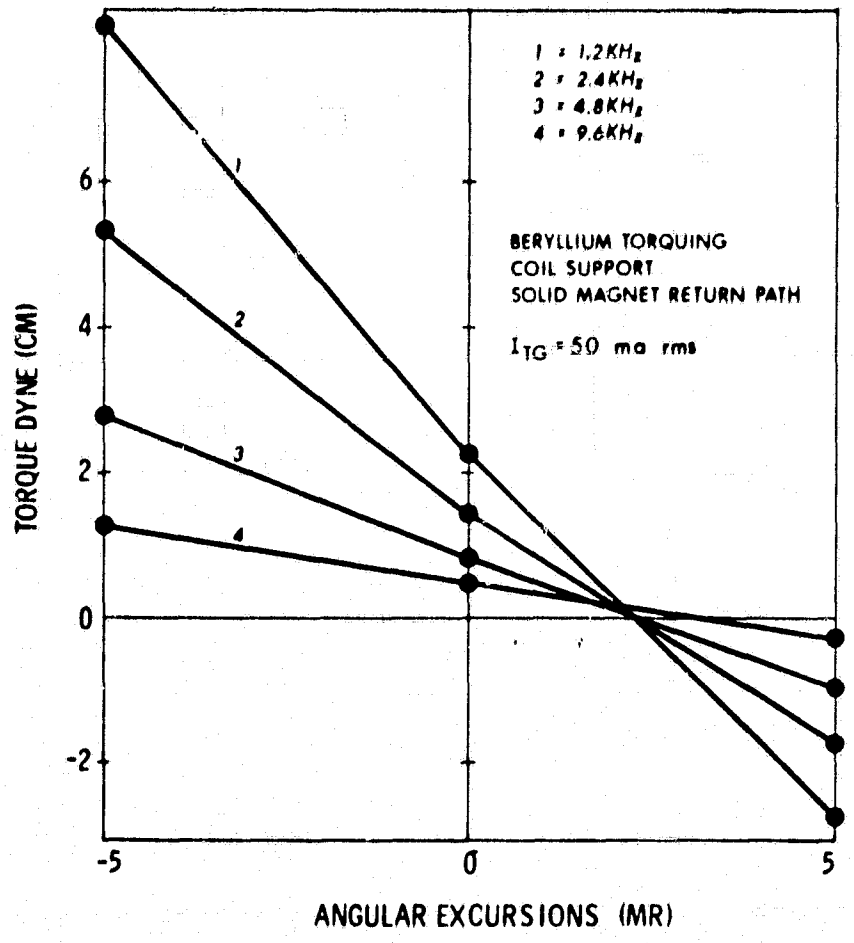

Fig. 6 - Reaction Torque vs Angle and Frequency

switching can best be accomplished if the load appears resistive to the switch. If the torque-generator coil is a single-pole lumped resistance and inductance, it can be tuned at all frequencies by a series resistor and capacitor shunting the coil. Variation of inductance with frequency, however, makes this tuning incomplete, inducing transients into the controlled current as it is switched from a dummy load to the torque generator. The transients saturate stages of the high-gain amplifier in the current control loop. This affects the area of the pulse. The effect varies with the rate and pattern of applied pulses causing a variation of scale factor with rate. In addition, the pulse rate and moding patterns are functions of the applied angular-input rate. The frequency content of the torquing current is, therefore, directly related to the input rate, and can also result in a scale-factor rate nonlinearity.

This type of nonlinearity was identified early in the 18 IRIG MOD B development and the coil holder was changed from beryllium to beryllium-oxide ceramic. This change resulted in better than a factor of three improvement in rate linearity. The GG334A gyro uses a potted epoxy coil support. From the standpoint of dimensional stability, a ceramic is ideal, but, because of the thin-wall sections of the holder, its manufacture is difficult. Plastics are generally less dimensionally stable and, since the coil support is mounted directly on the float member, some care is required before it is incorporated into a gyro design. The epoxy coil support used in the GG334A has not noticeably affected that gyro's drift stability.

1.2.2.3 Translational Displacement Sensitivity. The torque generator sensitivity can change due to a translational displacement between the torque-generator coils and permanent magnet (resulting from a float axial or radial displacement). This displacement can occur due to linear acceleration inputs or rates about the gyro output axis operating on the angular momentum of the wheel, causing a torque about the input axis. This sensitivity must be accounted for in system use as the gyro experiences dynamic inputs.

The pivot-to-jewel clearances of the GG334A gyro may allow radial or axial displacement between the torque coil and magnet. Such motion may result in a scale-factor change with dynamic input. This error coefficient has not been separated from other dynamic error terms for this gyro during the present reported test effort.

The effect of the dithered suspension on torque coil nonlinearities, dynamic error coefficients, drift stability and input axis alignment requires further investigation.

SECTION 2.0
GYRO AND REBALANCE LOOP EVALUATION

2.1 PRINCIPLES OF OPERATION

2.1.1 Pulsed Torque Electronics

All testing discussed in this report employs ternary float restraint as part of a ternary, incremental, digital conversion scheme. Command torque, thus, is applied in three levels: a positive value, its negative, and zero. A schematic, Fig. 7, shows how torque is applied. For illustrative purposes, mechanical rather than the actual semiconductor switches are shown. The switch status is shown in the positive-torque mode. Note that the torquing polarity is set by an H switch feeding current in the plus or minus direction of the winding. Switch S_5 operates so that current flows through either a dummy load or the torque winding.

The dummy load is a noninductively wound resistor approximately the same resistance as the torque winding mounted outside the torque electronics. The switch S_5 selects either command torquing (set position) or dummy load (reset position). Regardless of the torque-command state, the same current is fed into the scale-factor resistor. The voltage across this resistor is compared with a precision voltage reference at the input of a high-gain dc amplifier. The amplifier is part of a control loop that maintains a precise, fixed direct current level. Note also that an RC network shunts the torque coil. It tunes the coil so that the load seen by the switches and current source is purely resistive.

The control of the set-reset switch S_5 in Fig. 7 is clock synchronized to apply current as discrete pulses of fixed width. In each operational cycle, a clock issues interrogate, set, and reset command pulses. The signal-generator output is sampled at each interrogate pulse to determine if positive, negative, or no torque is required. If torque is required, S_5 is transferred to the set position by the set pulse and back to the reset position by the reset pulse. Thus, at least a small fraction of each cycle is spent in the reset position. During this period of zero current in the H switch, torque polarity can be reversed if required. A similar transient for every pulse is assured, whether the pulse occurs alone or as part of a long sequence. The average applied restraining force is proportional to the pulse rate and thus corresponds to the input angular rate.

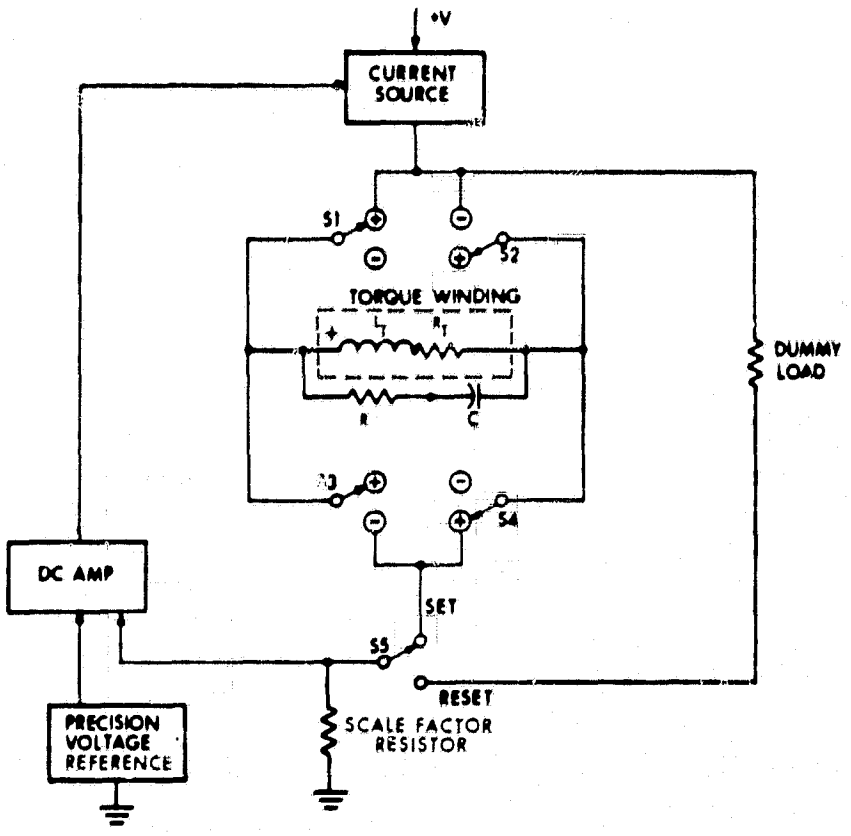

Fig. 7 Ternary Pulse Torque Switching

2.1.2 Gyro Lag Compensation

Multiple-pulsing is a bothersome performance characteristic occurring when the gyro is operated in a pulse-torque-to-balance control loop. It is caused by energy storage in the gyro float inertia and torque-coil inductance. The float response to a single torque pulse provides insight into the effect of lagged response on closed-loop operation. The response plotted in Fig. 8 for a single, fixed-magnitude pulse shows that only a small percentage of the total float motion occurs in the first sampling period. For instance, at the 3200-pps interrogation rate, approximately 34% of the travel has occurred by the time the next sample is made. At 9600 pps, the float has gone only 11% of its command travel at the next interrogation sample. Clearly, at 9600 pps, an angular rate about the gyro input axis, W_{IA}, that is in excess of 11% of the torque-loop full-on rate capability will result in at least double pulsing. For example, consider an initial condition in which a steady-state W_{IA} is applied such that the float travel in a sampling period is slightly in excess of 11%. At sampling time (assume the float crosses over the torquing threshold exactly at a control-loop sampling point) a restraining torque-command pulse is issued. The float sums the steady-state input and the pulse response. The input will exceed the pulse response over the next sampling interval , leaving the float outside the threshold to trigger another torque pulse. The effect will have been to command two $\Delta\theta$ increments in response to an input slightly in excess of one $\Delta\theta$. For the next few sampling periods, the float response to the two successive torque pulses dominates. Then, after a relatively long off time, another burst of two pulses will occur. The average indicated angle is correct over a long time, but the multiple pulsing has induced transient errors. Furthermore, the resolution of the system has degraded to two pulse weights.

A compensation technique to eliminate the multiple pulsing described above has been suggested for a pulse-rebalance loop.[1] This technique models all significant time constants in the gyro response such that the future response to stored command energy is continuously developed as an analog signal. This compensating signal, equal to the remaining float response to previous pulses, is added to the actual gyro SG output, thereby accounting for float-motion delays and eliminating the unnecessary multiple pulsing.

The effectiveness of such compensation is illustrated in Fig. 9 by comparing the response to an initial five-pulse offset with and without compensation. The torque history of the uncompensated system exhibits a limit cycle as shown on the left, whereas torque in the compensated system, at the right, settles immediately after five pulses. The time scale has been normalized to the interrogate sample

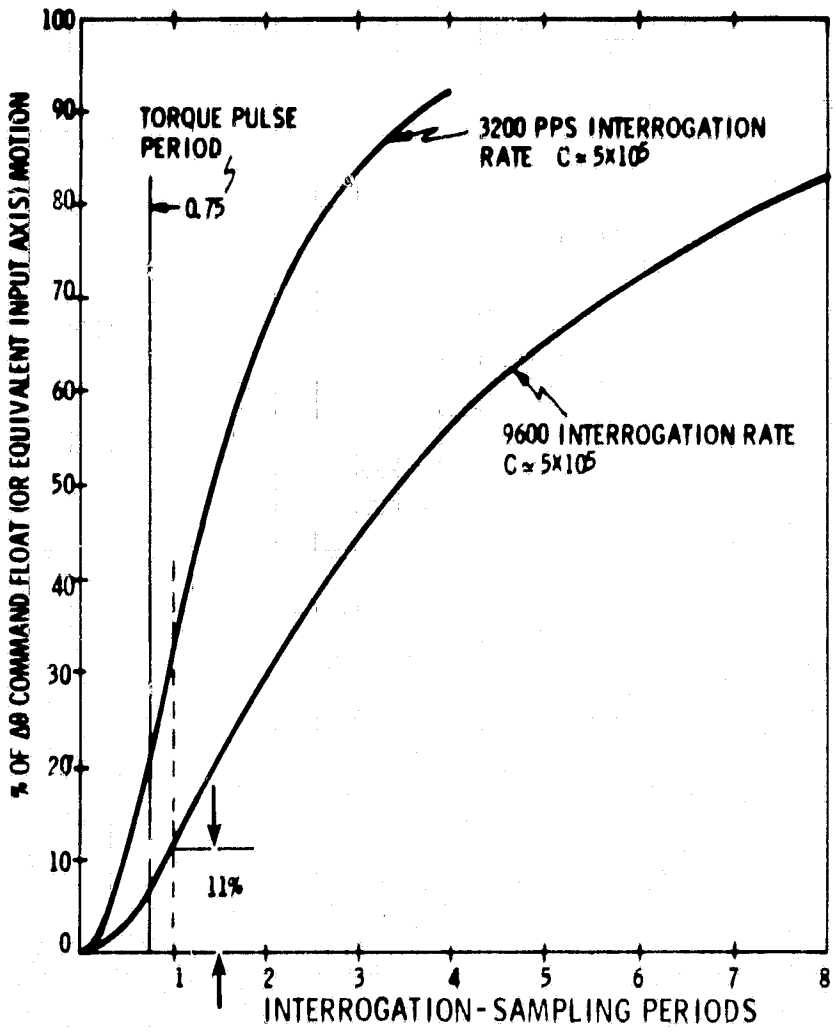

Fig. 8 Normalized Gyro Response to a Single Torque Pulse Command

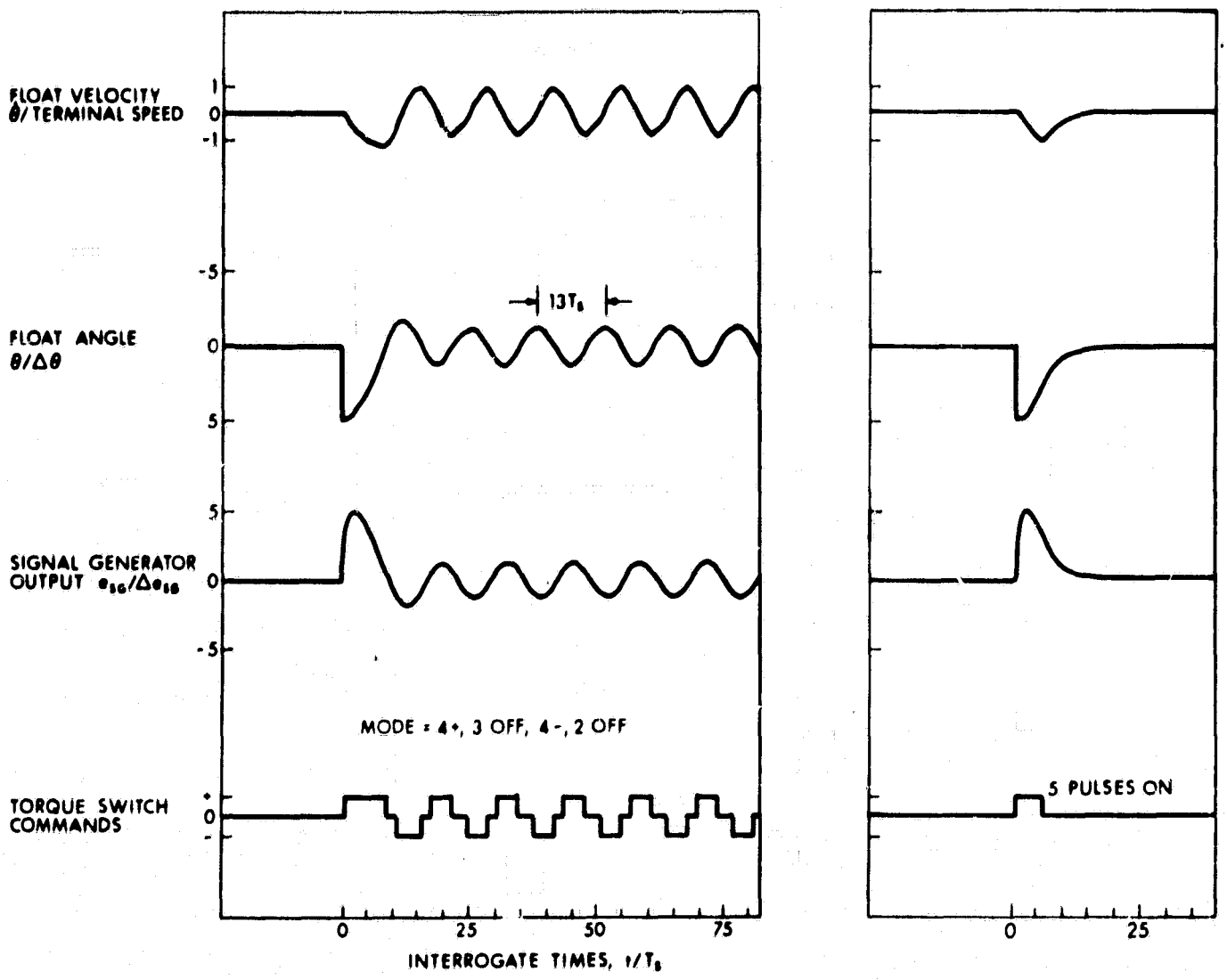

Fig. 9 - Response of Uncompensated and Compensated Systems to Initial Condition; $\theta = 5\Delta\theta$, Deadband = $\pm(3/4)\Delta\theta$

period, T_s. These figures illustrate that compensating the system removes the spurious output generated by the limit cycle. Test results on the GG334A gyro illustrating this mechanism will be described in Section 2.4.8.

2.2 DESIGN OF INSTRUMENT ELECTRONICS

A digital clock and pulse torque-to-balance electronics (PTE) were constructed to be used with the gyro during the entire program. These electronics are housed in two assemblies. The clock contains the primary timing reference for the system, a commercial crystal oscillator and oven. Count-down scalers plus logic contained in the assembly derive all synchronizing signals required by the PTE and the external ac power supplies. A special feature of the clock is a panel switch for selection of interrogation rate at 28.8, 14.4, 7.2, 3.6, or 1.8 kpps. The pulse duty cycle (ratio of pulse length to interrogate period) remains constant at 15/16 for all repetition rates.

The pulse-torque-electronics contain the rest of the torque circuitry. The constant-current source and H switch were derived from previous laboratory designs. The analog and interrogation decision sections, however, were completely redesigned. A high-speed integrated comparator was used to define each threshold. The major addition to the circuitry is the formation and introduction of the compensation signal which prevents pulse bursting. The rather simple circuit used is shown in Fig.10.

The clock and PTE are rugged units mechanically. Each is organized into a number of circuit boards which are bolted down along their edges to a one-piece aluminum frame. The electronics are completely enclosed by the installation of plate-aluminum covers to each side. This style of construction was chosen so that, if necessary, the clock and PTE could be vibrated with the gyro without significant flexure of the circuit boards.

2.3 SINGLE-AXIS TEST FACILITY

The single-axis test facility consists of a gyro rate table and a console adapted for this program. A block diagram illustrating the functional elements of the controls, various test monitors, and support equipment is shown in Fig. 11. The general technique used for both scale-factor (SF) stability and linearity testing is to set the table controls to the desired rate and to count the number of gyro incremental angle pulses ($\Delta\theta$) for a preset accumulation of table pulses ($\Delta\theta_T$) generated by the table-angle readout.

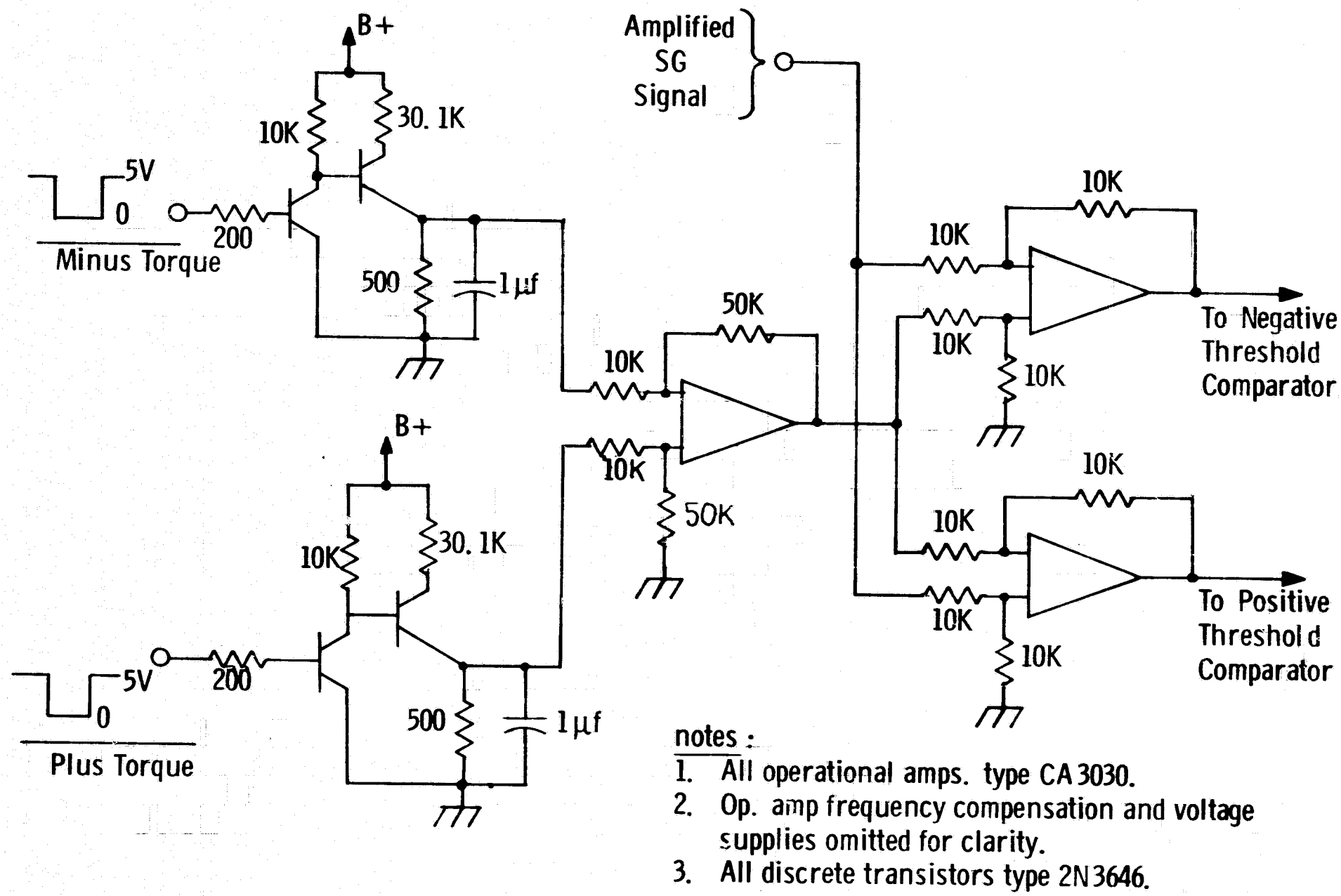

notes :

1. All operational amps. type CA3030.
2. Op. amp frequency compensation and voltage supplies omitted for clarity.
3. All discrete transistors type 2N3646.

Fig. 10 S-G Output Compensation Circuit

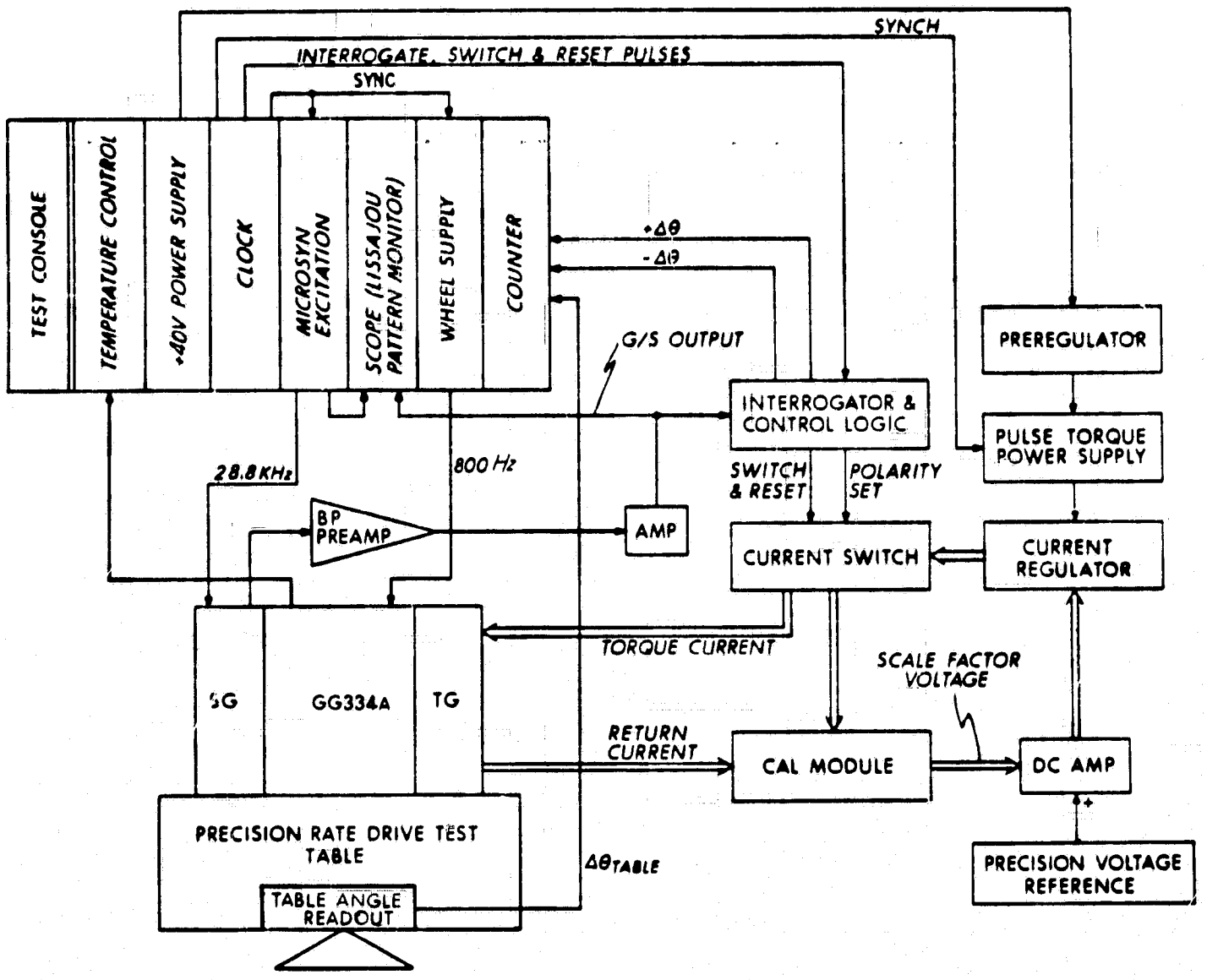

Fig. 11 Gyro in Pulse Torquing Electronic Test Setup

Since the outputs (table angle and gyro pulses) from this test occur as pulses, they can be interfaced directly to a digital computer allowing for on-line computation of the test data. Figure 12 illustrates the method used to perform this function with a small PDP-8/L computer. A computer program, while accounting for earth rate and gyro drift, calculates torque scale factor (input angle per pulse) and average table rate repeatedly during the test. Another computer program counts the sequences of torque pulses occurring at a fixed input rate. After counting a large sample, the program lists the count of each different pattern of adjacent torque pulses and adjacent non-torque interrogate samples. This program enables direct rapid observation of pulse bursting and confident evaluation of the compensation technique.

The computer installation was necessary to perform and analyze data for the large quantity of tests described in Section 2.4. This computer gyro testing provides flexibility, convenience, and utility far beyond that attainable with standard electronic instruments. Using analog-to-digital converters, the computer functions as an automatic test controller and sequencer. At the same time, it operates as a programmable data collection system of enormous proportions. Most important, perhaps, the program can reduce, scale to engineering units, and display data immediately after its collection. Many of the tests implemented were not practicable using conventional test equipment. For example, in some tests, the computer functions as over 3000 up-down counters. It is the only known way to gather pulse-pattern data such as that summarized in Section 2.4.8. Thus, the computer installation has reduced the level of data handling, greatly improved test accuracy, and allowed previously unattainable test techniques.

2.4 TEST RESULTS

The tests run on the GG334A gyroscope while on the single-axis test stand are described in this section. The measurments included are:

1. Torque-generator inductance at various frequencies
2. Torque-generator sensitivity at various direct currents
3. Torque-generator sensitivity at various alternating currents and float angles.
4. Bias and acceleration drift in the following modes:
   a. Inertial reference servo
   b. Analog torque-to-balance
   c. Pulse torque-to-balance
5. Pulse torque-to-balance parameters including:
   a. Scale factor stability and linearity at three interrogation rates (3.6, 7.2 and 14.4 kHz) without gyro lag compensation

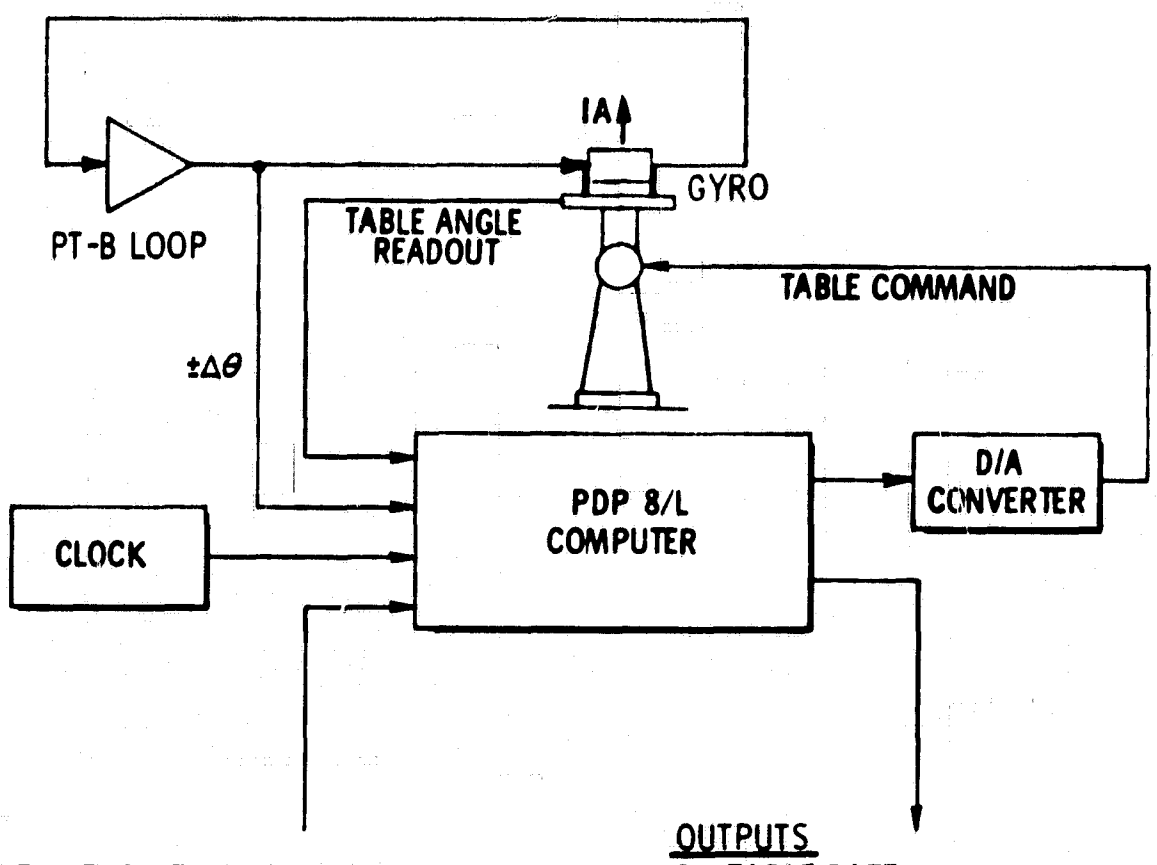

INPUTS

1. NUMBER REVS PER SF COMPUTATION
2. NUMBER OF TIMES TO REPEAT SF COMPUTATION AT EACH TABLE RATE
3. EARTH RATE GYRO DRIFT CORRECTION
4. NOMINAL GYRO SCALE FACTOR

OUTPUTS

1. TABLE RATE
2. SF DEVIATION FROM NOMINAL
3. MAX AND MIN VALUE OF SF AT EACH RATE
4. PUNCHED PAPER TAPE FOR PLOT

Fig. 12 On-Line Scale Factor Determination

b. Scale-factor stability and linearity at the same interrogation rates with gyro lag compensation

c. Scale-factor linearity improvement when reselecting torque-coil tuning components

d. Gyro pulse patterns vs. input rate, with and without gyro lag compensation, at the same three interrogation frequencies.

2.4.1 Torque Generator Inductance versus Frequency

Table 3 shows the permanent magnet torque (PMT) coil inductance vs. frequency. The inductance value decreased slightly (less than 1%) with an increasing frequency between one and ten kilo-Hertz. This trend could be caused by eddy-currents induced in the magnetic return path.

2.4.2 Torque Generator dc Sensitivity

The torque generator (TG) dc sensitivity is measured in an inertial reference mode. In that mode the loop drives the table to oppose earth rate, gyro drift, and dc inputs. To calculate dc torque generator sensitivity, gyro drift and earth rate inputs are removed.

The dc torque generator sensitivity data shows evidence of a small SG-to-TG misalignment. As previously discussed, such misalignment causes a different torque sensitivity for positive and negative current to the PMT coil. The curve (Fig. 13) also shows a 150 ppm dc nonlinearity over the test range of ± 70 ma (0.5 rad/sec). The mechanism causing this dc nonlinearity is under investigation.

2.4.3 Torque Generator ac Sensitivity

The torque generator sensitivity (Fig. 14) was measured using a one kHz alternating current. Magnitudes from 0 to 100 ma were used. The test was performed at three float angles to determine this sensitivity dependence on float angle. Measurements were made in an inertial reference servo mode since the ac coupling of the two torque coils made this test impossible in an analog torque-to-balance mode. The small slope of the ac sensitivity (0.000125 deg/hr/ma) illustrates a good SG to TG alignment for this particular unit. Displacing the float angle 1 mr increased the slope by 140%, illustrating the dependence of ac sensitivity on float angle. By plotting the ac sensitivity vs float angle (Fig. 15) the SG to TG misalignment angle, for this unit, is estimated as approximately 0.5 mrad.

Table 3 Inductance vs Frequency

GG 334A1 S/N C5 10/21/69	TORQUE COIL #1
FREQUENCY (K - Hz)	INDUCTANCE (mh)
1	6.07
2	6.07
5	6.05
10	6.02

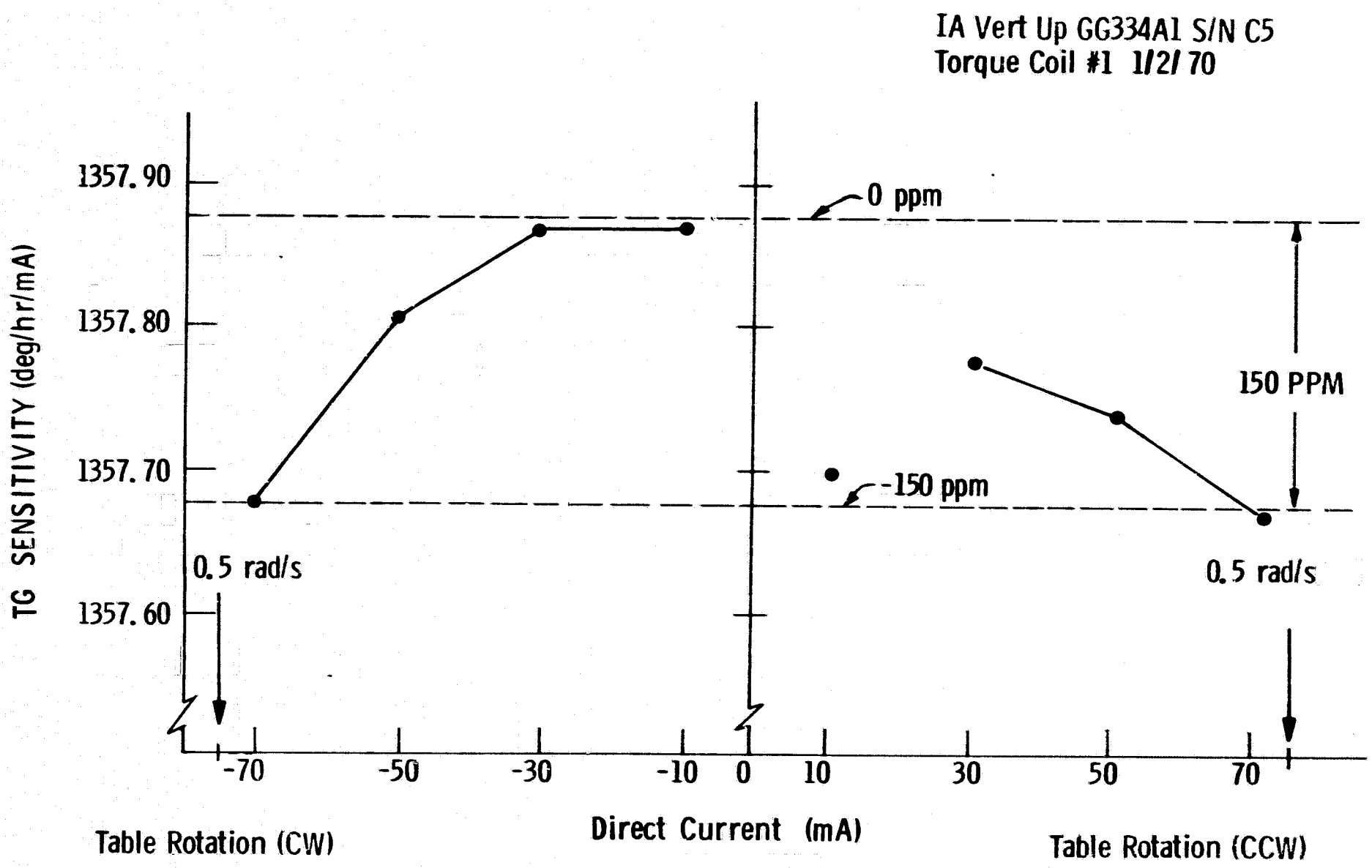

Fig. 13 D C Torque Generator Sensitivity

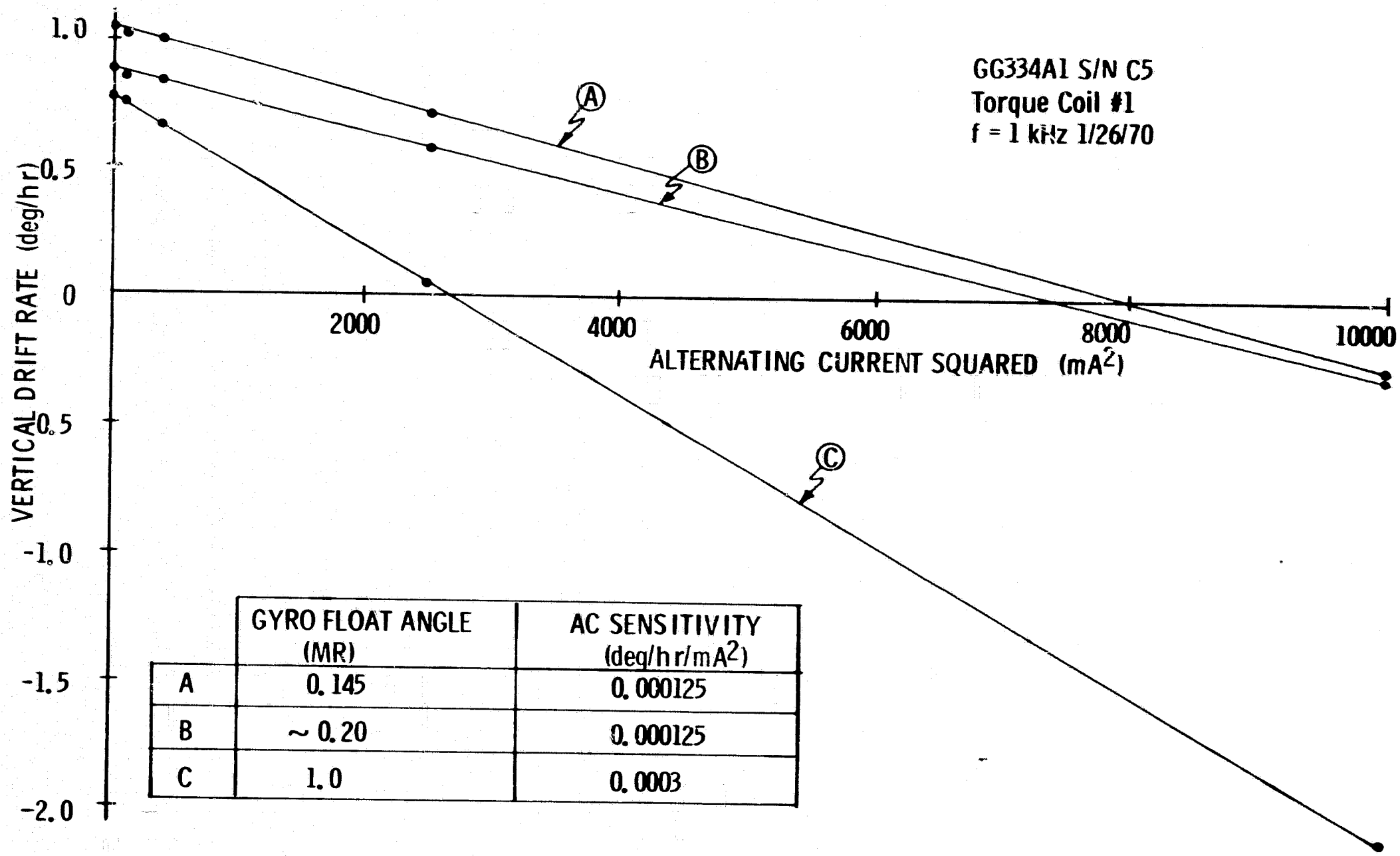

	GYRO FLOAT ANGLE (MR)	AC SENSITIVITY (deg/hr/mA²)
A	0.145	0.000125
B	~ 0.20	0.000125
C	1.0	0.0003

Fig. 14 AC Torque Generator Sensitivity

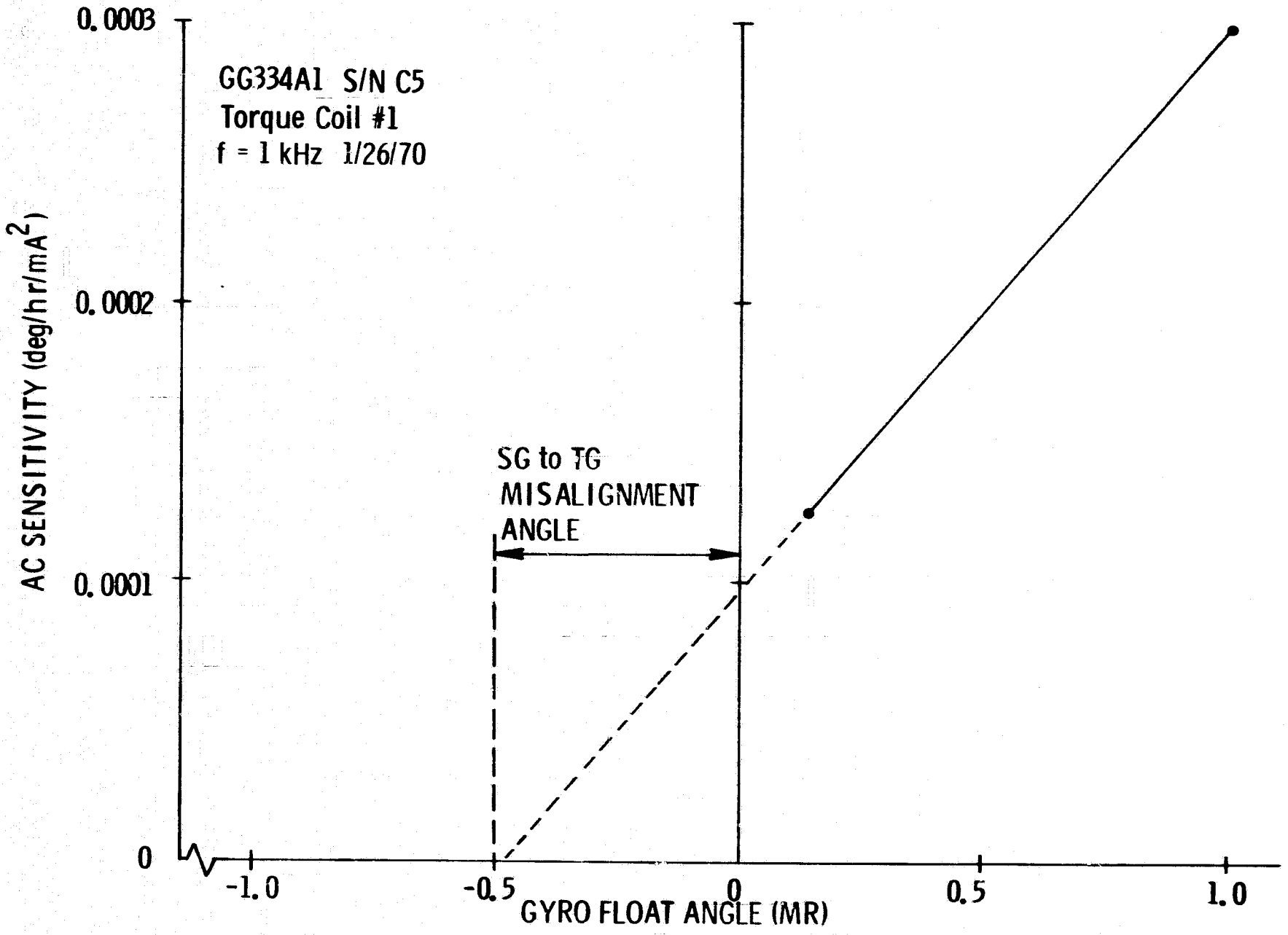

Fig. 15 AC Torque Generator Sensitivity vs. Float Angle

2.4.4 Bias and Acceleration Drift Measurements

The GG334A (S/N C5) bias and acceleration drift terms were measured in the three test modes tabulated in Table 4. In one mode, an analog torque-to-balance loop (ATBL) sends a dc to the torque coil (Coil No. 2) proportional to the gyro float angle. In a second test mode, a pulse-torque-to-balance loop (PTBL) applies pulses of current to the torque coil (Coil No. 1) at a rate proportional to the gyro input rate. In the inertial reference servo mode, the loop drives the table to oppose earth rate and gyro drift rates.

The acceleration insensitive drift (BD) and the drifts due to an acceleration along the input axis (ADIA), the spin reference axis (ADSRA) and the output axis (ADOA) are tabulated for data obtained in three test modes. Between tests at MIT/DL, the wheel was turned off and the unit cooled down. These terms showed a peak-to-peak spread of 0.19, 0.1 and 0.07°/hr/g respectively for data taken on this unit between 20 August 1969 and 24 January 1970. The changes from point to point in any term do not correlate with changes in the measurement loop used. This range of instability is typical for this class of gyro. In addition, there is good agreement between BD measurements in the analog-torque-to-balance and pulse-torque-to-balance modes ($<0.07^{\circ}$/hr). However, BD in the servo mode showed a 0.51°/hr range. This large BD range could result from a torque proportional to float angle, that is gyro elastic restraint. A 2-mr null difference between these servo tests would account for this magnitude of bias spread.

2.4.5 Scale Factor Stability

The quantization size (angle/pulse) is proportional to the maximum rate in which the loop must function, and inversely proportional to the interrogation frequency. The strapdown system designer must trade between the desire for high interrogation frequencies, and thus fine quantization as needed for attitude algorithm calculations, and dynamic compensations against the timing and switching problems these higher frequencies present. For the GG334A gyro under test, interrogation frequencies of 3600, 7200, and 14400 Hz gave scale factors of approximately 60, 30, and 15 seconds of arc per pulse respectively. This test program showed that the MIT torque loop design used can operate through this range of interrogation rates with equivalent linearity and scale factor performance.

Figure 16 shows a 50-hr PTBL scale-factor run without gyro lag compensation at a 3600 pps interrogation rate. Each point is the average scale factor measured over 250 table revolutions (1.75 hours per data point). A total excursion of 10 ppm

Table 4 Bias and Acceleration Drift Measurements

Test Location	Honeywell	MIT	MIT	MIT	MIT	MIT	MIT	MIT
Type of Loop	ATBL	ATBL	SERVO	SERVO	PTBL	SERVO	PTBL	PTBL
Date	1/69	8/20/69	9/29/69	9/30/69	12/12/69	12/18/69	12/23/69	1/24/70
BD (deg/hr)	- 0.26	- 0.17	- 0.45	- 0.43	- 0.10	+ 0.06	- 0.15	- 0.17
ADSRA (deg/hr/g)	- 0.22	+ 0.07	+ 0.05	+ 0.07	+ 0.15	+ 0.15	+ 0.14	+ 0.14
ADIA (deg/hr/g)	+ 0.74	+ 1.04	+ 1.01	+ 1.14	+ 1.01	+ 0.97	+ 1.00	+ 1.16
ADOA (deg/hr/g)	+ 0.29	- 0.04	- 0.04	+ 0.02	+ 0.03	+ 0.03	+ 0.03	+ 0.03

(GG334A1 S/N C5)

ATBL = Analog Torque to Balance Loop

PTBL = Pulse Torque to Balance Loop

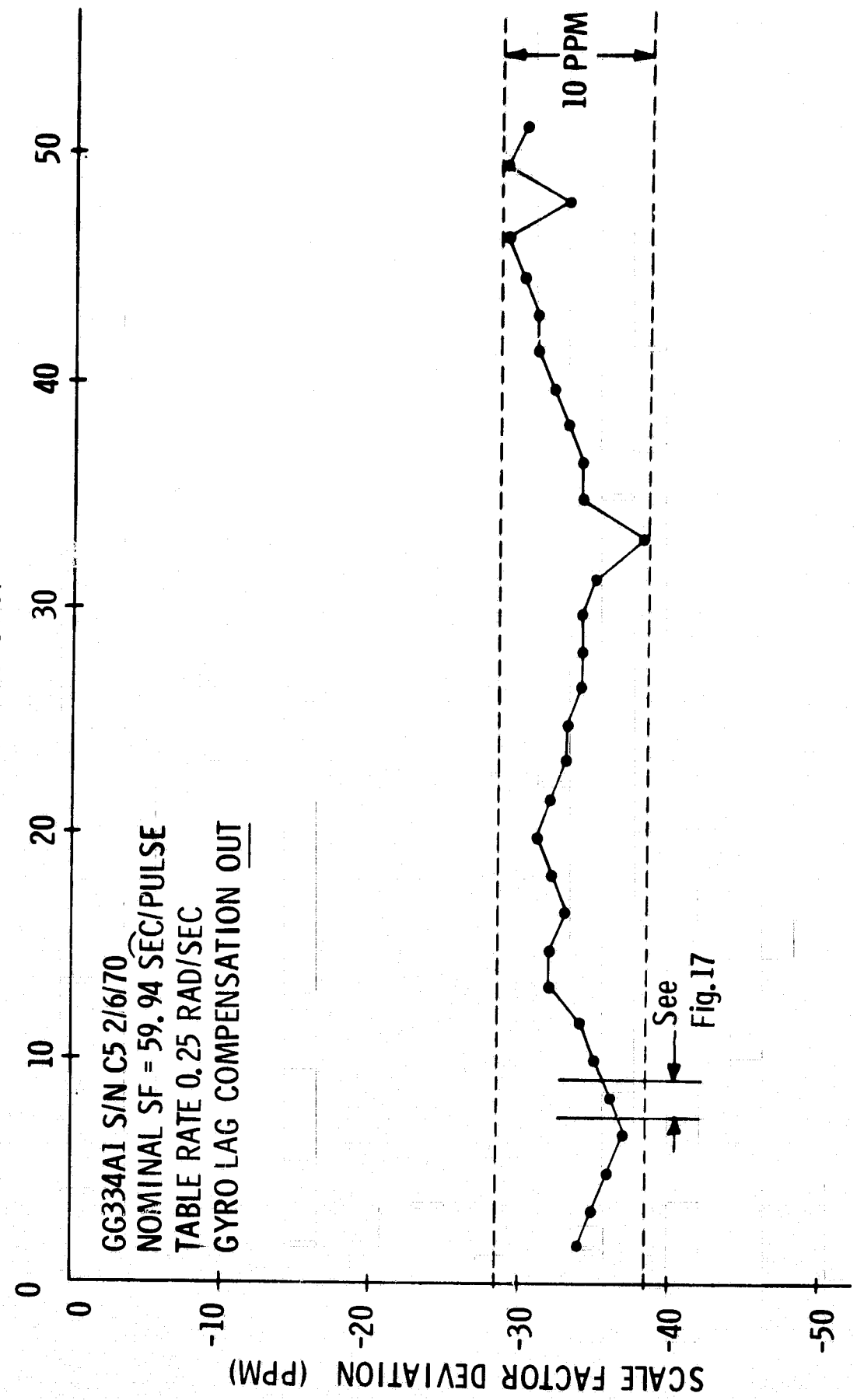

Fig. 16 Scale Factor Stability Interrogation Frequency = 3.6 kHz

was obtained. Figure 17 shows a small portion of Fig. 16 expanded and plotted for scale factor averaged over 10 revolutions (4.2 minutes per data point). A one-pulse uncertainty results in a 5 ppm error when scale factor is averaged over 10 table revolutions. When averaged over 250 table revolutions, the quantization error becomes negligible. Figure 17 illustrates loop quantization error of ± 1 pulse or 10 ppm. Figure 16 illustrates long-term stability when quantization error is negligible.

Similar stabilities were obtained at interrogation rates of 7200 pps (Fig. 18) and 14.4 Kpps (Fig. 19). Even though the quantization decreases with increasing interrogation rate, the point-to-point stability remains nearly constant for the three interrogation rates when the loop is not compensated. The 10 ppm stability at 3600 pps correspond to ±1 pulse whereas this stability at 14.4 Kpps correspond to ±4 pulses. Thus at the higher interrogation frequency the improved quantization is offset by an increase pulse burst length maintaining a near constant angular uncertainty. The scale factor at 14.4 Kpps shows a slight decrease with time which has been typical for tests at that frequency. The cause of the downward trend, whether due to the torque loop or gyro, could not be identified at this time. It does not represent a significant finding, but will be investigated during the continuing effort on this program.

Figure 20 at 14.4 Kpps interrogation rate with the gyro lag compensator illustrates a characteristic of loop compensation. For this 14-hour test, a 5 ppm point-to-point stability was obtained. (This curve has a downward trend similar to the uncompensated data.) The improved point-to-point stability with the compensator (comparing Fig. 20 to Fig. 19) results since the gyro lag compensation elminates pulse bursting. Without compensation, the gyro is torqued by a string of pulses. This multiple pulse bursting will cause data uncertainty equal to the length of a pulse burst. When the PTBL gyro lag compensation is installed, the pulse bursting is eliminated, reducing this error to a one-pulse uncertainty. Thus when the loop is compensated an increased quantization occurred with increased interrogation frequency. This did not occur for the uncompensated case as described above.

2.4.6 Scale Factor Linearity

Using gyro lag compensation, tests were run on the GG334A gyro to determine how scale factor linearity varies with loop interrogation frequency. Interrogation frequencies of 3600, 7200 and 14400 Hz were selected, and input rates from 0.15 to 0.95 radians per second were used. As shown in Figs. 21, 22 and 23, these three interrogation frequencies gave equivalent linearity of approximately 130 ppm. This

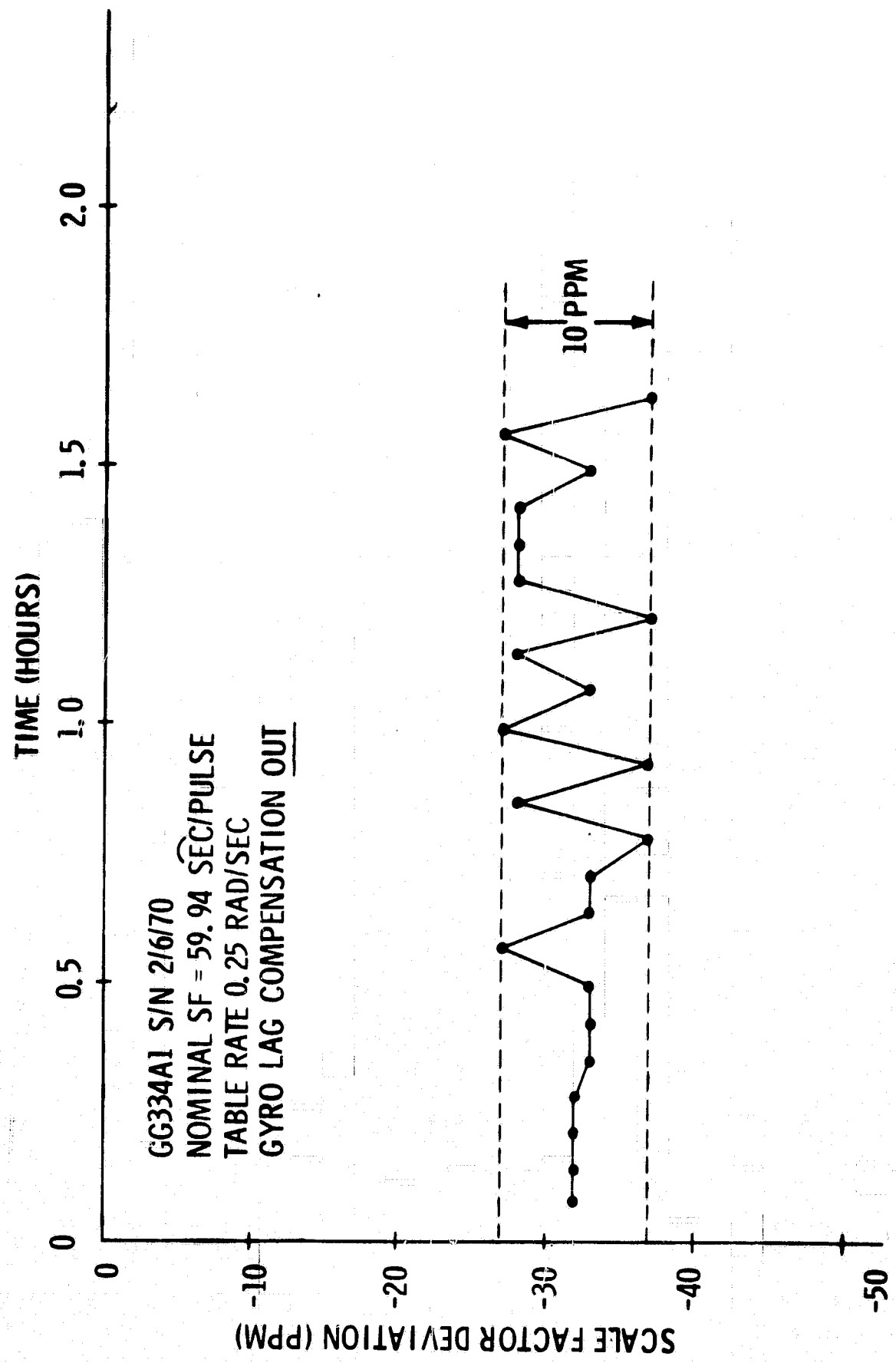

Fig. 17 Scale Factor Stability Interrogation Frequency = 3.6 kHz

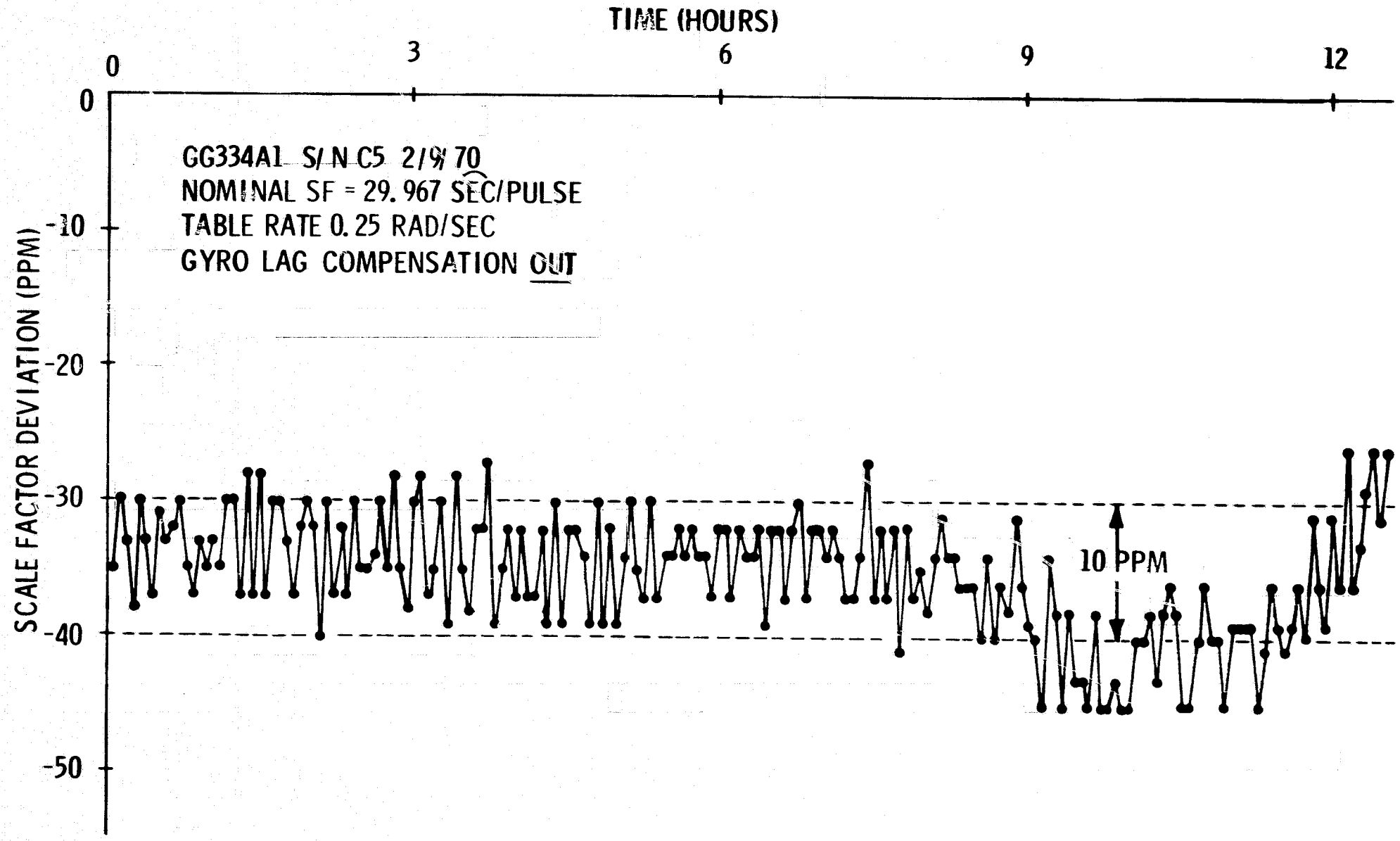

Fig. 18 Scale Factor Stability Interrogation Frequency = 7.2 kHz

GG334A1 S/N C5
NOMINAL SF = 15.0239 SEC/PULSE
TABLE RATE 0.15 RAD/SEC
GYRO LAG COMPENSATION OUT

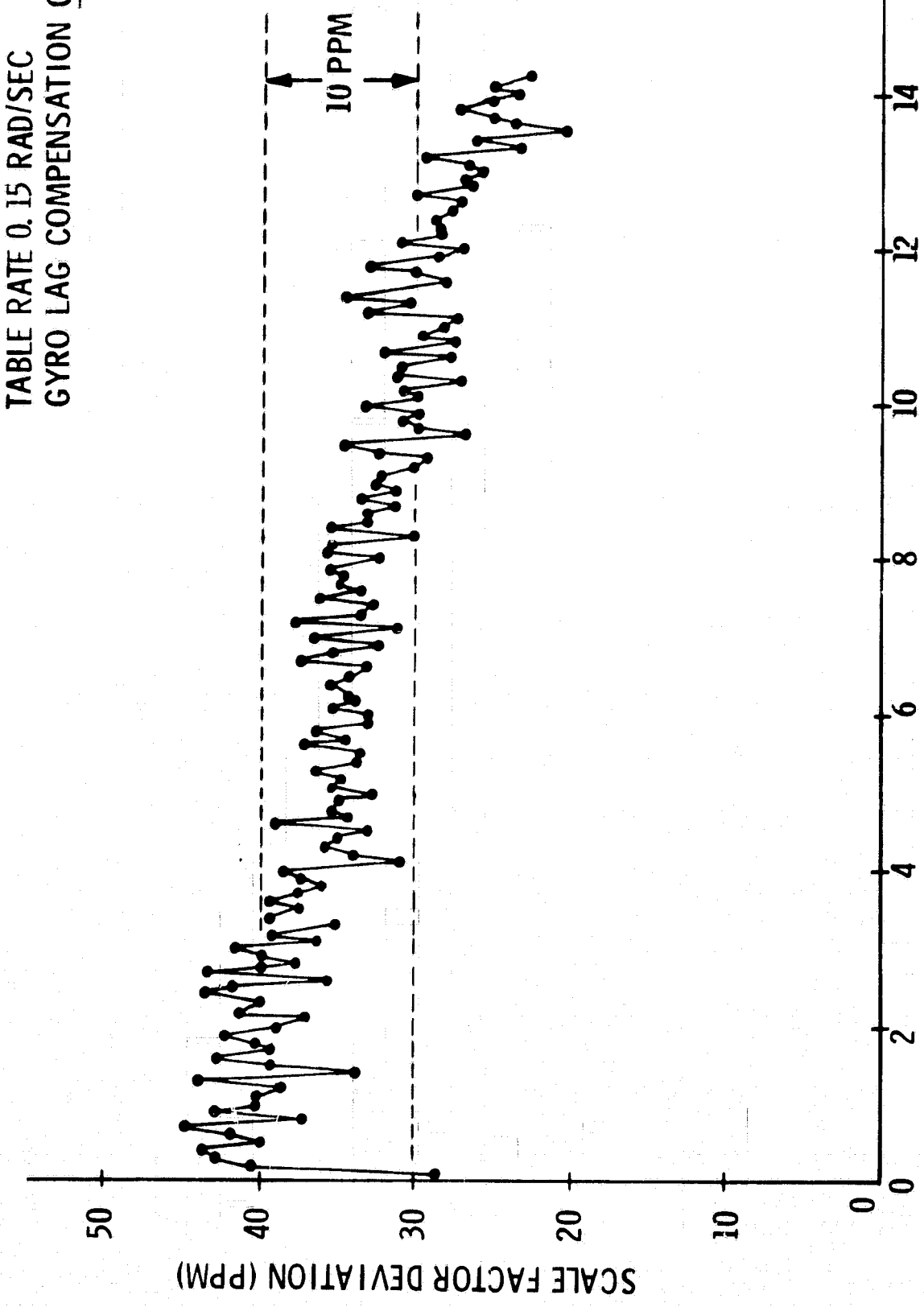

Fig. 19 Scale Factor Stability Interrogation Frequency = 14.4 kHz

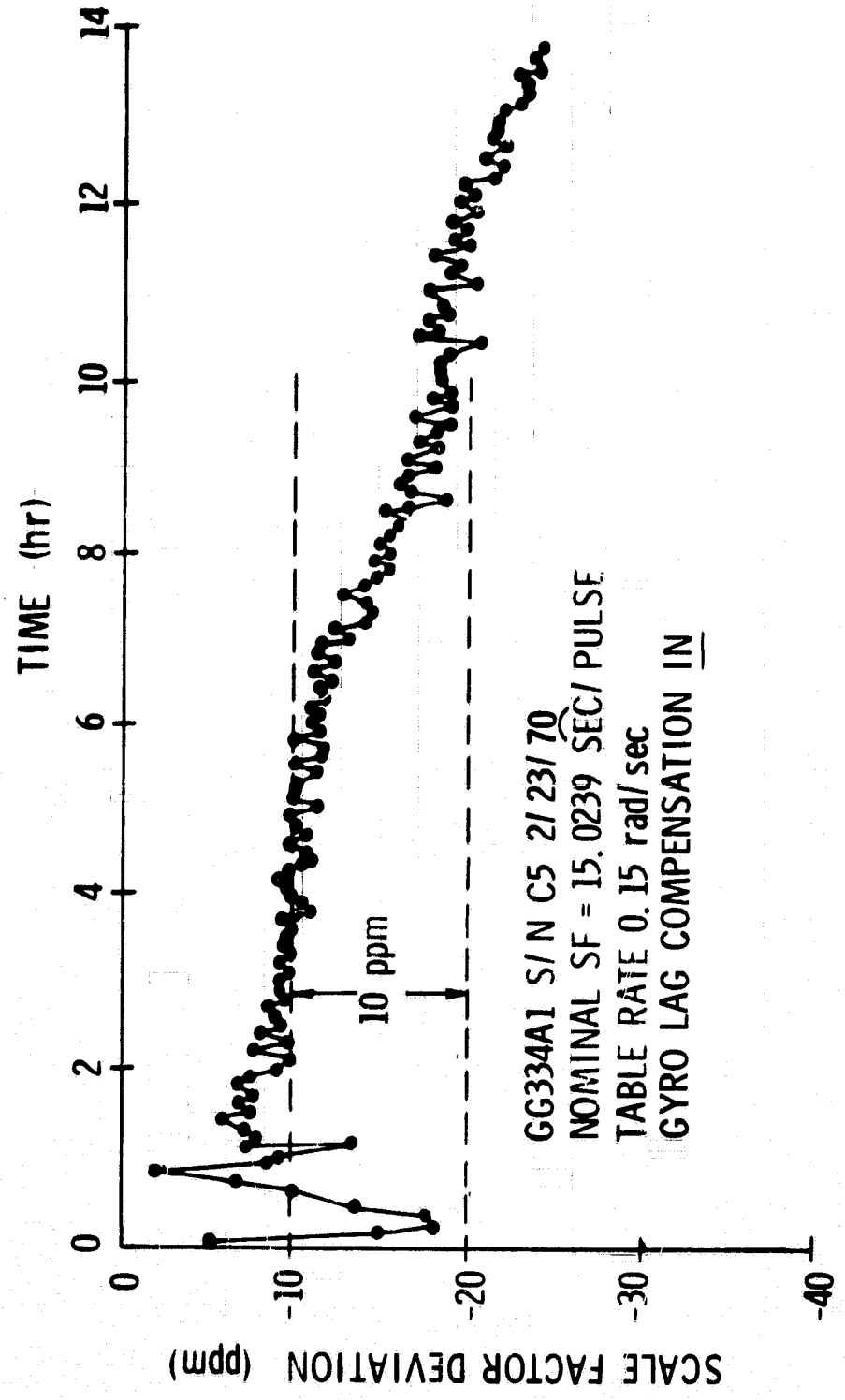

Fig. 20 Scale Factor Stability Interrogation Frequency = 14.4 kHz

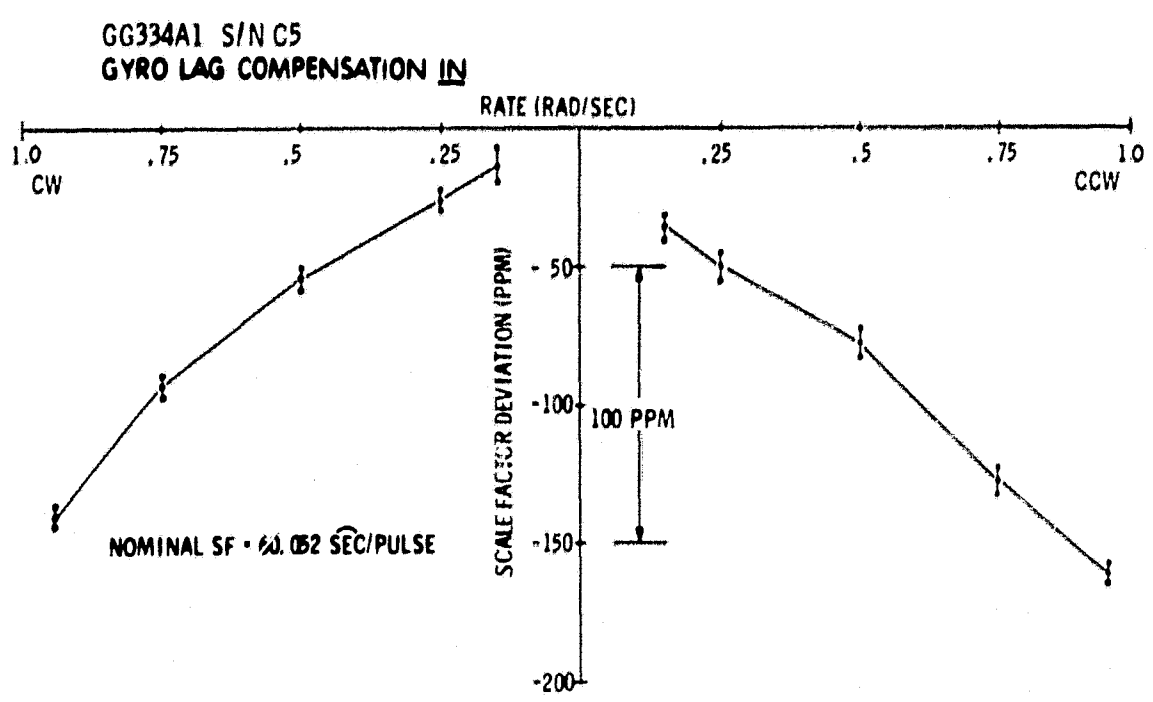

Fig. 21 Scale Factor Linearity: Interrogation Frequency = 3.6 kHz

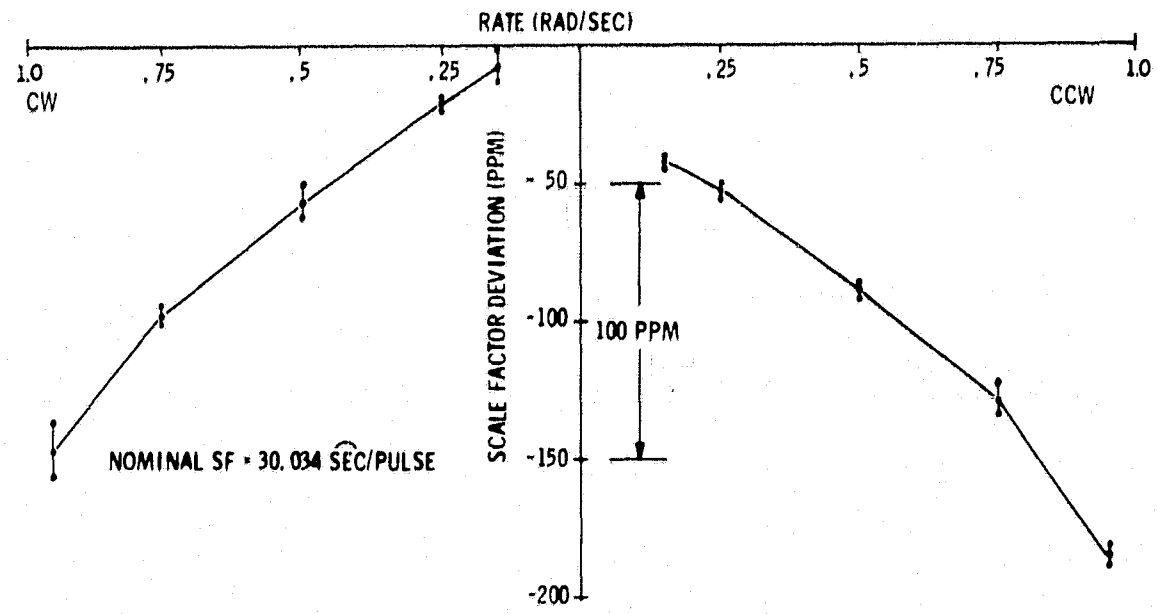

Fig. 22 Scale Factor Linearity: Interrogation Frequency = 7.2 kHz

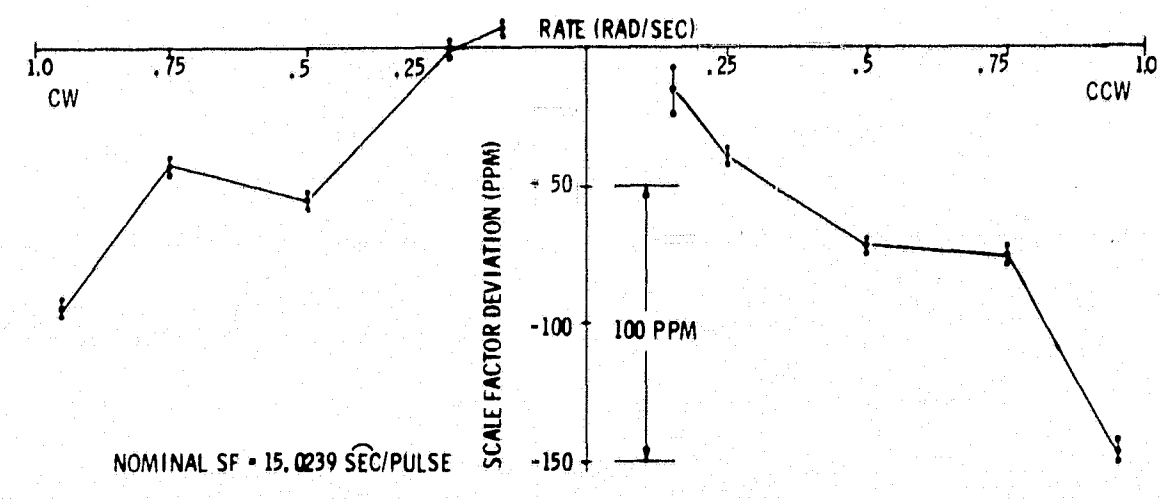

Fig. 23 Scale Factor Linearity: Interrogation Frequency = 14.4 kHz

data illustrates the frequency insensitivity of this instrument, which is due to the use of a potted coil support (Units with conductive coil supports are frequency sensitive.) and torque-coil tuning which was carefully adjusted to make the coil look resistive to the current switch.

The rate linearity tests without gyro lag compensation at interrogation frequencies of 3600 pps (Fig. 24) and 7200 pps (Fig. 25) are equivalent to the tests with compensation (Figs. 21 and 22). A change in linearity with loop compensation would not be expected, since the data presented is averaged over many revolutions, and thus the quantization improvement obtained with loop compensation is not illustrated. The data serves to illustrate that the compensation concept is compatible over the entire rate region, since no linearity degradation is observed.

For all rate linearity tests, the average SF for a positive rate about the gyro input axis (IA) was greater in magnitude than for a negative rate about IA, due to either a pulse torque-to-balance loop unbalance and/or an instrument SM to TG misalignment. The PTBL linearity curves are of similar shape to the dc sensitivity curve (Fig. 26). Similarity between PTBL scale factor and dc linearity was also noted on the 18 IRIG MOD B gyro; however, its curves are concave upward.

Table 5 summarizes SF stability and SF linearity data at the three interrogation frequencies with and without gyro lag compensation. Notice the test results are independent of interrogation frequency and only scale factor stability is improved by the gyro lag compensator.

2.4.7 Torque-Coil Tuning for Improved Linearity

All previous linearity tests shown were run with three series RC networks, each shunting the coil. These components were selected to make the load look as nearly resistive as possible. Figures 27 and 28 show the effect of mistuning the coil for improved linearity at 3600 pps interrogation rate. Figure 27, run at an interrogation frequency of 3600 pps shows a 60 ppm nonlinearity over the test range of ± (0.25 to 0.95) rad/sec. Figure 28 run over the same test range but at a 7200 pps interrogation frequency showed a linearity of 220 ppm. Thus tuning to improve linearity has made the linearity dependent on interrogation frequency. The generation of a model for the scale factor nonlinearity mechanism and the development of a standard procedure for optimizing rate linearity should be an area of future investigation.

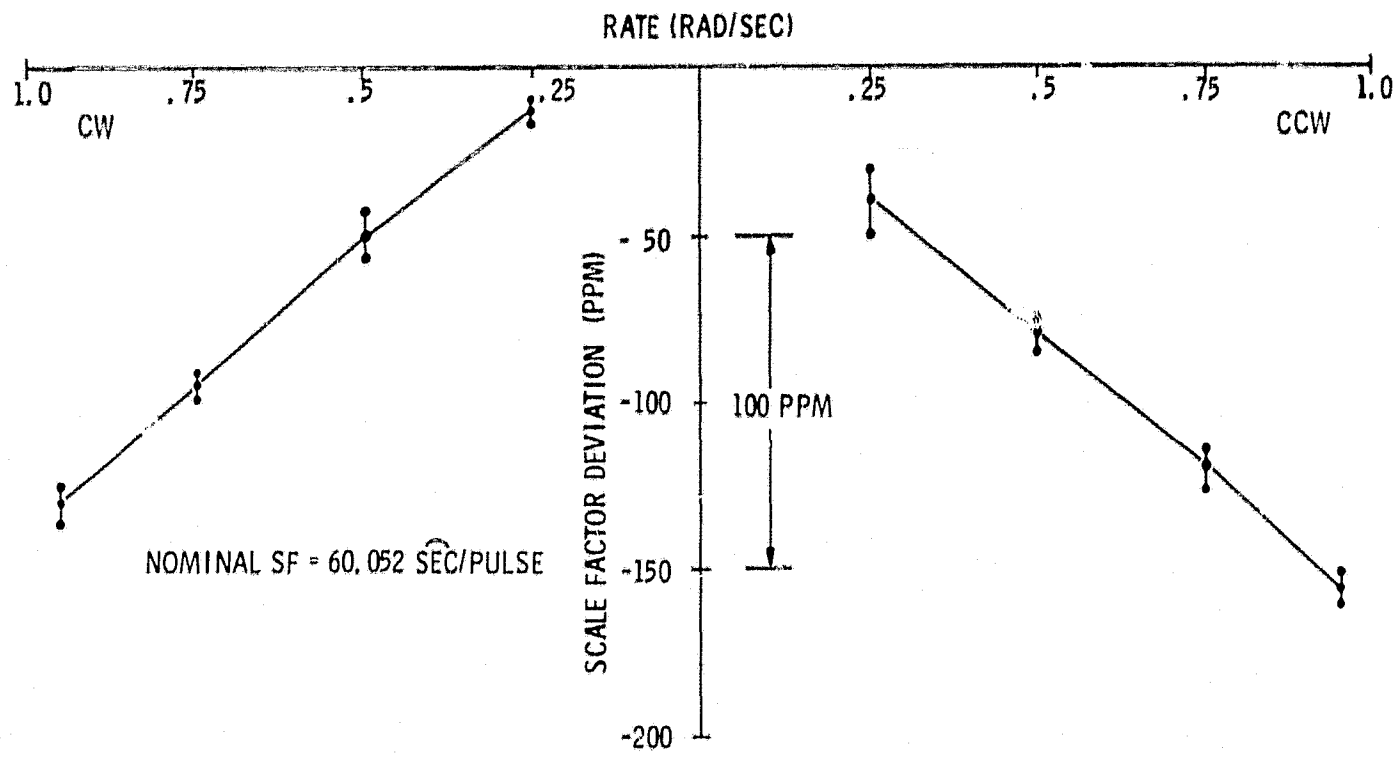

Fig. 24 Scale Factor Linearity: Interrogation Frequency = 3.6 kHz

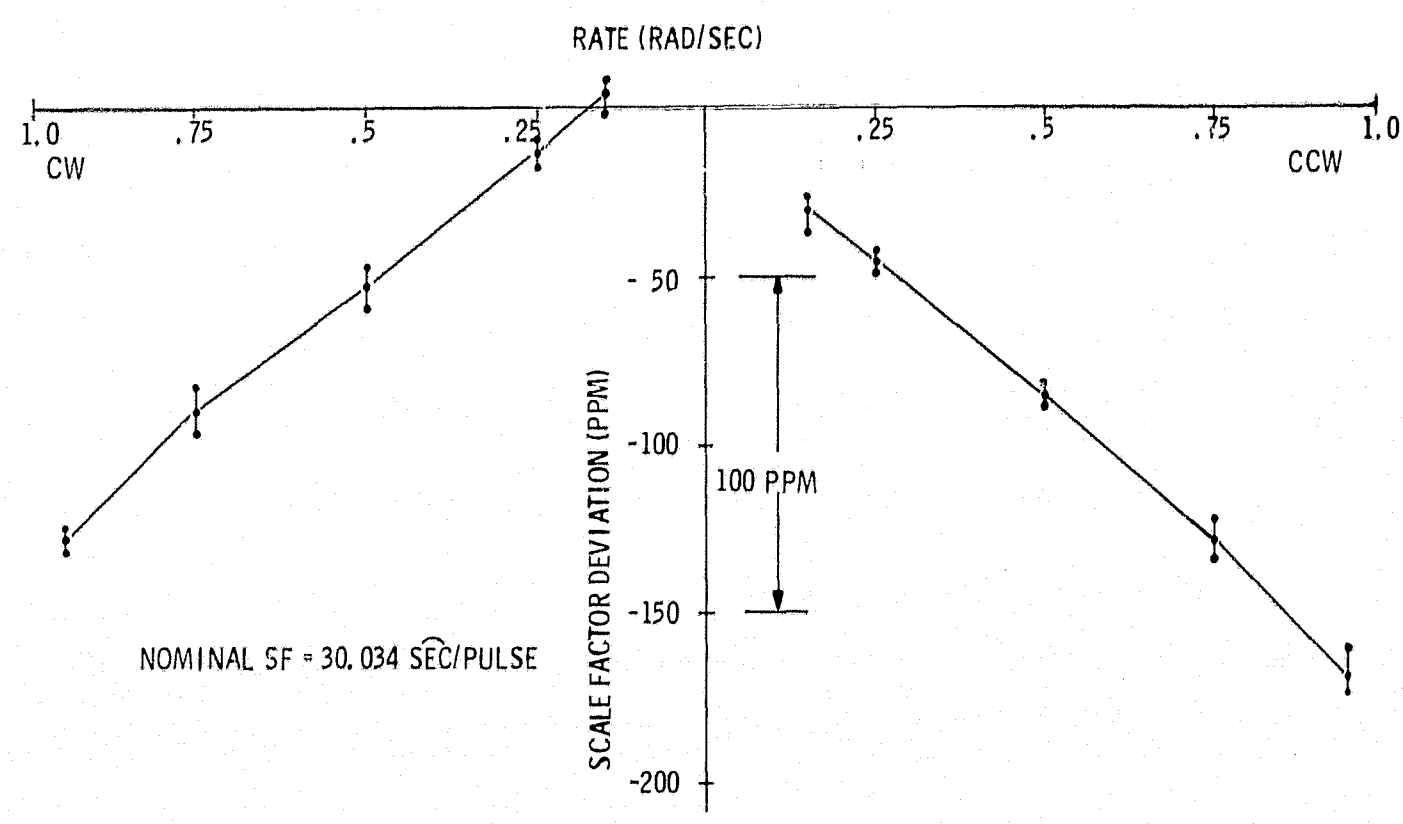

Fig. 25 Scale Factor Linearity: Interrogation Frequency = 7.2 kHz

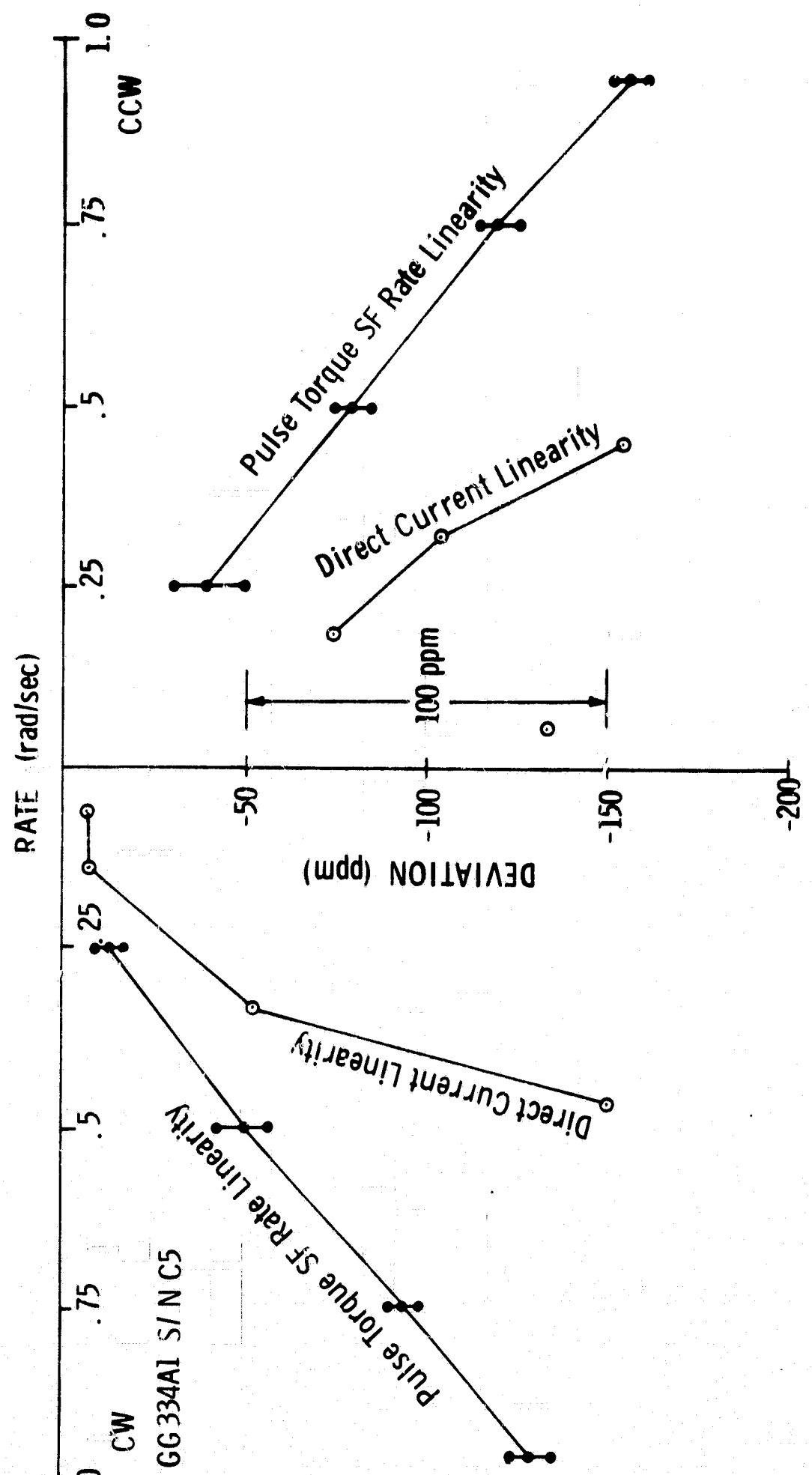

Fig. 26 Comparison of DC and Pulse-Torque Scale-Factor Linearity

Table 5 Scale Factor Stability and Linearity Summary

GG334A1 S/N C5
2/24/70

INTERROGATION FREQUENCY	GYRO LAG COMPENSATION OUT		GYRO LAG COMPENSATION IN	
	SF STABILITY	SF LINEARITY	SF STABILITY	SF LINEARITY
(PPS)	(PPM)	(PPM)	(PPM)	(PPM)
3600	10	120	---	115
7200	15	125	---	130
14400	10-15	---	5	110

SF LINEARITY PERFORMANCE OVER A TEST RANGE OF ±(0.25 - 0.95) RAD/SEC

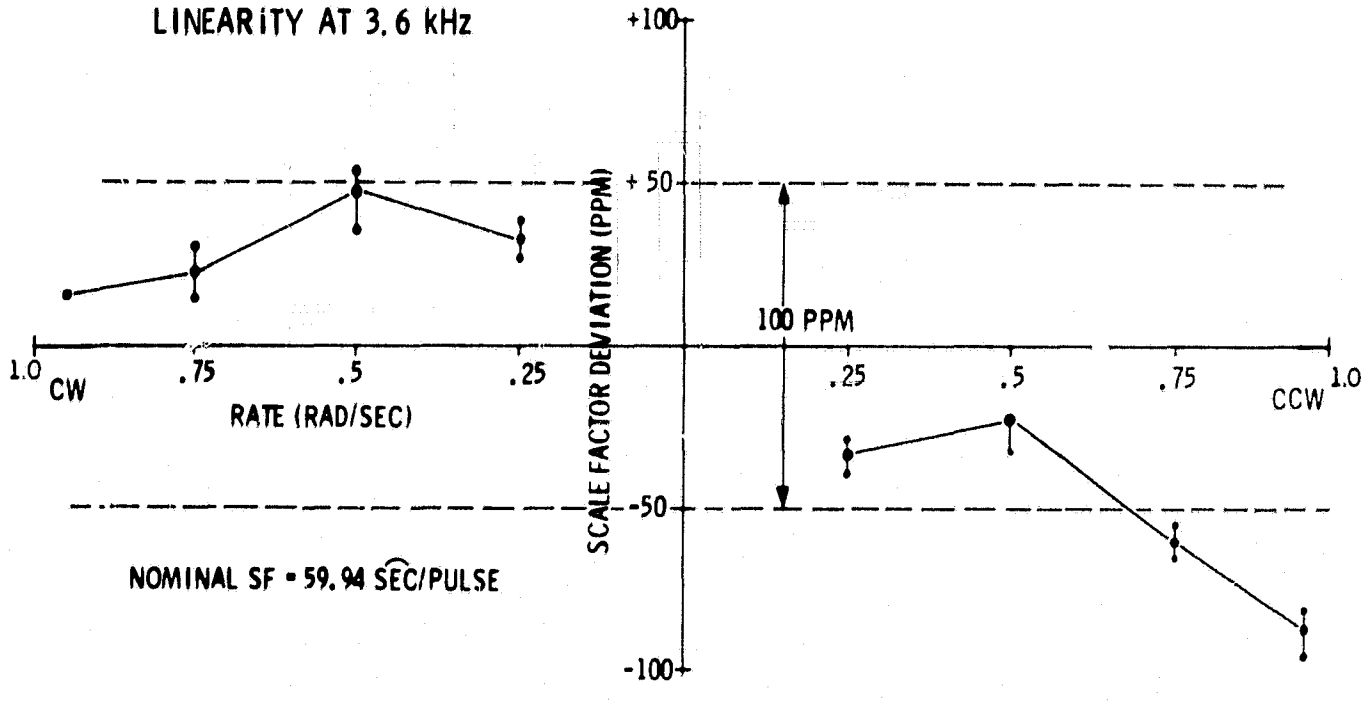

Fig. 27 Scale Factor Linearity: Interrogation Frequency = 3.6 kHz

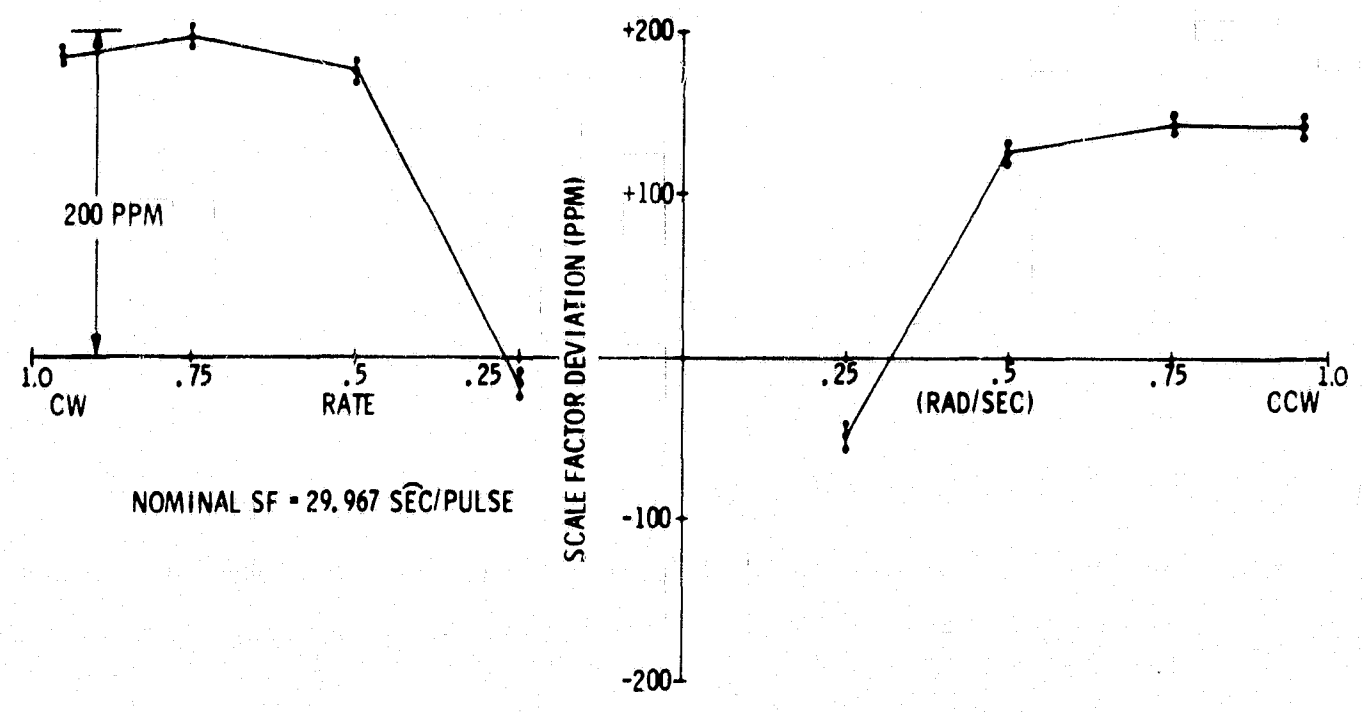

Fig. 28 Scale Factor Linearity: Interrogation Frequency = 7.2 kHz

2.4.8 Gyro Lag Compensation Testing

Table 6 is a distribution of the pulse torque patterns for an uncompensated loop when operated at 1/4 of maximum rate and an interrogation frequency of 14,400 pps. The first column represents the number of times that a particular mode occurred. The second column represents the number of ON pulses of the pattern while the third column represents the number of OFF pulses which followed. The table illustrates the number of times each pulse pattern occurred over the test period. The most common patterns occurred near 7 ON followed by 21 OFF pulses, 6 ON followed by 18 OFF pulses and 8 ON followed by 24 OFF pulses. Other pulse patterns occurred less frequently. This table illustrates the ambiguous information available in a string of pulses describing the rate inputs for an uncompensated pulse torque loop.

Table 7 shows the pulse torque distribution for a compensated loop for the same input rate and interrogation frequency of Table 6. A pattern of 1 ON followed by 3 OFF pulses occurs most of the time with slight variations due to table rate variations. More importantly, the system never produces more than one ON pulse in a row. Compensating the gyro lags has reduced the multiplicity of patterns by eliminating pulse bursts. For this reason, the compensated system will have a smaller error in indicated attitude than the uncompensated system. Since fewer narrow decisions are required with compensation, the variety of patterns is also reduced by an increase in noise rejection.

Figure 29 is a plot of the pulse burst length vs input rate for three interrogation frequencies. Burst lengths that occurred less than 5% of the time were not plotted in the range shown for each case. This figure is essentially a graph of resolution versus IRA rate. For rates up to one half maximum rate, a burst is defined as the number of adjacent ON pulses. Above this rate, a burst is defined as the number of adjacent OFF pulses. The large number of pulses per burst occurring near half maximum rate represents a loss of resolution and accuracy of the indicated angle. The higher interrogation frequencies yielded the larger burst lengths showing that shortening the sample period cannot alone improve the quantization beyond a certain point. For all interrogation frequencies and all input rates tested, multiple pulsing occurred with the uncompensated loop, whereas it was eliminated by the compensation. This data demonstrates the effectiveness of compensation in eliminating multiple pulsing and thereby reducing the error in indicated position.

Table 6 Gyro Moding Patterns
Interrogation Frequency = 14.4 kHz
Gyro Lag Compensation Out

GG334A1 S/N C-5
TABLE RATE ~0.25 RAD/SEC
2/25/70

NUMBER OF OCCURRENCES	ON	OFF	NUMBER OF OCCURRENCES	ON	OFF
3	1	1	1	5	1
1	1	2	2	5	11
1	1	18	5	5	12
1	2	3	75	5	13
1	2	5	195	5	14
1	2	9	282	5	15
1	3	3	249	5	16
1	3	4	102	5	17
2	3	5	22	5	18
3	3	6	4	5	19
3	3	7	2	5	20
1	3	8	12	6	15
1	3	9	227	6	16
1	3	10	964	6	17
3	3	11	1797	6	18
3	3	13	1588	6	19
1	3	14	442	6	20
1	3	15	58	6	21
1	3	17	3	6	22
1	4	5	6	7	18
3	4	7	252	7	19
1	4	8	2156	7	20
4	4	9	4095	7	21
8	4	10	2149	7	22
22	4	11	339	7	23
31	4	12	12	7	24
33	4	13	7	8	21
12	4	14	196	8	22
4	4	15	1026	8	23
2	4	16	1380	8	24
2	4	17	507	8	25
1	4	19	41	8	26
1	4	20	3	9	25
			40	9	26
			36	9	27
			3	9	28

Table 7 Gyro Moding Patterns
Interrogation Frequency = 14.4 kHz
Gyro Lag Compensation In

GG334A1 S/N C5
TABLE RATE~0.25 RAD/SEC
5/25/70

NUMBER of OCCURRENCES	ON	OFF
390	1	2
4095	1	3
379	1	4
1	1	5
1	1	6

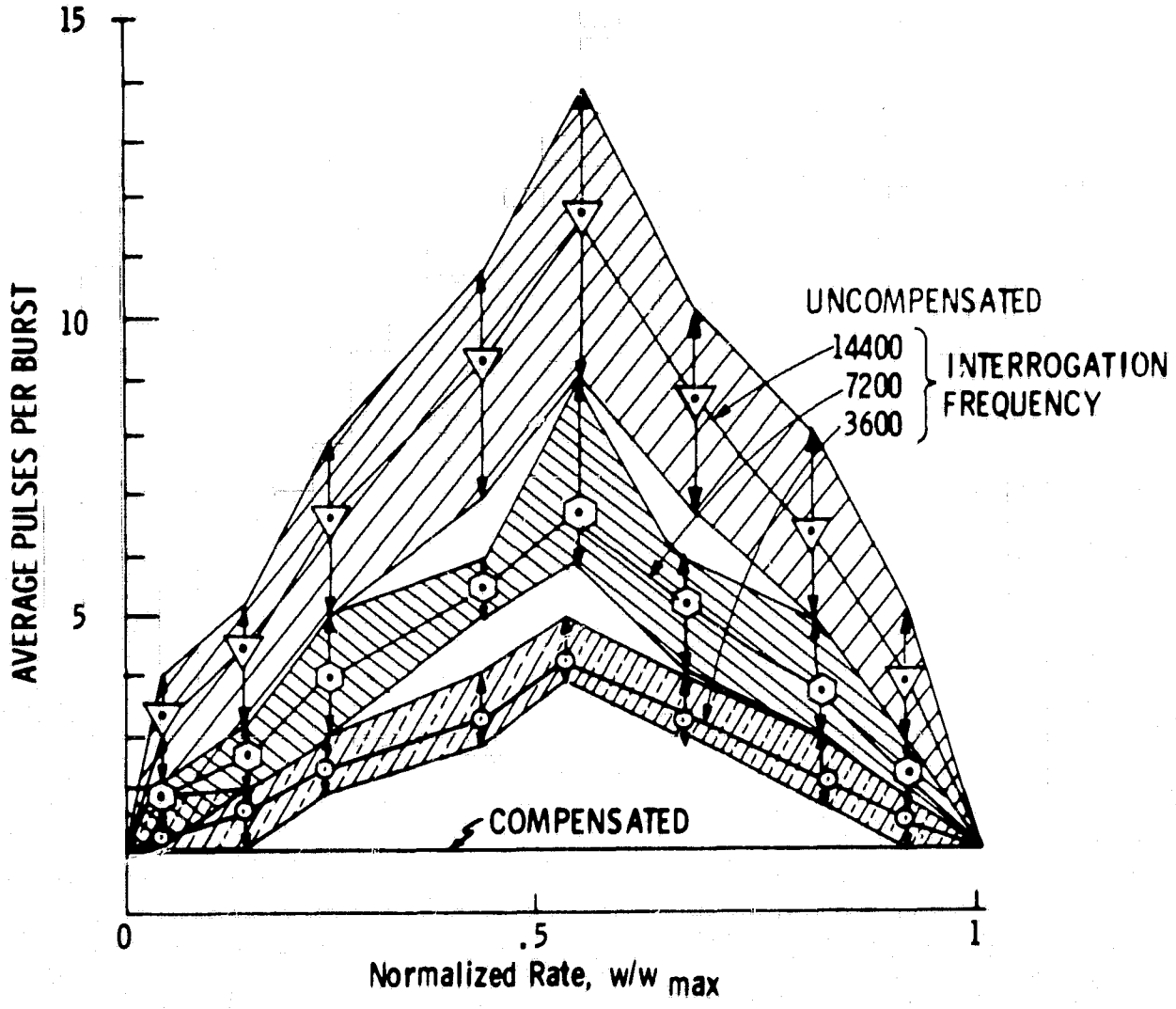

Fig. 29 Burst Length vs Rate

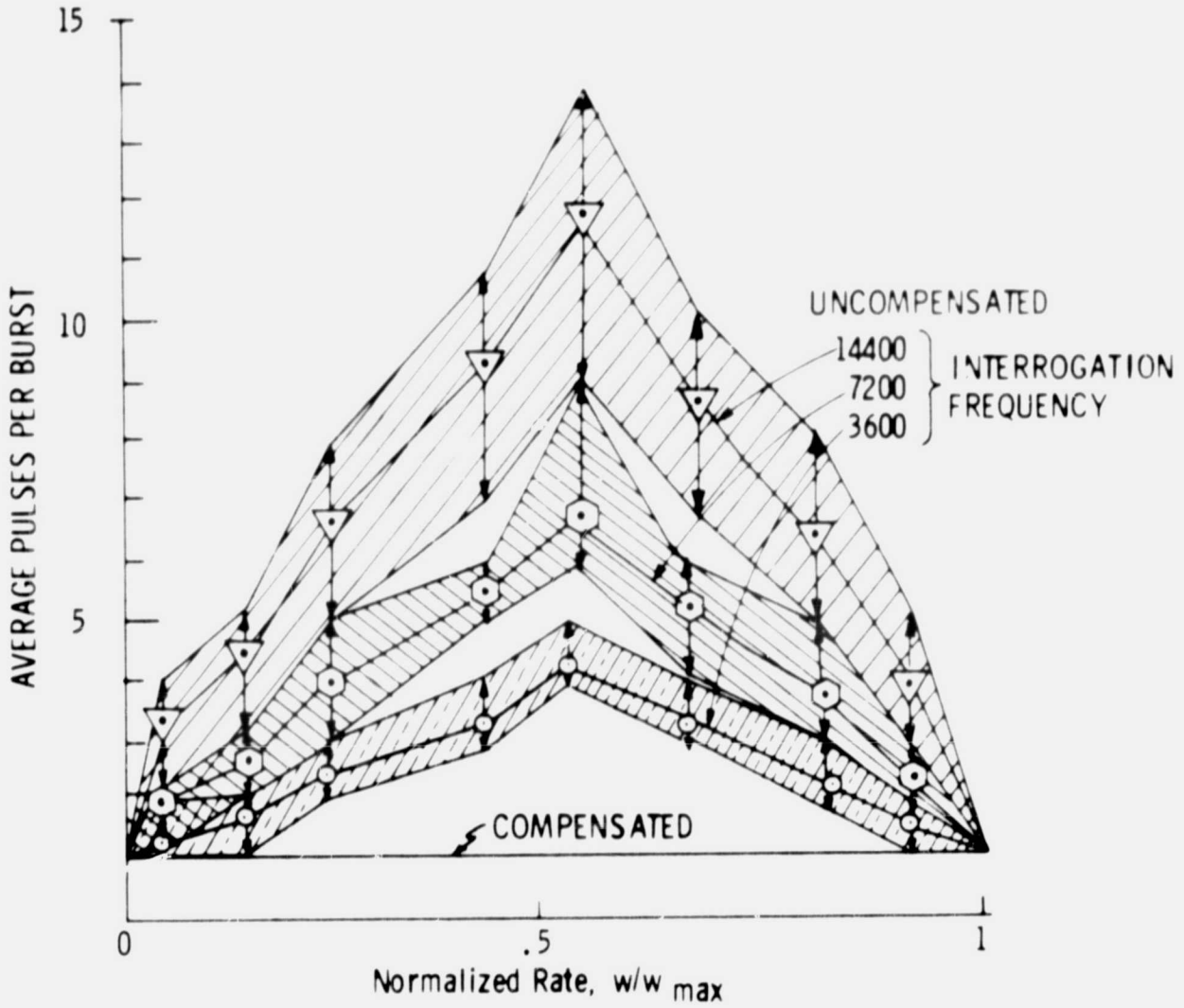

Fig. 29 Burst Length vs Rate

2.5 CONCLUSIONS AND RECOMMENDATIONS

2.5.1 Conclusions

A number of conclusions can be reached from the results of this section.

1) For the GG334A (S/N C5) gyro used with the MIT ternary torque-to-balance loop, the following performances were obtained:

   a. Scale-factor stability of 10 ppm was achieved at 3600-pps interrogation rate over a 50-hour run.
   b. Scale-factor rate linearity of 125 ppm over rates of 1/8 to 1 radian per second were obtained at repetition rates of 3600, 7200, and 14400 pps.
   c. Scale-factor rate linearity of 60 ppm for rates from 1/4 to 1 radian per second were achieved at a 3600-pps interrogation rate when the torque coil was detuned to achieve better rate linearity.
   d. During the month of testing, the drift stabilities measured in the pulse-torque-to-balance loop were 0.07°/hr for bias, 0.01°/hr/g for ADSRA, and 0.16°/hr/g for ADIA drift terms.

2) When a permanent-magnet torque generator is used to rebalance a strapdown gyro, the stability and linearity of its scale factor are critical limiting parameters for system use. Several design and assembly practices have been described and analyzed. It is concluded that careful alignment of the torque coil to the signal-generator null is necessary to reduce plus-to-minus scale-factor difference and alternating-current sensitivity. The use of non-conductive material for the coil holder eliminates eddy currents (the major source of nonlinear impedance) simplifying tuning of the coil and improving scale-factor linearity.

3) The pulse-torque and dc scale factor appear to have the same general shape vs. rate, suggesting that thermal effects are another important source of nonlinearity.

4) If the torque coil is tuned to appear resistive to the current switch, scale factor linearity and stability are independent of interrogation rate from 3.6 to 14.4 kpps.

5) Scale-factor nonlinearity can be reduced at fixed interrogation rate by mistuning the torque coil. Such mistuning can improve linearity if it is judiciously chosen to cancel existing nonlinearity from other causes. But it is only effective at the interrogation rate at which chosen; otherwise linearity becomes much worse.

6) The construction and testing of the compensation for command torque lags has validated the analysis and design technique. Both smaller errors and lower effective resolution in quantization are achieved through the elimination of pulse bursting.

7. Although not shown here, a direct implication of other analysis[1,9] is that the pulse bursting phenomena is common to all types of torque loops which do not have a compensation feature as described above. If the period between decisions is comparible to the gyro time constant, compensation is required to achieve single-pulse quantization over the entire rebalance range, regardless of the type of rebalance loop used.

2.5.2 Recommendations

It is recommended that:

1) Empirical testing be required of the hypothesis that nonlinear scale factor results from thermal effects. This may be accomplished by combining alternating and direct current in the coil so as to keep the power dissipation constant during a linearity test.

2) The technique of mistuning the torque coil to improve linearity should be examined in some detail, particularly as it relates to the stability and reliable operation of the torque-to-balance electronics. The shape of nonlinearity induced in a good unit for variations in the resistor and capacitor should be mapped. In addition, a more general program to reduce torque-scale-factor nonlinearity should be developed.

3) The compensation of gyro time constants should be considered for all new designs. Testing it in a binary delta modulator and in a forced binary loop is recommended.

4) The design of a high speed H Switch is recommended to investigate the possibilities of ultra high interrogation rate pulse torquing.

SECTION 3.0
ANGULAR OSCILLATION TESTS

by
Charles B. Lory

3.1 INTRODUCTION

3.1.1 Purpose

The purpose of these tests is to measure the apparent average input rate of rotation indicated by a pulse-rebalanced gyroscope when the gyro case is oscillated angularly about any two of its principal reference axes. In order to demonstrate the integrity of the equipment and procedures, similar tests with the torque loop open are measured and compared to existing theory.

As a secondary item, tests were included to measure the open-loop transfer function of the same gyroscope when forced by a single-axis angular oscillation. Such tests help evaluate the predictive value of several float and spin-bearing compliance models which have been advanced.

3.1.2 Background

Three problems beset the analysis of the gyro dynamics studied here.

1. If the simplest model of the gyro which seems adequate produces equations which cannot be solved in closed form, how can one best seek useful solutions?
2. What constitutes a "useful" property or solution.
3. How complex a model is adequate?

The main purpose of our tests centers around the first two problems above. Interest in two-axis oscillations from the system designer's point of view concentrates on the lower frequencies where the classic assumptions for a single degree-of-freedom integrating unit would seem adequate. If the unit is pulse-rebalanced, however, the resulting output-axis equation is still a mathematical challenge. (See, e.g., assumptions by Schneider,[4] p. 19 and his resulting Eq. (2-12), p. 22.) Direct testing or point-by-point numerical solution of the output-axis equation are the available ways of erradicating some of ones ignorance. Since specification of a useful solution is part of the problem, there has been little guidance as to what to test.

Single-axis, open-loop tests are included in an effort to discriminate between models of varying complexity. One of the classic simplifying assumptions is that the wheel spins in a perfectly rigid bearing and float structure. Weinstock,[5] and Weinstock and Marchese[6] relaxed the assumption to a constant, symmetric compliance between wheel and float about the input and output axes. They solved for the open-loop, single-axis responses and for the apparent time-average input rate with two-axis oscillations, again open-loop. This model was extended to a non-constant compliance by Schneider (op. cit., pp 23-26), specifically to the Honeywell gas-bearing gyro tested here. He estimates gas-bearing stiffness as proportional to rate capability versus frequency, solving with a shifting apparent resonant point as the excitation frequency changes.

3.1.3 Scope of Work

Most of the work reported here is experimental. This fact is in keeping with the contract and, furthermore, is consequent to the infant state of analytical solutions. Thus the two-axis average-rate tests started as a broad scan, articulating all combinations of axes over a range of frequencies for several phase shifts. Until the resulting data acted as a catalyst to someone's imagination, one could only check data by its consistency and continue to scan.

This report provides an initial analytic breakthrough enabling prediction of some data. The assumptions and results will be given in Section 3.2 below. Limited in usefulness as these are, they illustrate that this work must include intuition if progress is to be made.

Single-axis, open-loop tests were run first. This was not done to study wheel-to-float compliance models in any depth. Indeed, Sher and Weinstock[7] have shown the need for a rather powerful high-frequency angular vibration for that task. Rather the tests serve to make sure that compliance effects do not affect the gyro at more moderate frequencies. Such conservatism is recommended by lingering doubts as to the applicability of some of the theory. High frequency response at low amplitudes was obtained in hope that some useful hints might transpire.

3.2 PREDICTED RESULTS

3.2.1 General

The general mathematical problem in the single-degree-of-freedom integrating gyro is well illustrated by the classical form of output-axis equation as derived by

Schneider for the GG334A gyro. He obtains

$$I_{OA}\ddot{A}_{OA} + C_{OA}\dot{A}_{OA} = H_s W_{IRA} + M_{tg} - I_{OA}\dot{W}_{ORA} + A_{OA}\left[(I_{SA} - I_{IA})(W_{IRA}^2 - W_{SRA}^2) - H_s W_{SRA}\right] + (I_{SA} - I_{IA}) W_{IRA} W_{SRA}. \quad (3.1)$$

His symbols and others used here are included in the definition of symbols in the front matter. Note the distinction between case motions about case reference axes and the float motions (with respect to the case) about its principal axes. The W's represent, for the body-mounted gyro, the independent angular forcing functions supplied by the environment, expressed in case reference coordinates.

The linearity of this equation depends on the character of the applied output-axis torque between float and case, M_{tg}. If this term is independent or is a linear function of A_{OA} (and its first two derivitives) the equation is linear, albeit with a time-dependent coefficient of A_{OA} for non-constant forcing functions. Schneider (op. cit., p. 44) observes that for two-axis sinusoidal forcing functions this has no known general solution. He follows Weinstock (op. cit.) in obtaining a series solution by iterative approximations. (These solutions are not of direct interest to us here except to note that quadrature-phase, low-frequency oscillations about SRA and ORA, which produce an IRA cone, were used as a calibration input.) Such techniques depend for rapid convergence on relatively small values of the A_{OA} term. When the float is pulse rebalanced, the term M_{tg} is a discontinuous, sampled function of A_{OA} and its derivitives (and, in the case of gyro lag compensation, on the past history of M_{tg}). The equation is still linear within intervals of fixed command, but the value of the command-torque is a nonlinear function of the system state at the last sample time. Worst yet, mode patterns of the controller can interact, possibly regeneratively, with cross-coupled torque if it is strong.

Nevertheless, one can see at least a vague general guide for seeking analytic solutions. First, understand the control of command torque intimately. Next choose sets of conditions corresponding to some test or proposed environment. For each set, see if the sizes of the terms in Eq. (3.1) can be estimated without actually solving the equation. Finally, study these for helpful approximations. One such approximation has been found in this program. It is described in Section 3.2.4.2 below as the IRA-dominate case.

3.2.2 Anisoinertia and the Wheel

The wheel of a gyro has long been observed to "hunt" about synchronous speed at a low frequency. This is easily understood. The wheel is driven by a hysterisis

motor which, being non-salient pole, produces torque proportional to the sine of the so-called torque angle. This is the angle between the rotor field and the rotating armature field measured in electrical degrees. Over reasonable displacements, the sine is quite linear and one can picture an inertia controlled in mechanical phase with respect to the armature field by a linear spring. This system has an undamped natural frequency of

$$f = \frac{1}{2\pi}\sqrt{\frac{K}{I_{W,SA}}} \qquad (3.2)$$

where K is the stiffness of the motor in torque per unit mechanical angle and $I_{W,SA}$ is the inertia of the wheel about the spin axis. This natural frequency is typically in the range from one to five Hertz for gyros such as the GG334A.

The significance of the wheel hunt here is its effect on anisoinertia. The actual torque on the float about the spin axis due to the wheel inertia is limited to that which the motor torque can transmit. As noticed by Gelb and Sutherland,[8] this means that the wheel phase fails to accelerate with the float above the hunt natural frequency. Obviously this means the motor torque acting on the float is negligible compared to the inertial reaction torque which would occur if the wheel were rigidly fixed. Thus a good approximation of the anisoinertia term for the frequencies tested here (10 Hz and above) is

$$(I_{F,SA} - I_{IA})\,W_{IRA}W_{SRA} \qquad (3.3)$$

rather than that shown in Eq. (3.1). For the GG334A, this gives a difference of inertias of -57 gm-cm^2 rather than +23 gm-cm^2. Schneider took note of the change in high frequency anisoinertia (op. cit., p. 38), but unfortunately used +23 gm-cm^2 in his results at all frequencies (ibid, pp 68-69).

3.2.3 Open-Loop Theory

With the exception of the anisoinertia term just discussed, Schneider's application of theory to angular oscillations of the Honeywell GG334A are taken as the predicted results for open-loop operation. In each case, his "ideal" gyro responses are shown, i.e., those without account for wheel-to-float compliance.

3.2.4 Closed-Loop Theory

3.2.4.1 General. For practical application, Eq. (3.1) seems sufficient to describe the indications of a single-degree-of-freedom integrating gyro subjected to two-axis

C.2

angular oscillations. For pulse rebalancing, however, no general method for getting even approximate closed-form solutions has been found.

A few general observations about Eq. (3.1) will help in understanding its nature.

1. The anisoinertia term, $(I_{SA} - I_{IA})\, W_{IRA}\, W_{SRA}$, is not influenced by float output angle. A dc drift will therefore occur whenever W_{IRA} and W_{SRA} have in-phase components, regardless of the rebalance technique.
2. The term $(I_{SA} - I_{IA})\,(W_{IRA}^2 - W_{SRA}^2)$ will contain a dc term and a double frequency term due to the squaring. It will then not give an average value when multiplied by A_{OA} unless the pulse rebalancing introduces double frequency terms into the float angle. Anyway, it is small compared to $H_s\, W_{IRA}$ for the tests reported here.
3. The major source of difficulty in the equation is in the term $-A_{OA}\, H_s\, W_{SRA}$. The problem is severe when this term is one of the major torques other than rebalance torque. In that case, a rebalance pulse is initiated by the action of cross-coupled torque. The pulse then changes the float angle, A_{OA}, and therefore changes the cross-coupled torque. This interactive system is made all the more difficult to characterize when IRA and ORA rates are simultaneously present.

3.2.4.2 The IRA Dominant Case. Let us proceed to analyze the pulse-rebalance case for which an approximate solution can be found. Suppose the control of pulses is dominated by the input precession torque, $H_s\, W_{IRA}$. This means that the float position is controlled as if only IRA rates were applied. Then modest SRA rates, and the resulting cross-coupling and anisoinertia, would contribute only a dc perturbance without significantly affecting the float angle. For quasistatic input rates, the time average float angle for the compensated loop considered here is[9]

$$A_{OA} = \frac{H_s T W_{max}}{10\, C_{OA}}\, \text{signum}(W_{IRA}) + \frac{H_s}{C_{OA}}\left[T + \sum_{i=1}^{n} (\tau_i)\right] W_{IRA} \qquad (3.4)$$

where the signum function is defined as

$$\text{signum}(x) = \begin{cases} 1, & x > 0 \\ 0, & x = 0 \\ -1, & x < 0 \end{cases} \qquad (3.5)$$

and where the summation is taken over all time constants (such as the float time constant and the torque coil L/R) in the interrogated signal response to commands of torque. This was perceived to apply to sinusoidal inputs if there is a large number of pulses per oscillation cycle and if the interrogate period, T, is short compared to the oscillation period.

One can now consider the inputs

$$A_{SRA^*} = a \sin(\omega t) \tag{3.6}$$

$$A_{IRA} = c \sin(\omega t + \epsilon) \tag{3.7}$$

where "c" is much larger than "a" to meet the required approximations. The SRA* is the outer gimbal axis, which aligns with the SRA at zero inner gimbal angle. Thus

$$A_{SRA} = A_{SRA^*} \cos(A_{IRA}) \approx A_{SRA^*} \tag{3.8}$$

for small angles. We then have the input rates

$$W_{SRA} = a\omega \cos(\omega t) \tag{3.9}$$

$$W_{IRA} = c\omega \cos(\omega t + \epsilon) \tag{3.10}$$

If one divides Eq. (3.1) through by H_s, each term on the right-hand side except the command torque can be interpreted as a contribution to equivalent input rate, W_D. This rate, then, is made up of all terms which are measured as input, whether or not they are caused by IRA rotations. For the inputs now under discussion, only the terms having a nonzero time average are included, giving

$$W_D = - A_{OA} W_{SRA} + \frac{I_{F,SA} - I_{IA}}{H_s} W_{IRA} W_{SRA} \tag{3.11}$$

For compactness, let us express Eq. (3.4) as

$$A_{OA} = K_1 \text{ signum}(W_{IRA}) + K_2 W_{IRA}. \tag{3.12}$$

Substituting into Eq. (3.11) and carrying out the time average operation on each term, one obtains

$$W_D = \left[- \frac{2}{\pi} K_1 a + \left(\frac{I_{F,SA} - I_{IA}}{H_s} - K_2\right) \frac{a c \omega^2}{2} \right] \cos(\epsilon) \tag{3.13}$$

as the apparent input rate for simultaneous IRA-SRA rates.

For the GG334A in the compensated pulse rebalance loop we have

$$K_1 = 2.9 \times 10^{-6} \text{ radians}$$

$$\frac{I_{F,SA} - I_{IA}}{H_s} = -285 \times 10^{-6} \text{ seconds}$$

$$K_2 = 246 \times 10^{-6} \text{ seconds}$$

The factor K_1 is sufficiently small that the term proportional to ω can be neglected, giving

$$W_D \approx \frac{1}{2}\left(\frac{I_{F,SA} - I_{IA}}{H_s} - K_2\right) a\, c\, \omega^2 \cos(\epsilon). \qquad (3.14)$$

This can be conveniently normalized by dividing through by $(a\, c\, \omega^2)$, the product of the peak applied velocities. However, one must be careful to remember that, whether or not normalized, this approximation only applies for the conditions specified in its derivation.

3.3 TEST EQUIPMENT

The test equipment consists of a gimbaled vibration fixture, gimbal-angle servomechanisms and read-outs, safety circuits, gyro-support electronics, and general support electronics. Each of these items is described below. Considerable savings were achieved by maximum use of existing government-owned equipment, especially in the use of an Apollo guidance gimbal system for the vibration fixture. Only such items as the gyro mounting fixture, the specialized gimbal-readout demodulators, and the safety circuits needed to be designed and built for the tests.

> NOTE.—The detailed description of the test equipment will not be of interest to all readers. Those who feel they can understand the data without this background should skip to Section 3.4. A glance at Fig.'s 31 and 32 first will help in understanding the general organization of the oscillation drive and readout.

3.3.1 Vibration Fixture

The vibration fixture was made by using the housing, gimbals, torque motors, resolvers, slip rings, and wiring from a prototype Apollo Block I inertial measurement unit (IMU). Its housing and gimbals are made of hydroformed portions of a sphere brazed to machined mounting flanges. These aluminum parts are light, but due to spherical shape and careful stress relief they are rigid and dimensionally stable. Each of three axes of freedom is connected by two intergimbal assemblies, one at

each end. An intergimbal assembly consists of two close-tolerance ground beryllium members held together by a precision duplex ball bearing. Each gimbal end mounts a slip-ring assembly, a dc torque motor, and at least one resolver. At one end of each axis, the resolver is a sixteen-speed transmitter having a peak error of 20 arc sec. At the other end, a three-minute one-speed resolver transmitter is located. One of the one-speed resolvers was rewired as a control transformer to better utilize available angular control equipment.

To utilize the inertial measurement unit parts as an angular vibrator, two major changes were made. First the inner-most gimbal, which was the stabilized platform, was discarded. It was replaced by a machined aluminum member designed to mount just a GG334A gyro. Second, since only two degrees of freedom were required and the gimbals provide three, the outer gimbal was held by a clamp which could immobilize it at any cardinal point. The resulting vibration fixture is shown partially assembled in Fig. 30. In the center, the gyroscope can be seen clamped in the aluminum fixture. The screw with the large knurled knob is used to adjust the gyro case about its ORA prior to tightening the clamp screws, after which it can be removed to retain dynamic balance. The small board of electronics at the right is the signal-generator preamplifier. At each end of the center aluminum member is an intergimbal assembly for the inner axis, at the top and bottom of the picture are the intergimbal assemblies for the middle axis, and those for the outer axis are seen mounted in the case on the left and right. To help maintain close temperature control of the gyro, the inner member which mounts it is provided with a thermistor for sensing and two heating elements.

The design and performance capabilities of the vibration fixture have been reported in considerable detail in Ref. 4, Sec. 3 and Ref. 12, Chap. 3 and 4.

3.3.2 Gimbal-Angle Controller

The gimbal angle control system consists of two servomechanisms, position commanded by the two outputs of a variable-phase oscillator. The system is illustrated in Fig. 31 for one axis. Gimbal angle is measured with a one-speed resolver. The desired static (or average) angle is commanded by the setting of the resolver bridge. The output of the resolver and bridge operating as a transmit-receive pair, is proportional to deviation from the static setting. After demodulation with respect to the 3200 Hz reference signal, this difference is compared with the ac command from the variable-phase oscillator. The difference is amplified to drive torque motors at each end of the gimbal axis.

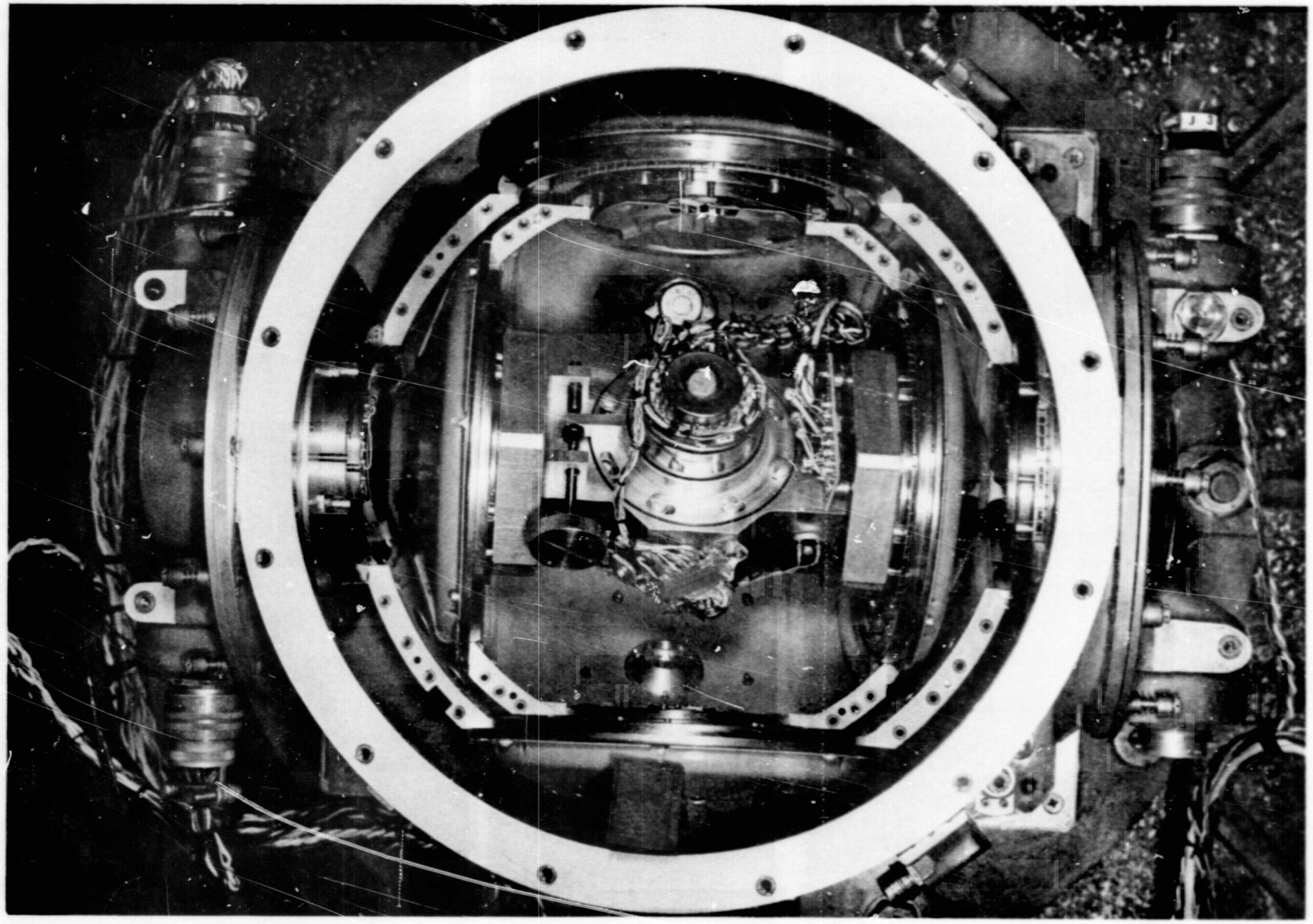

Fig. 30. Vibration Fixture with Half of Each Gimbal Removed to Show the GG334A Gyro and Its Mounting

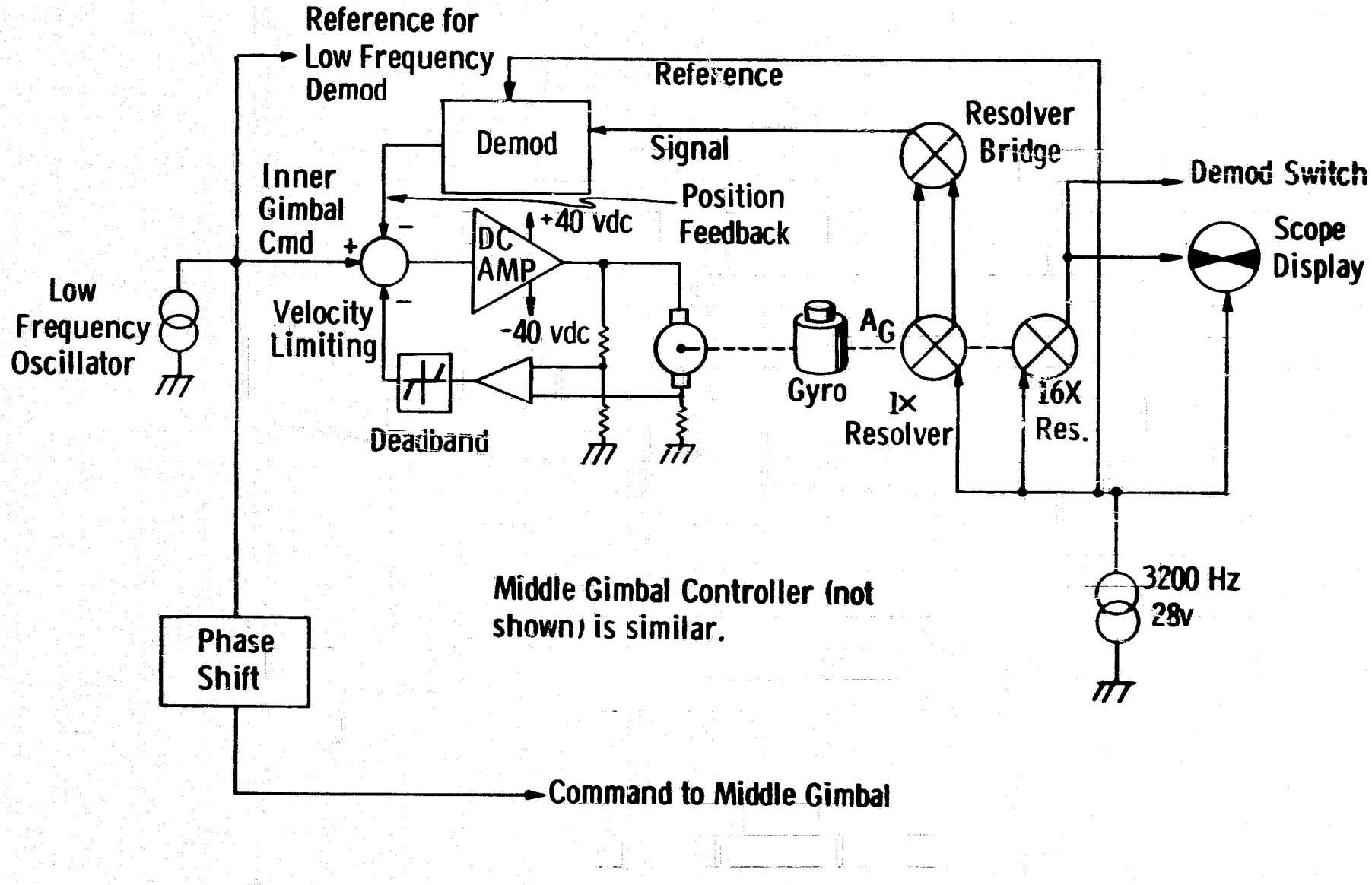

Fig. 31 Gimbal-Angle Control Mechanization

When the control system described is combined with the modified IMU, a two-axis angular vibrator of considerable flexibility and power is formed. The gryo can be driven at its maximum rebalance rate (1.05 radians per sec.) up to about 40 Hz. Float motion greater than the quantizer dead zone is achieved out to 200 Hz. Open-loop transfer functions are obtainable up to 600 Hz. There is no low-frequency limit on operation: In fact the system can even be modified to provide slew rates.

The stabilization loops designed for the gimbals have excellent compensation, achieving stable performance with high static accuracy. The electronics, however, were all potted, cordwood assemblies which could not easily be adapted for use here. Instead, ground support gimbal electronics, which are open on circuit boards, were used. The ring demodulators were replaced with a FET-switch design having linear response over a much wider amplitude range. Also, the voltage supply to the output stages was raised from ±28 Vdc to ±40 Vdc, the highest value the output transistors could handle. The poor response provided by these electronics was improved to an acceptable level by improving the lead-lag compensation. The resulting performance is only adequate, but gives safe control at all frequencies of interest.

3.3.3 Gimbal-Angle Readout

Since all tests are run with the gimbal angles at cardinal points (see Section 3.4.1), the oscillations take place about nulls of the sixteen-speed resolver sine outputs. The motion is measured as in Fig. 32, which illustrates a scheme of double demodulation. The first demodulator and filter, which removes the carrier frequency, was designed and built especially for the task. Its output is measured by the second demodulator and filter, a commercial phase-angle voltmeter using one phase of the low-frequency position command as its reference signal. At frequencies below ten Hertz, this voltmeter must be replaced by a phase-sensitive demodulator and a chart oscillograph.

The carrier-frequency demodulator is made entirely of integrated circuits. A panel switch first chooses unity or ten-to-one resistive attenuation. The signal is then buffered and amplified by one, ten, or 1000. The reference switches a FET demodulator. The resulting signal is smoothed by a fourth-order active Butterworth filter having a cutoff frequency of 1460 Hertz. This phase shifts the envelope information in degrees by 10% of its frequency in Hertz over all frequencies used here. Since the same circuit is switched to measure both gimbal motions as well as the gyro response, the phase shift is not significant. Care was taken, however,

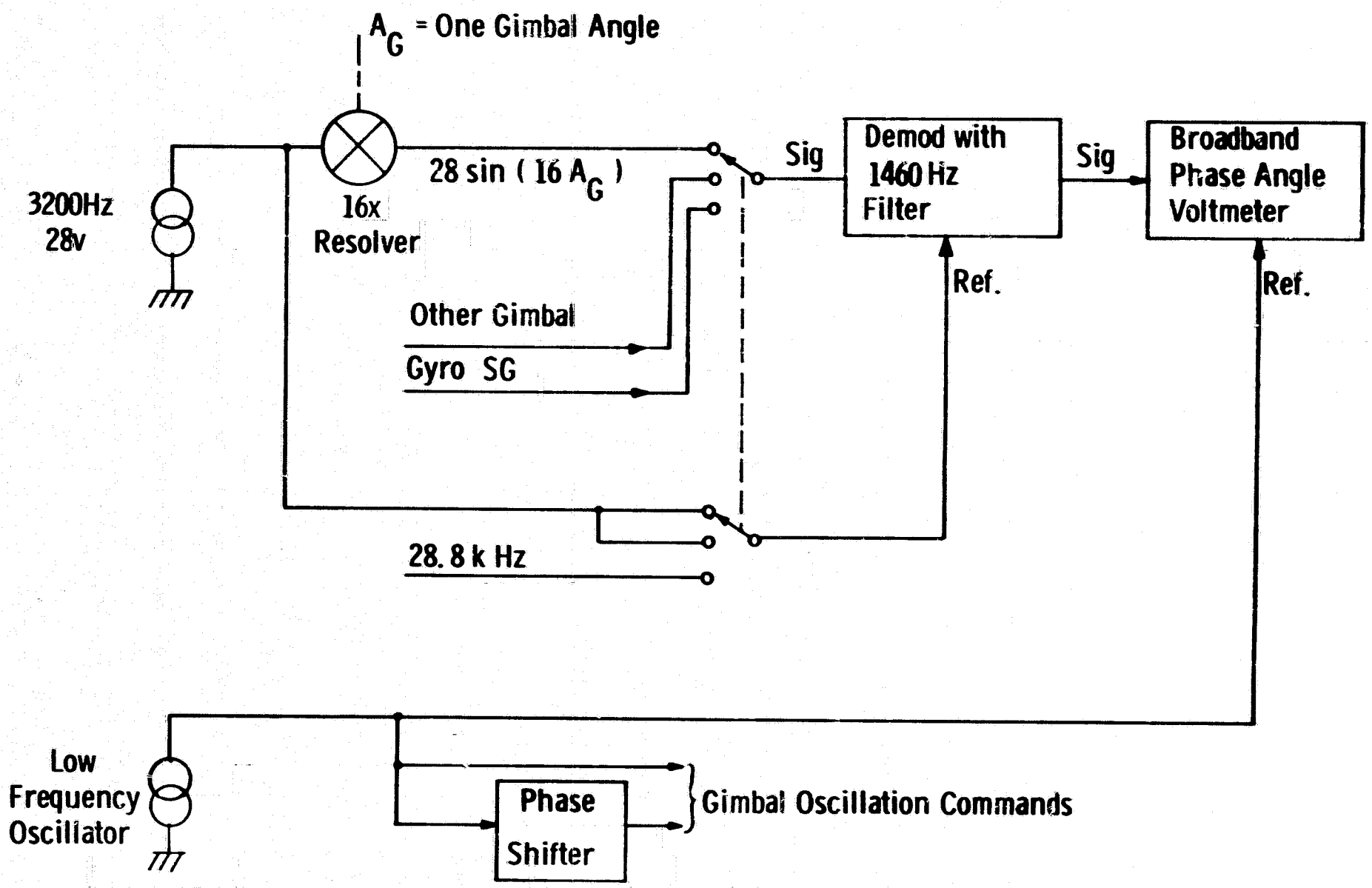

Fig. 32 Gimbal Oscillation Measurement Mechanization

to run most of the tests with ten times as large a motion on the inner axis as on the middle (which has about ten times the moment of inertia to move). By appropriate setting of the 10:1 attenuator, the signal level was kept similar within the measuring circuitry for each axis; this minimizes the most important measurement error, that from relative phase shift between the motions.

3.3.4 Safety Circuits

The principal purpose of the safety circuits is to reduce the probability of applying gyro rates in excess of the gas bearing capability. One type of circuit is used to control rate by velocity feedback to the servo. This circuit shows in Fig. 31 where a bridge circuit derives a signal proportional to torque-motor EMF. If this exceeds the breakdown voltage of a pair of zener diodes, strong velocity limiting is introduced into the loop. The remainder of the safety circuits limit rate by disabling the servos if various signals exceed preset limits or if essential excitations are not present. Disablement is by simultaneous disconnect of the servo power amplifier 40V supplies. The following conditions trigger and latch the disablement:

a. Excess rate as sensed from the back-EMF circuit mentioned above. This circuit is active at all times independent of the control usage of the signal. (The control usage is introduced only during gimbal slewing.)
b. Large signal amplitude on the one-speed resolver control nulls. This detection is disabled in the slew mode.
c. Failure of the +28 Vdc supply, which powers the safety circuits.
d. A drop below 25V of the 28V, 3200 Hz supply voltage.

In addition, deviation of either temperature controller by more than ±1 F sounds an alarm and disables the wheel supply.

3.3.5 Gyro-Support Electronics

The support electronics for the gyro are rack-mounted items of more or less standard design in quality gyro testing. Included are all circuits needed to operate the gyro except the clock and pulse-torque electronics. These are:

a. A dual temperature controller. One half heats the gyro to its operating temperature while the other assists by heating the mounting structure to about 10F cooler.
b. A two-phase, 800 Hz, 26V wheel supply.
c. A 28.8 kHz, 5V signal generator primary excitation supply.
d. A precision direct-current supply for the second torque coil.

3.3.6 General Support Electronics

In the category of general support electronics are ac and dc power supplies plus oscilloscope monitors. The power supplies provide needs such as the resolver excitation and the variety of regulated dc voltages required by the pulse-torque electronics and the various support electronics.

3.4 TEST PROCEDURES

> NOTE.—The reader who is not interested in procedures in detail should read only Sections 3.4.1 and 3.4.5. The former gives a guide to the table and illustrations describing test positions. Section 3.4.5 contains the closed-loop, two-axis procedures: it should probably not be skipped if the important aspects of the associated results are to be properly understood.

3.4.1 Test Positions

The test positions were selected to keep the input axis of the gyroscope parallel to the earth's polar axis for all tests. In this position, the earth rate component along the IA is almost constant. Earth rate and the static drift can be nulled prior to applying test oscillations using direct current in the second torque winding. The positions then provide the capability of oscillating all possible pairs of axes from among the input-, output-, and spin-reference axes.

All of the positions used are summarized in Table 8 and illustrated in detail in Fig.'s 33 through 39 inclusive. To achieve these positions, the IMU case was positioned with its -Z axis ($-Z_{nb}$) along the polar axis and its X axis horizontal and west as shown in Fig. 33. Note that Apollo nomenclature has been retained for all coordinate axes and gimbal angles. Thus case coordinates are subscripted "nb" for Navigation Base, and gyro-holding-fixture coordinates are designated "sm" for Stable Member. The triads are colinear in X, Y, and Z respectively when all gimbal angles are zero and, from this position, positive gimbal angles result if the case is rotated clockwise with respect to the gyro when looking in the +X, +Y, and +Z directions. To drive all pairs of gyro axes with the inner and middle IMU axes, the gyro must be able to mount with either the IRA or the SRA along $-Y_{sm}$ as shown in Figs. 34 and 35 respectively. Even though the same two axes are articulated, position 1a and 4a are both used; because the middle axis accelerates about ten times as much inertia as the inner, widely different test conditions are thus achieved.

Table 8 Gyro Test Positions - Option A

POSITION NO.	GYRO AXES	ALIGNMENT OF GYRO AXES			INNER GIMBAL ANGLE	MIDDLE GIMBAL ANGLE	OUTER GIMBAL ANGLE
		WITH EARTH	TEST FIXTURE	GIMBAL AXES			
1A	IA	POLAR	$-Y_{sm}$	-INNER	0	180	90
	OA	WEST	$-X_{sm}$	-OUTER*			
	SRA		$-Z_{sm}$	-MIDDLE			
2A	IA	POLAR	$-Y_{sm}$	-INNER	90	180	90
	OA		$-X_{sm}$	-MIDDLE			
	SRA	EAST	$-Z_{sm}$	-OUTER			
3A	IA	POLAR	$+Z_{sm}$		90	90	90
	OA		$-X_{sm}$	-MIDDLE			
	SRA	EAST	$-Y_{sm}$	-INNER			
4A	IA	POLAR	$+Z_{sm}$	-MIDDLE	180	90	0
	OA		$-X_{sm}$				
	SRA	EAST	$-Y_{sm}$	-INNER			

* Positive Gimbal Rotation Produces Negative Gyro Rotation

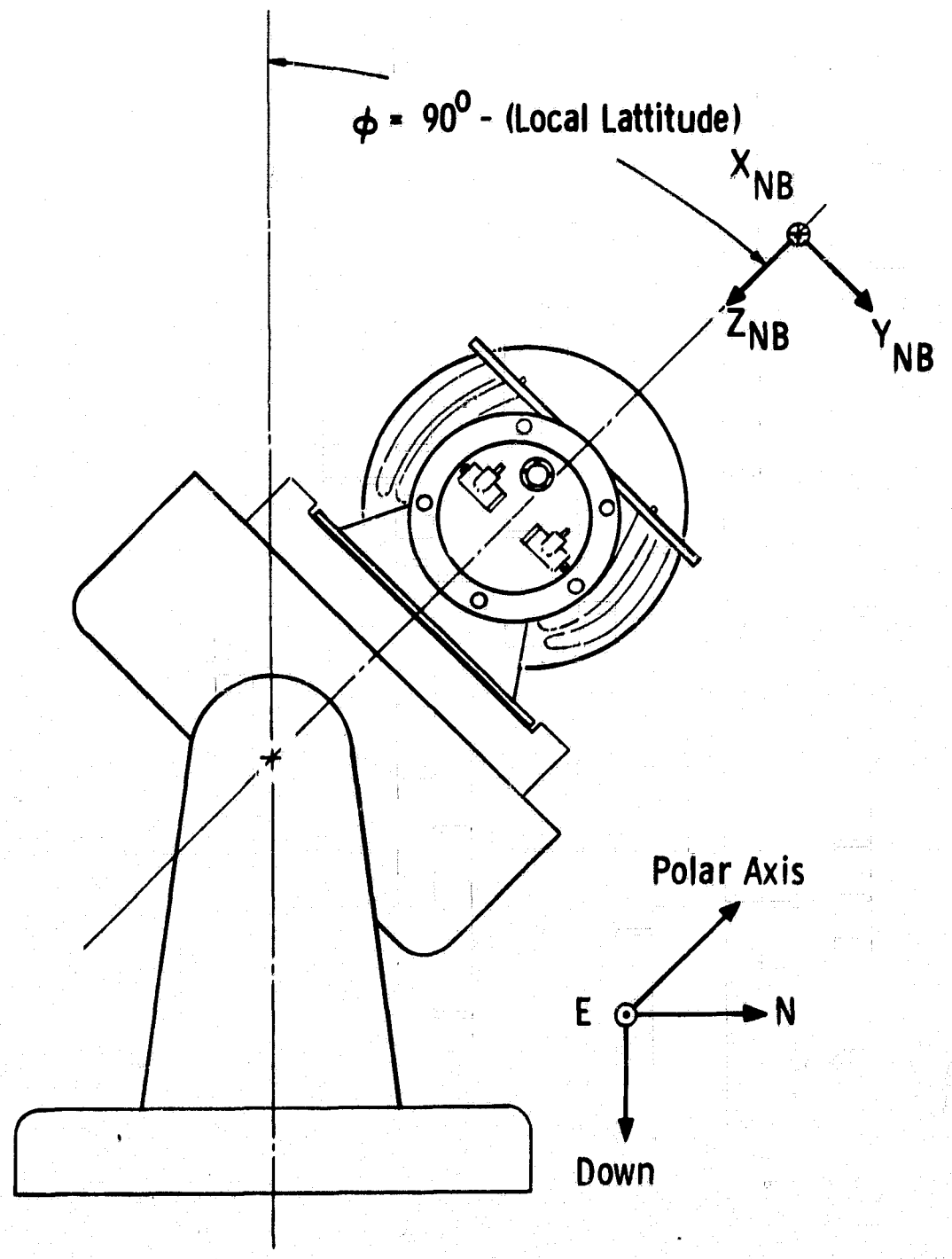

Fig. 33 IMU Position For All Tests

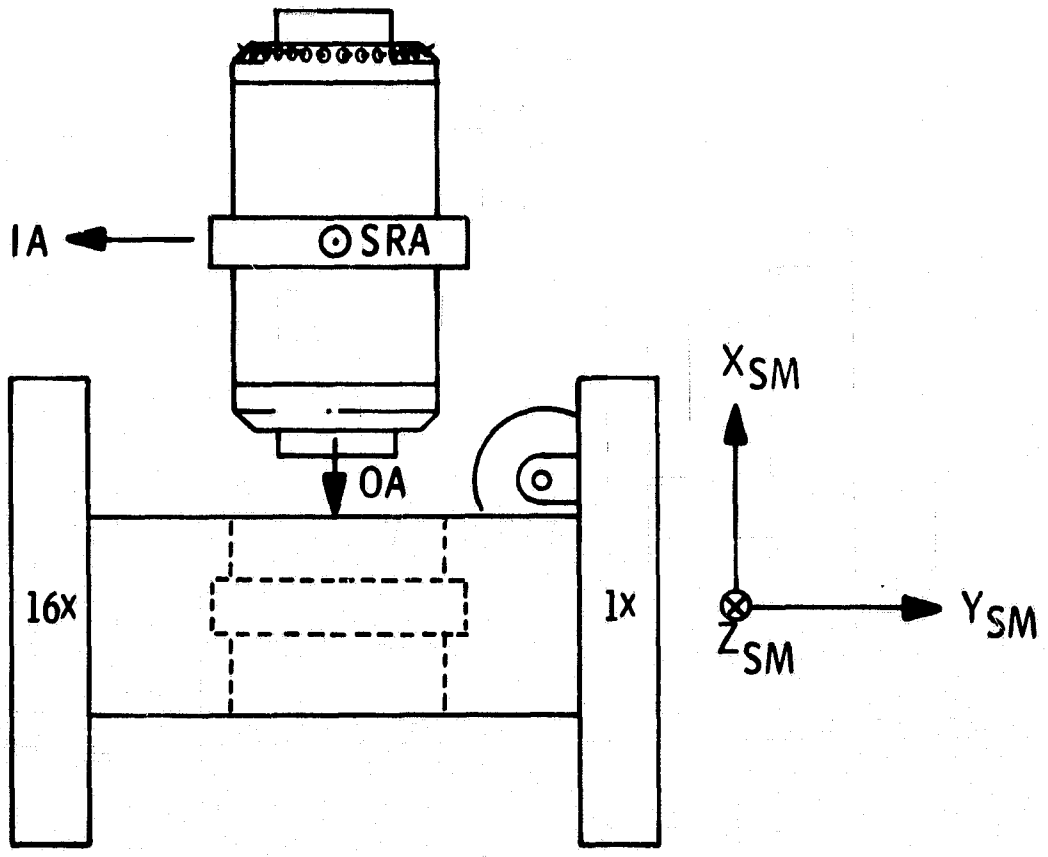

Fig. 34 Gyro Orientation For Positions 1 & 2

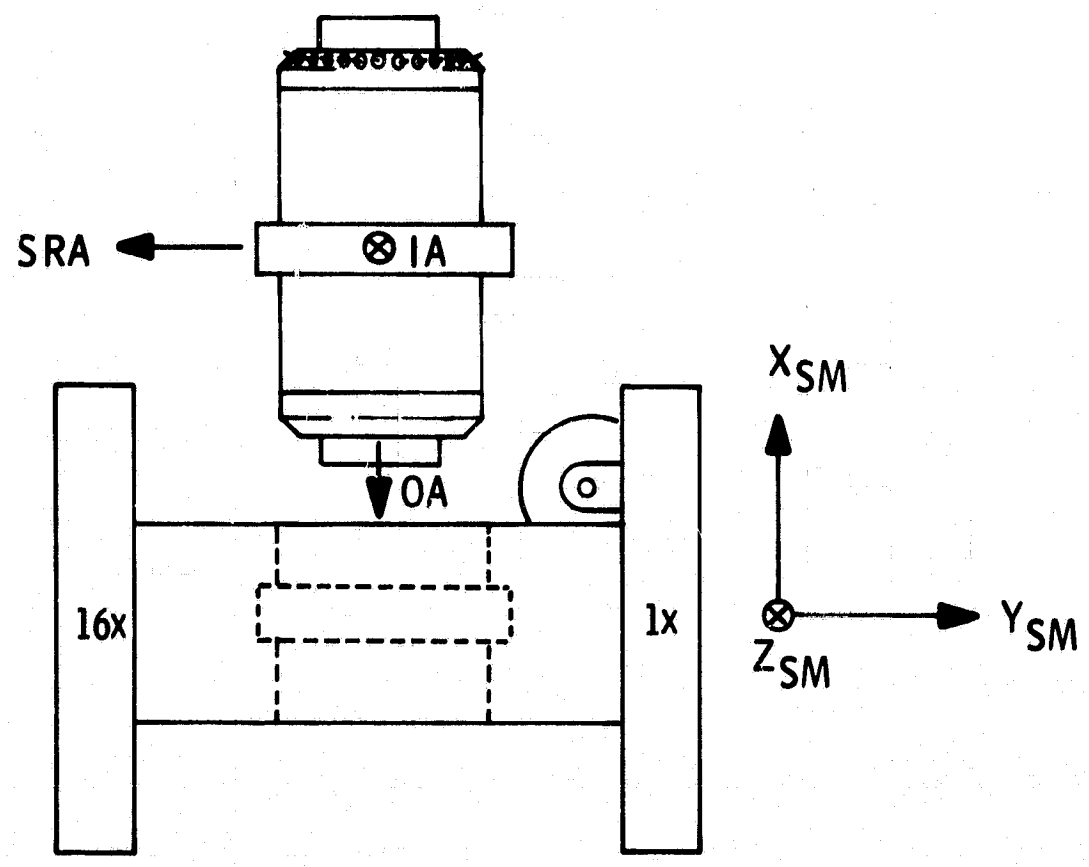

Fig. 35 Gyro Orientation For Positions 3 & 4

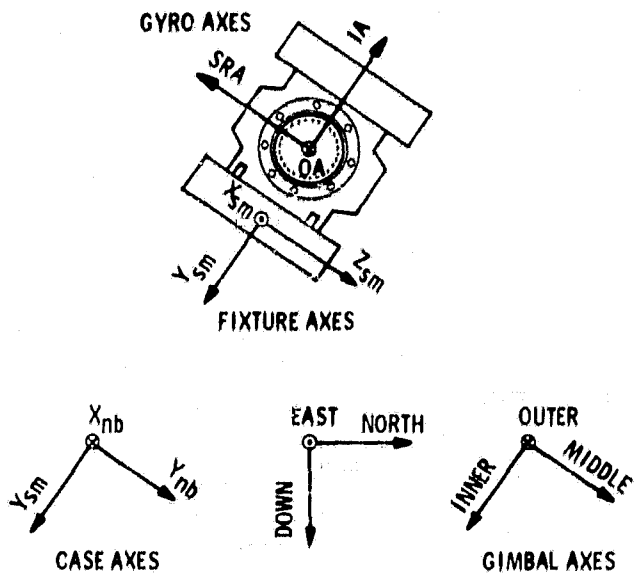

Fig. 36 Position 1A (Looking West)

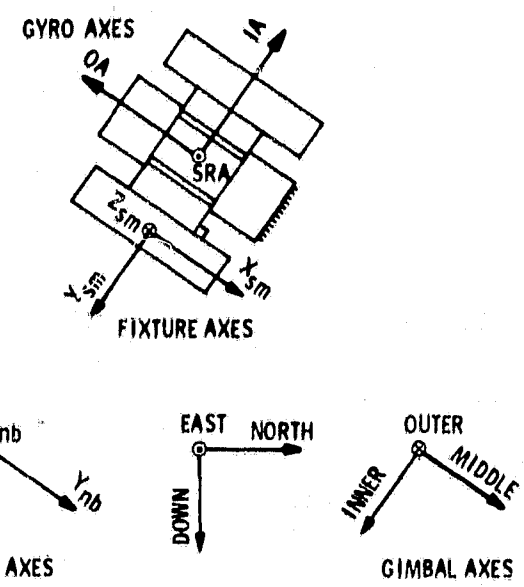

Fig. 37 Position 2A (Looking West)

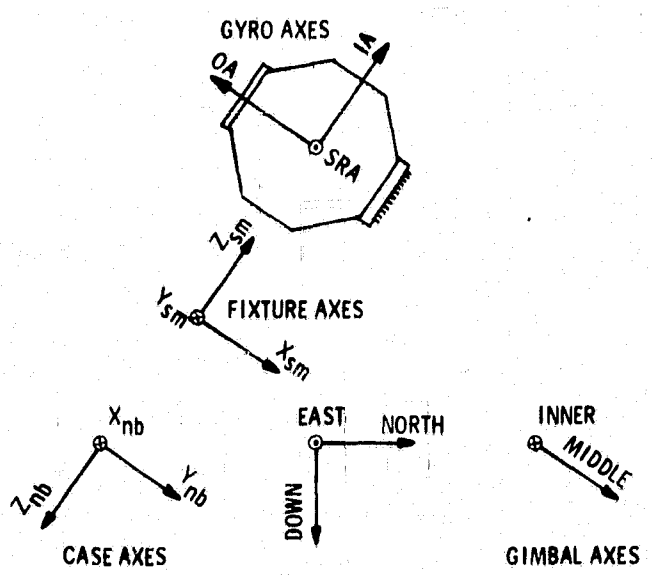

Fig. 38 Position 3A (Looking West)

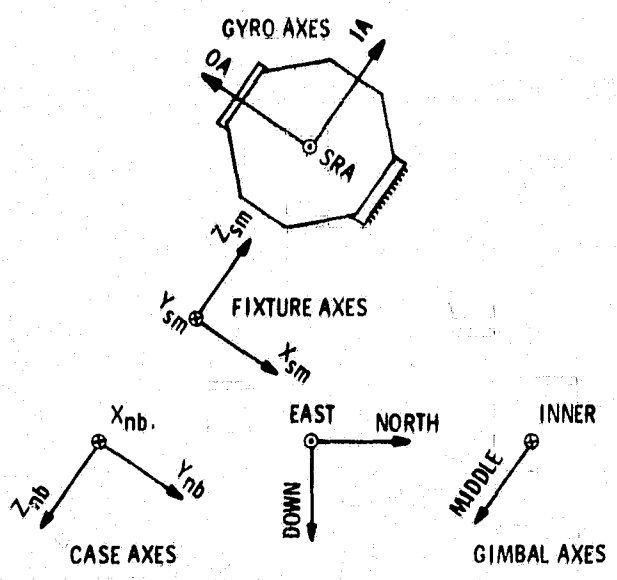

Fig. 39 Position 4A (Looking West)

3.4.2 Gyro Alignment

To achieve test positions 3a and 4a, the gyro must be placed with the input reference axis, IRA, orthogonal to the inner gimbal axis with high accuracy. This was accomplished by oscillating the inner gimbal at 10 Hz and rotating the gyro about its output axis until no oscillation could be observed in the gyro signal-generator output. Next, it is necessary to get the best possible alignment of the ORA with the middle gimbal axis for position 3a. This cannot be done exactly. Due to small machine tolerances in the inner element and gimbals, the middle gimbal axis will not lie in the ORA-IRA plane, which cannot be adjusted. However, by oscillating the middle axis in position 3b, the inner axis zero point was adjusted for no SG oscillation, giving the best alignment about SRA.

Alignment with the IRA along the inner axis to achieve test positions 1a and 2a is more difficult. A large oscillation at 10 Hz was commanded on the middle gimbal axis with this axis nominally along the SRA. The inner gimbal angle was carefully held at zero. Now two components of oscillation would be seen in the SG output: IRA inputs due to misalignment about ORA, and output axis coupling due to misalignments about IA. At 10 Hz, the IRA response lags the motion by just under two degrees while the output axis response leads the motion by over 88 degrees. The adjustment about ORA to get IRA orthogonal to the middle gimbal axis (which is the critical one) was accomplished by rotating until the SG oscillation showed no component at the phase of the IRA response.

3.4.3 Single-Axis Response Tests

3.4.3.1 ORA Driven. The response to oscillation about the ORA was measured in position 3a. The middle axis was commanded over a frequency range from 25 to 200 Hz with the torque loop open. The amplitude and phase of the middle axis and the SG output were measured for each frequency.

3.4.3.2 IRA Driven. The response to oscillation about the IRA was measured in position 1a. The inner axis was commanded over a frequency range from 10 to 640 Hz with the torque loop open. The amplitude and phase of the inner axis and the SG output were measured for each frequency. In the vicinity of local resonant peaking at 452 Hz, a number of closely spaced points were obtained.

3.4.4 Open-Loop Two-Axis Test Procedures

Two-axis angular oscillation tests were performed open loop for each test position except 2a. In each other position, in-phase and 90°-phase oscillations were

applied at octave steps of frequency from 10 to 160 Hz. Direct current from a precision supply was passed through torque coil No. 2 at each test point. The current was adjusted until no average float velocity could be observed. The difference between this current and the current required to oppose earth rate acting alone was used to calculate the equivalent input resulting from oscillation.

One important use of the open-loop two-axis tests was the end-to-end calibration of the gimbal-angle readout. Electrical measurement of the resolver voltage transmission ratios for the middle and inner axes showed equal sensitivity. Thus, the end-to-end sensitivity of the entire measuring system for both axes in volts per radian was obtained by measuring a large IRA cone at 10 Hz. The sensitivities were then calculated to make the data agree with the theoretical average IA rate generated by the coning motion. The only alternative method of obtaining end-to-end calibration would have been to disassemble the vibration fixture down to the bare inner gimbal assemblies. Those containing the 16-speed resolvers would then be set up on an angular indexing stand and the voltage output for standard angles would be measured. Calibration by the gyroscope response to a cone avoided the large time and expense which would have resulted from disassembly and indexing.

At the higher frequencies, only small oscillation amplitudes can be obtained. Due to the inability to identify zero float rate with high accuracy (especially when IRA is aligned with a driven axis, making the float follow any drift in average gimbal angle), the tiny equivalent input rates cannot be accurately measured. Such low confidence data were not included in that to be presented in Section 3.5.2.

3.4.5 Closed-Loop Two-Axis Test Procedures

The procedure for closed-loop two-axis angular oscillation tests is similar to the open-loop tests with some important exceptions:

1. The current in torque coil No. 2 was maintained throughout at the value required to oppose earth rate acting alone.
2. Testing was also performed in position 2a.
3. Tests with 90° phase shift were performed with both leading and lagging phase.
4. Data were first accumulated with only the IRA oscillation applied. The resulting apparent input rate was judged to represent plus-to-minus scale-factor difference. With two axes oscillated, changes from the plus-to-minus difference were interpreted as the significant equivalent input rate.

All tests were run with an interrogation rate of 14,400 pps. For many of the tests, separate answers were accumulated for a compensated and uncompensated loop; the differences, however, were not considered significant quantitatively in evaluating the benefits of the compensation. Hence, only results for compensated operation of the rebalance loop are to be presented.

Each test point was obtained as a fixed-time oscillation with separate accumulation of plus and minus $\Delta\theta$ pulses. To start, the gimbal axes were placed in the desired position. The dc in torque coil No. 2 was adjusted until a negligible net pulse count was accumulated over a period of 12 or more hours. Then the oscillations were commanded and adjusted in magnitude and phase until the desired motion was indicated by the measurement electronics. The oscillation command was then turned off; the gimbal angles were adjusted to the 16-speed resolver nulls; and, while maintaining this position, the $\Delta\theta$ counters were cleared and gated open. The oscillations were then commanded for exactly 300 seconds. After the command had ceased, the gimbal angles were again adjusted to the same nulls. (The stability of the 16-speed resolver nulls is better than a microradian, giving excellent repeatability of the initial and final position.) The readings of the two $\Delta\theta$ counters were recorded. Any resulting difference in the readings is the test result and contains negligible components of earth rate or fixture motion.

3.5 TEST RESULTS

Only test results will be given in this section. Since many of the important conclusions will arise from comparisons between different tests, all discussion of results is deferred to Section 3.6.

3.5.1 Single-Axis Responses

Two open-loop single-axis transfer functions were obtained, one with the IRA driven, one with the ORA driven. For oscillation about IRA, Fig. 40 shows the magnitude and phase of $(A_{OA})/(A_{IRA})$. When the oscillation was about ORA, the magnitude and phase of $(A_{OA})/(A_{ORA})$ as shown in Fig. 41 was obtained.

3.5.2 Open-Loop Two-Axis Test Results

The equivalent input rate for open-loop two-axis oscillations are plotted in Fig. 42. The results are normalized by the product of the oscillation amplitudes and plotted as a function of frequency. Note the excellent agreement between the data in position 1a and those in position 4a. Since the amplitudes of oscillation for

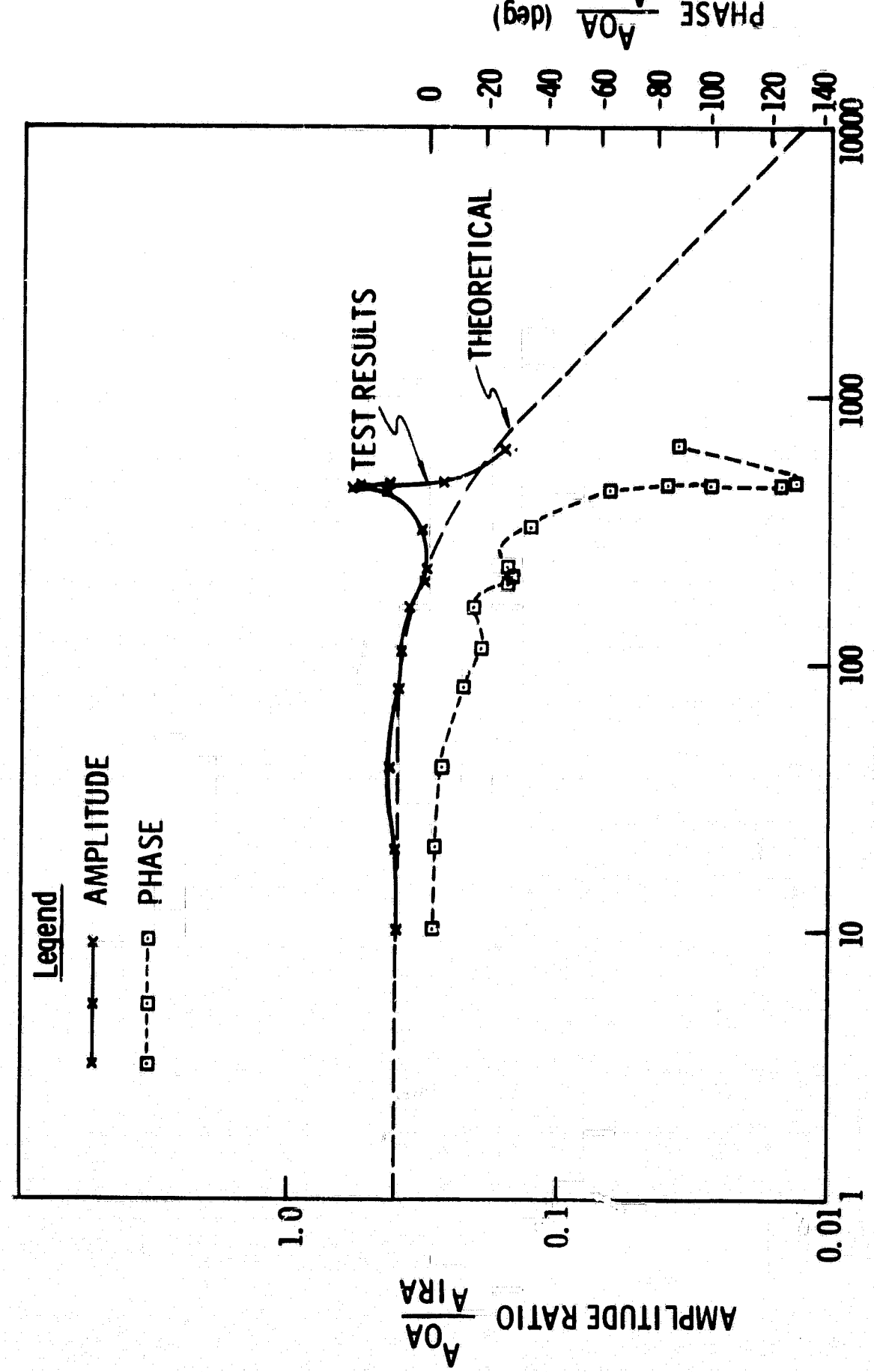

Fig. 40 Float Response to Sinusoidal Input Axis Case Motion GG334 Gyro

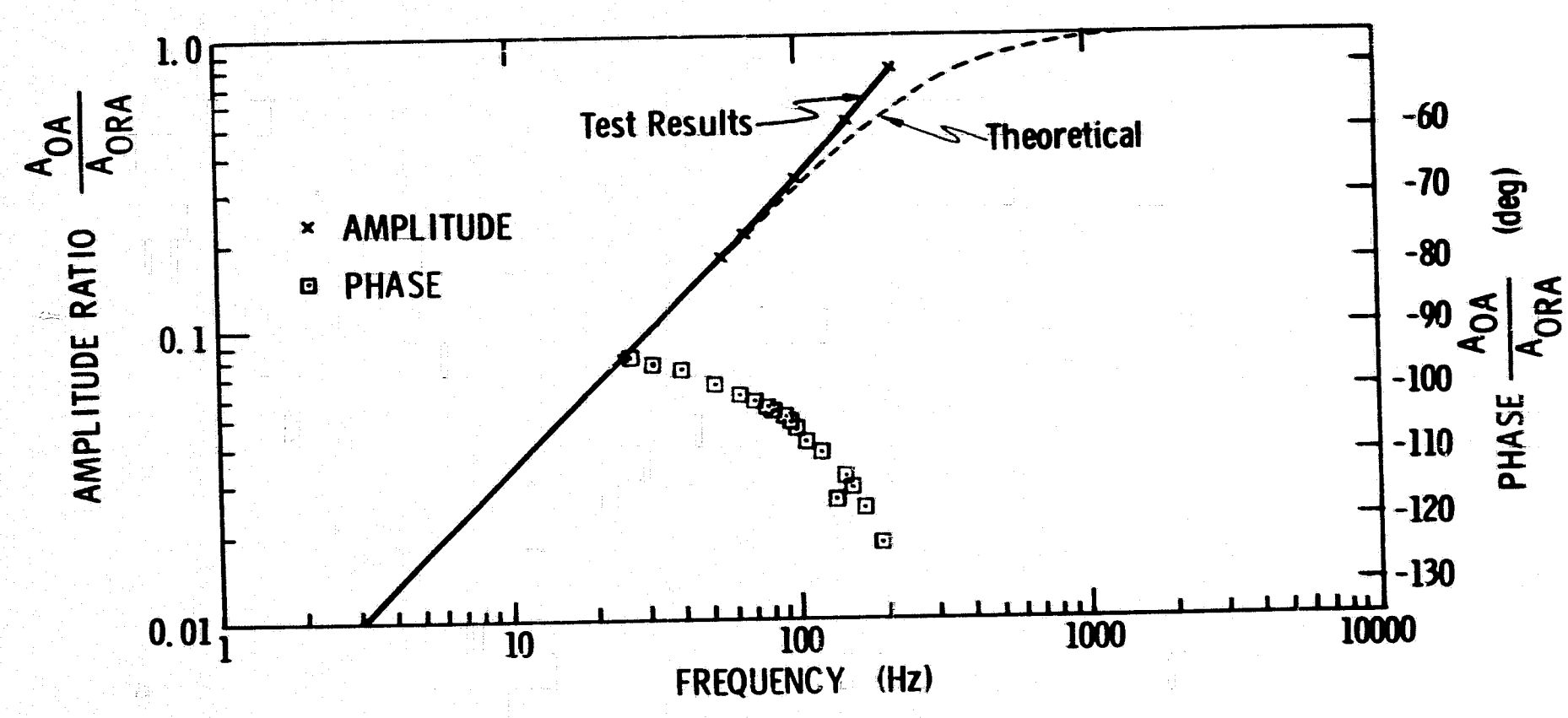

Fig. 41 Float Response to Sinusoidal Output Axis Case Motion GG334A Gyro

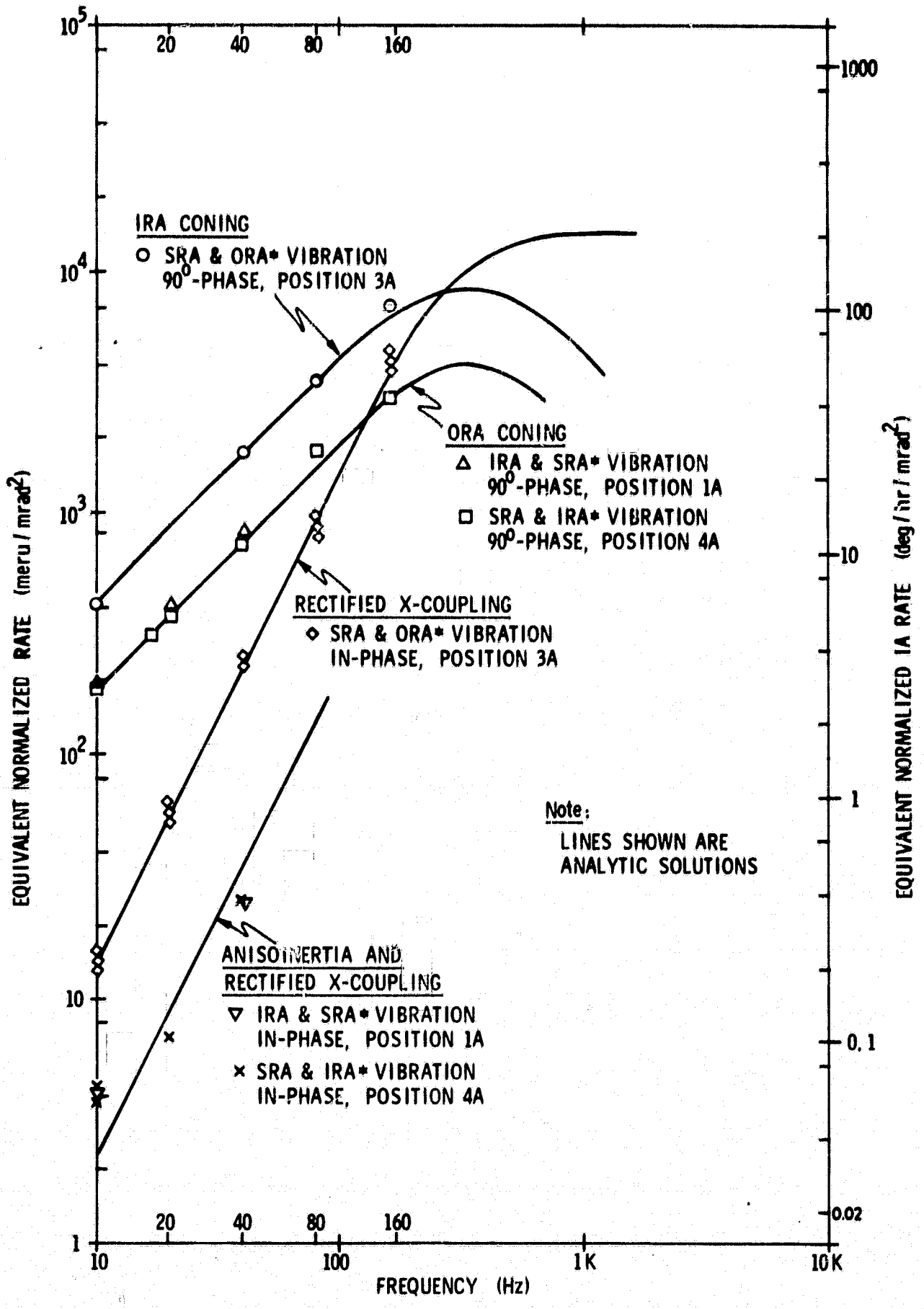

Fig. 42 Open-Loop Indicated Rate with Two-Axis Oscillations

a given gyro axis differ by a factor of ten between positions, the agreement in data verifies the linearity of the measurement electronics.

3.5.3 Closed-Loop Two-Axis Test Results

The equivalent, or apparent, input rate resulting from closed-loop operation during two-axis angular oscillations is shown in Fig. 43 through Fig. 50 inclusive. Experimental results for each position are shown with a data point at each frequency from 10 to 160 Hz in octave steps, shown on a logarithmic scale. Care must be taken to observe the vertical scales. Most are a logarithmic scale of IA rate, but several are linear and several others give IA rate normalized to the input peak velocity product.

3.5.3.1 Position 1a In-Phase Results. The equivalent IA rate as measured with in-phase IRA-SRA* oscillations (position 1a) is shown in Fig. 43 normalized to the input peak velocity product.

> NOTE.—An axis marked with a star, such as SRA*, is the outermore oscillated gimbal axis. This is aligned with the corresponding gyro case reference axis, but only when the inner gimbal angle is zero.

Also shown is a theoretical line, the normalized solution of Eq. (3.14). The peak IRA and SRA* rates applied as well as the amplitude of the IA expressed in pulses are also plotted. One should note the approximately constant rate inputs from 10 to 40 Hz, followed by approximately constant acceleration from 40 to 160 Hz. Since the same inputs were applied for position 1a quadrature oscillation and all position 2a oscillations, this input data will be omitted from the next two graphs. Note especially the high IRA rate attained at the lower frequencies.

3.5.3.2 Position 1a Quadrature Results. The equivalent IA rate is shown on a linear scale in Fig. 44, for the SRA* motion both leading and lagging the IRA motion by 90°. One sees that the ORA coning term evident in the open-loop data has been much attenuated but not entirely eliminated by the pulse restraint.

3.5.3.3 Position 2a Results. Apparent IA rate is shown in Fig. 45 for three phase relationships between the ORA* and IRA motions. The resulting rate scales are linear. These tests, which are run in position 2a, result in rocking or coning of the SRA.

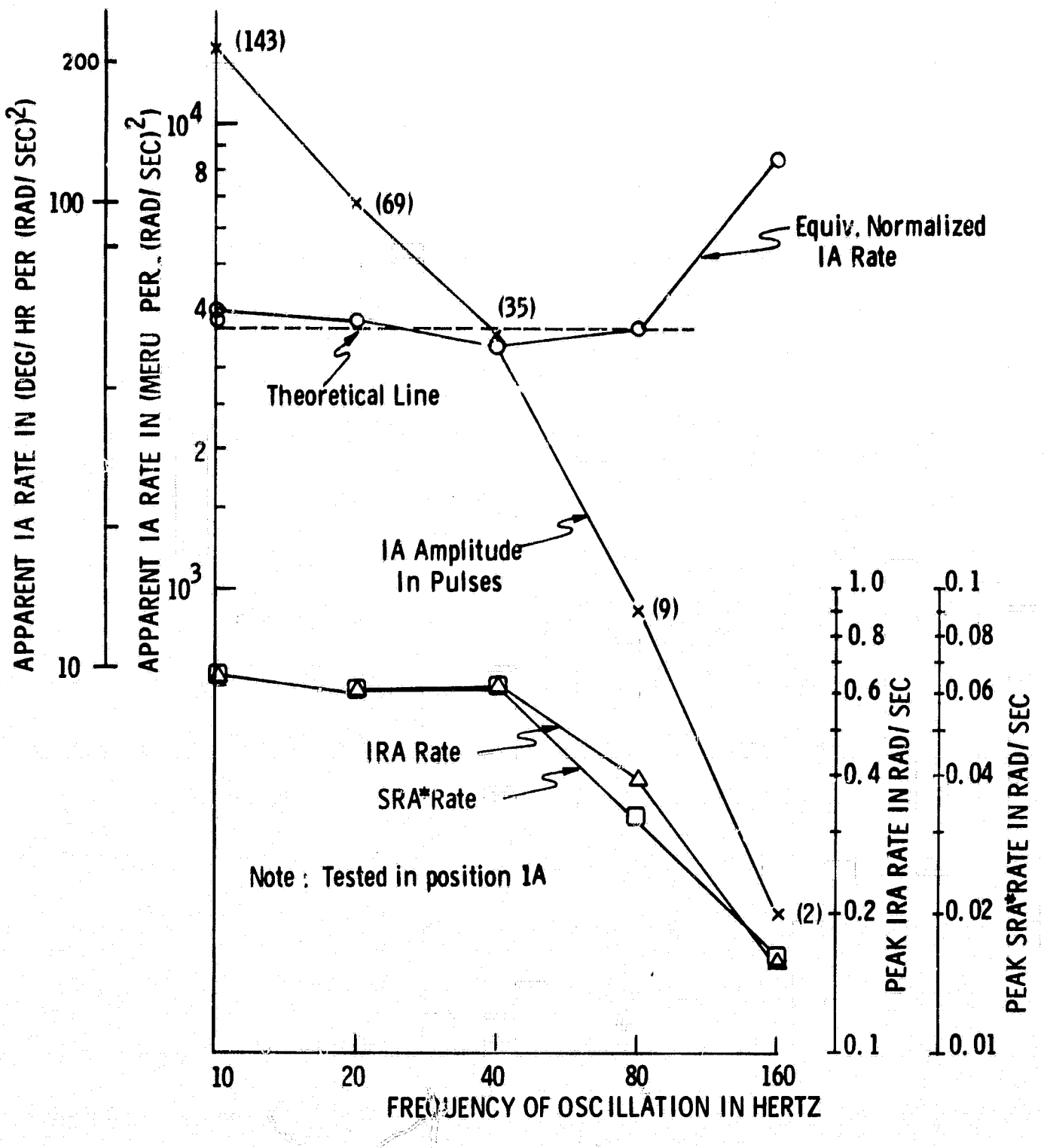

Fig. 43 Apparent IA Input Rate Normalized to Peak Velocity Product For In-Phase Angular Oscillations About IRA and SRA*

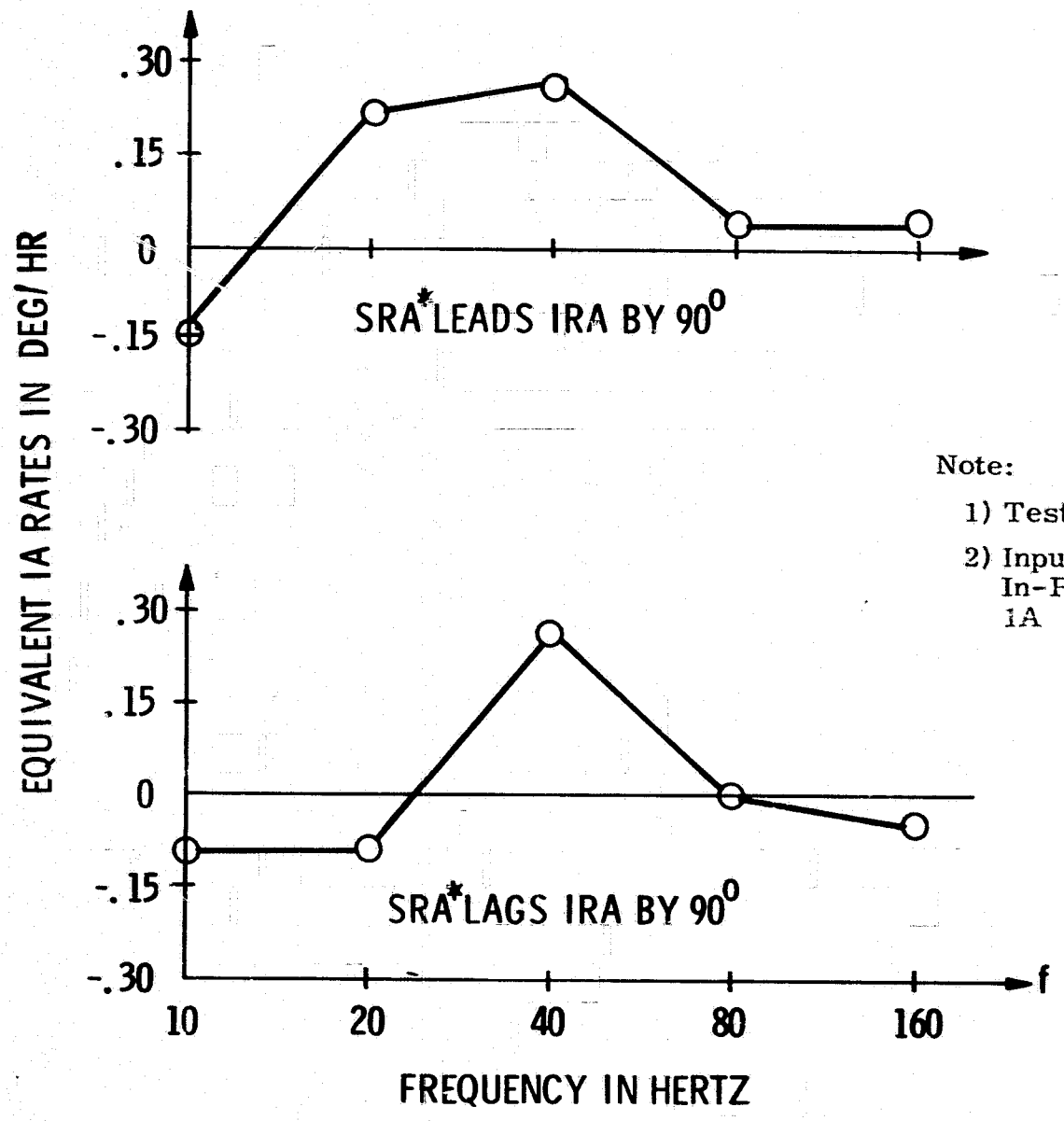

Note:

1) Tested in Position 1A
2) Input Rates Similar to In-Phase Test in Position 1A

Fig. 44 Apparent IA Input Rate For Quadrature-Phase Linear Oscillation About IRA and SRA*

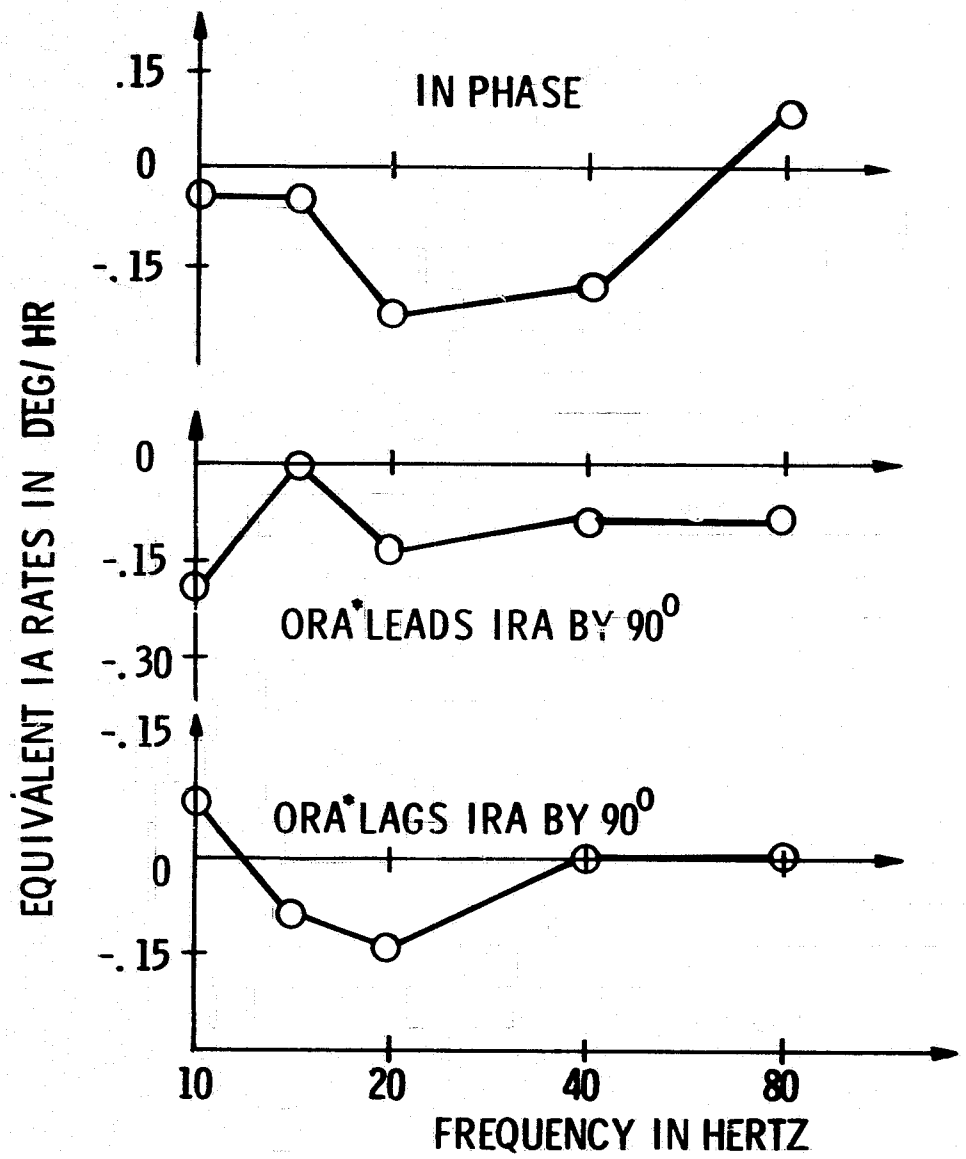

Notes:

1) IRA Rates Similar to Tests in Position 1A
2) ORA* Rates Similar to SRA* Rates in Tests in Position 1A
3) Test Run in Position 2a

Fig. 45 **Apparent IA Input Rate For Angular Oscillation About IRA and ORA***

3.5.3.4 Position 3a In-Phase Results. The previous positions were run with the IRA along the inner axis of the vibration fixture. Thus, they were the result of large IRA motion. Positions 3a and 4a, which will now be presented, have the large inner axis motion along the gyro SRA axis. The first case is SRA-ORA* in-phase oscillations, shown in Fig. 46. Equivalent IA rate and the oscillation amplitudes applied are plotted. The average indicated rate at 160 Hz is truly zero as indicated on the graph, not merely extremely small. The float was observed to be in a stable cyclic motion requiring an equal number of plus and minus pulses per cycle. Small disturbances (made by varying the current in torque coil No. 2) changed the phase at which the torque pulses were applied, but did not result in any net count regardless of the length of the test. This test point was our first indication that pulse rebalancing and high SRA rates could interact to cause deadbanding in the measurement of IRA inputs.

3.5.3.5 Position 3a Quadrature Phase Results. The equivalent IA rates indicated for quadrature-phase oscillation about SRA and ORA* (position 3a) are shown normalized by the peak velocity product in Fig. 47. The open loop theoretical curve, the actual average IRA rate applied by the coning motion, and the open-loop data are presented along with the closed-loop results. Preliminary analysis indicates that the rise in closed-loop indicated rate which can be seen in the data is to be expected.

3.5.3.6 Position 4a In-Phase Results. The data in Fig. 48 shows the equivalent IA rate and the amplitudes of the oscillations for in-phase testing in position 4a, in which the SRA and IRA* are driven. Note that the passage through zero rate is inferred from the sign reversal between 40 and 80 Hz, so that the shape of the line in this area is artistic rather than factual. The data are replotted normalized by the peak velocity product in Fig. 49. In contrast to the position 1a in-phase data of Fig. 43, agreement here with theory as expressed in Eq. (3.14) is poor.

3.5.3.7 Position 4a Quadrature-Phase Results. Equivalent IA rate and the input oscillations amplitudes are plotted in Fig. 50 for the case in which the SRA motion leads the IRA* motion by 90° (position 4a). Note that this data, obtained with relatively large SRA articulation, contrast quite sharply with the large IRA motion result shown in Fig. 44.

3.6 DISCUSSION OF RESULTS

3.6.1 Single-Axis Response Tests

There remains considerable doubt as to the significance of the measured single-axis open-loop responses. The response to ORA oscillation, Fig. 41, shows

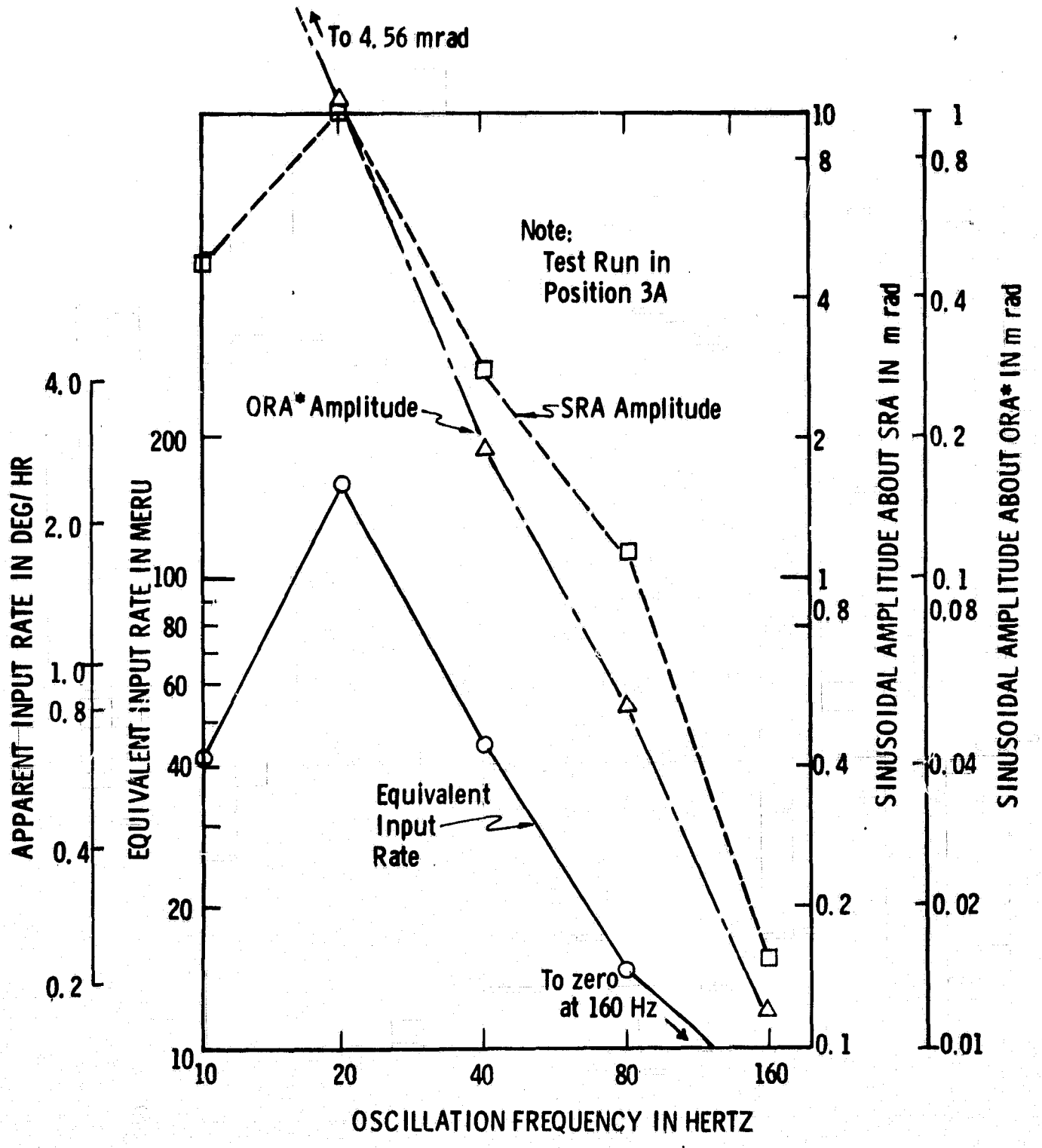

Fig. 46 Apparent Input Rate and Oscillation Amplitudes For In-Phase Oscillations About ORA* and SRA

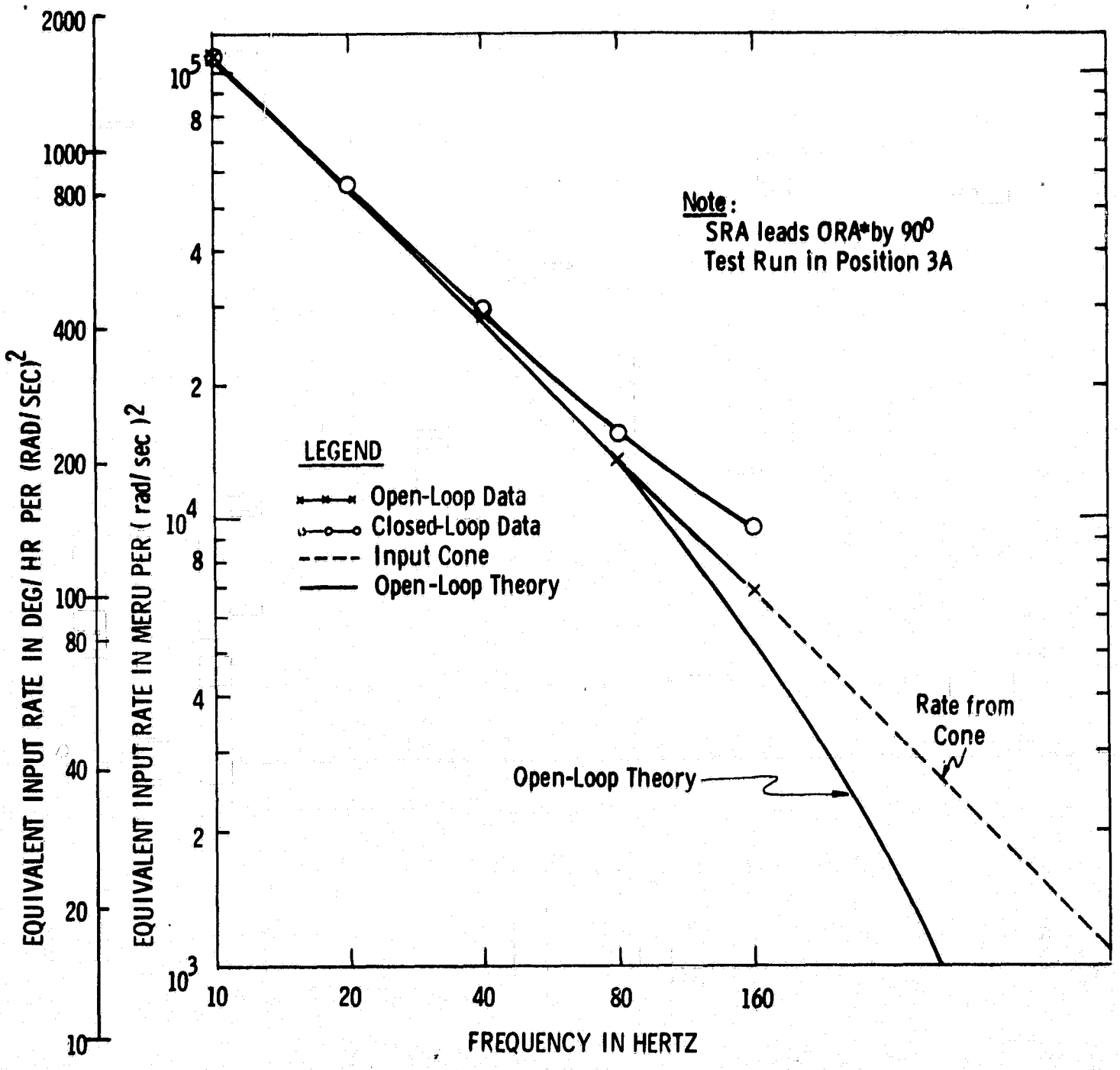

Fig. 47 Equivalent Input Rate Normalized by the Product of the Peak Velocity For Quadrature Oscillation About ORA* and SRA

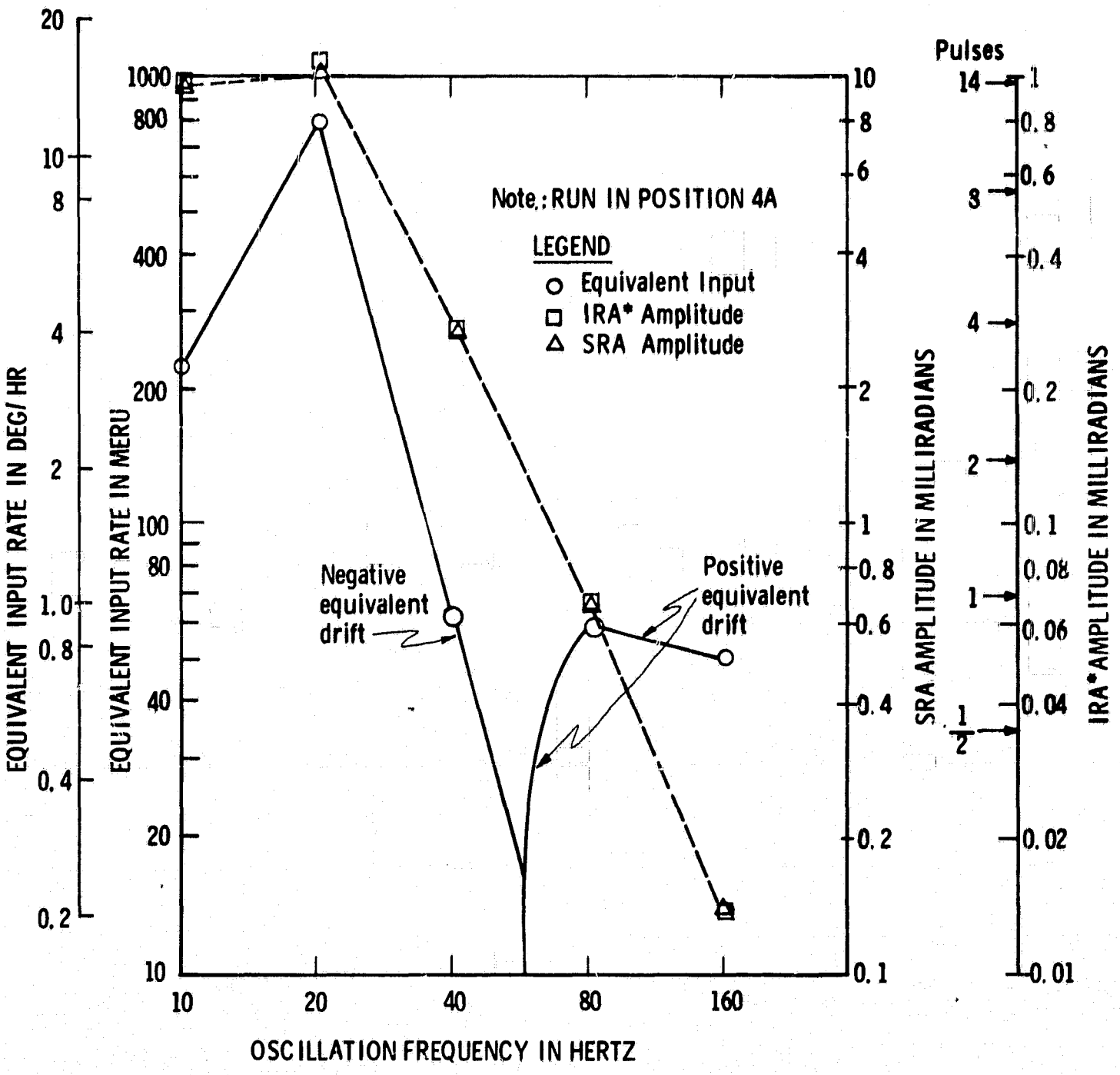

Fig. 48 Apparent Input Rate and Oscillation Amplitudes For In-Phase Angular Oscillations About IRA* and SRA

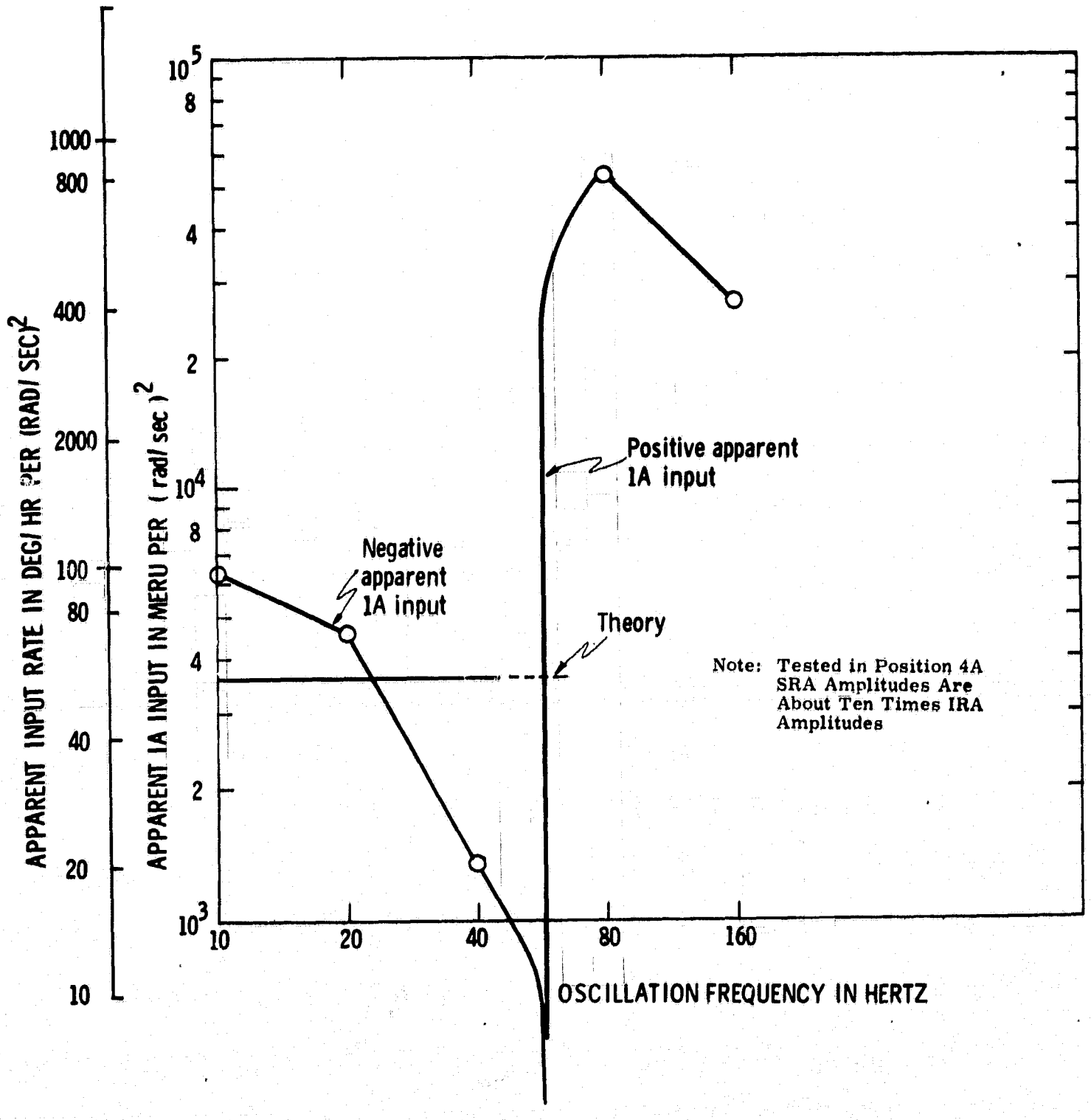

Fig. 49 Apparent IA Input Rate Normalized to Peak Velocity Product For In-Phase Angular Oscillations About IRA* and SRA

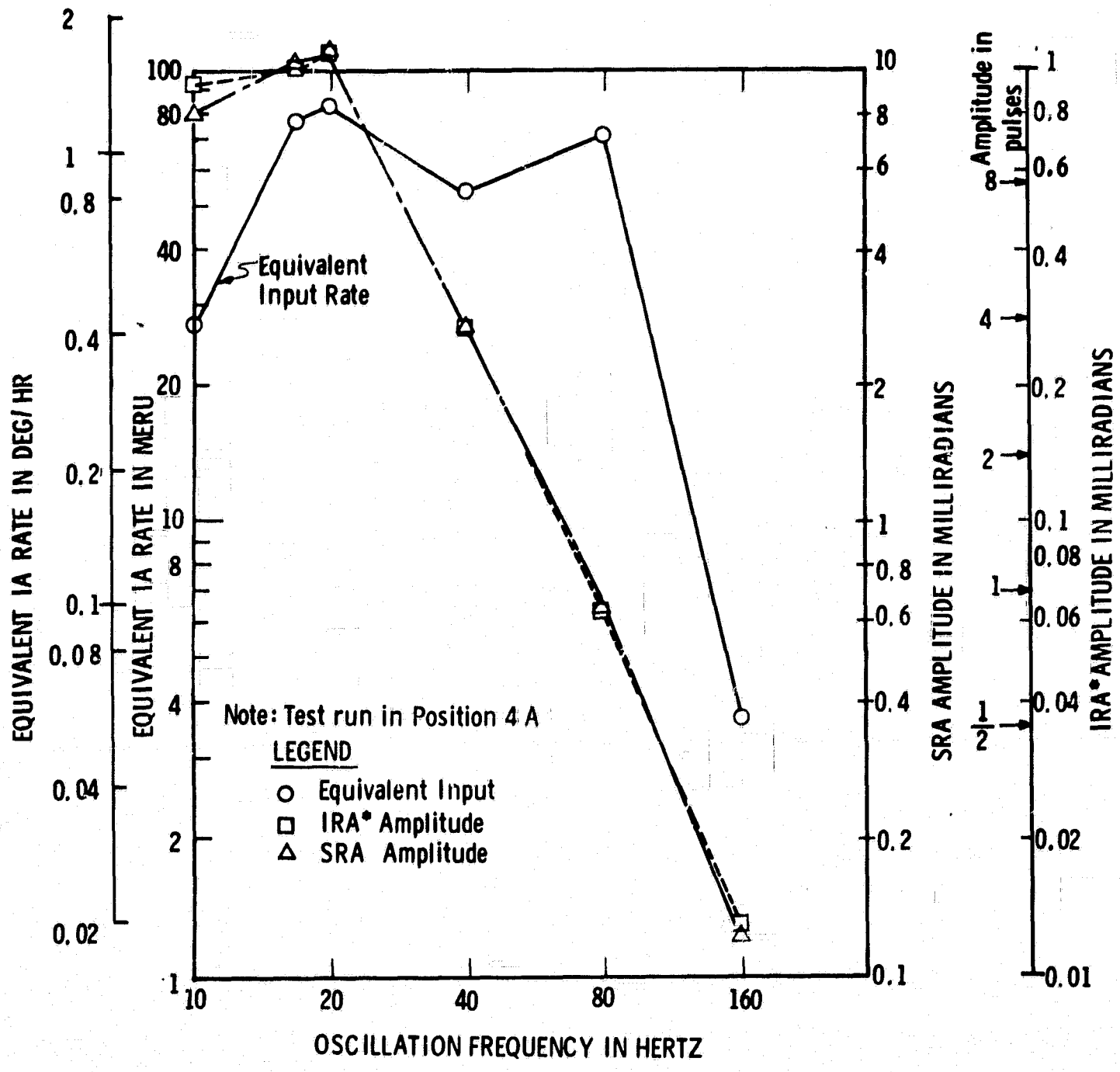

Fig. 50 Apparent IA Input Rate and Oscillation Amplitudes For Quadrature-Phase Angular Oscillation About IRA* and SRA

a noticeable rise in amplitude over a theoretical solution not including spin bearing compliance effects. The response to IRA oscillation in Fig. 40, however, disagrees with the non-compliant theory only in having a resonant peak at 452 Hertz. Since the two tests were run in different positions of the vibration fixture, the most plausible explanation of both variations from theory would be compliance of the vibration fixture, rather than compliance within the gyro. One must admit, nevertheless, that the ORA disagreement is just about what Schneider predicted with wheel-to-float compliance. (See ref. 4, Fig. 2-7, p. 32.) A conclusive determination cannot be made as to the gyro compliance effects using any vibration fixture currently in existence.

Regardless of the source of compliance, the fact still remains that Fig. 41 shows amplified response for ORA oscillation above 80 Hertz. This will cause a similar small rise in single-axis, open-loop data when the ORA is oscillated. For instance, such a rise is seen in the open-loop coning plus rectified cross-coupling illustrated in Fig. 47. (The closed-loop data presumably is also affected; it, however, has an even larger rise due to another cause as mentioned in Sec. 3.5.3.5 above.)

3.6.2 Two-Axis Open-Loop Results

As expected, the results of the open-loop, two-axis tests serve mainly to confirm theory and thus establish confidence in the oscillation fixture and measurements. Other than the compliance effect just noted, the data in Fig. 42 generally agree with the analytic solutions. This is a necessary and valuable prelude to the closed-loop tests. It not only validates the measurement technique, but assures us that our analytic model is sufficient to encompass all significant effects.

The only significant deviation from the theory is in the anisoinertia and rectified cross-coupling data, resulting from in-phase oscillation of the SRA and IRA. The data, appearing near the bottom of Fig. 42, were obtained in positions 1a and 4a. One must appreciate that the accuracy of this data is in question due to the low level rates induced by the oscillations. The rates range from about 0.03 to 0.4 degree per hour, i.e., 2 to 26 milli earth-rate units (meru). Despite this, however, the two points at 40 Hertz and the three points at 10 Hertz show sufficient repeatability to lend credence to the data. It is not known whether the concave upward trend to this data is an actual characteristic of the gyro or if it is a systematic error in the measurements. One can be sure that it is not caused by the variation in spin-axis inertia with frequency. (See Section 3.2.2 above for discussion of this subject.) The extremely small equivalent input rates for these tests results from the fact that, in this range of frequencies, the effect is the <u>difference</u> between anisoinertia

and cross-coupling, anisoinertia being the larger. For the GG334A, if we continued to lower the frequency of the test, the magnitude of the anisoinertia must decrease, thus decreasing the overall effect including cross-coupling. (The overall would, in fact, go to zero and reverse sign if one tested to low enough frequency.) We must conclude, therefore, that the known variations in anisoinertia would produce a concave downward trend and that the data has an unidentified characteristic. Fortunately, it is not at all necessary to discern such low average float rates in order to accomplish our main purpose, the measurement of two-axis effects with a closed pulse-torque loop.

3.6.3 Closed-Loop Two-Axis Results

3.6.3.1 The IRA Dominant Case. At the onset of this test program, each individual test point obtained constituted an independent, unpredicted result. Now, however, the development of Eq. (3.14) provides a bench mark from which much of the data can be judged. In particular, the IRA-SRA* oscillation results shown in Fig. 43 and 44 directly confirm the predictive value of the new analysis in Section 3.2.4.2 when the assumptions are sufficiently well met. Both the fit for in-phase oscillation up to 80 Hertz and the approximation to zero for 90° data are within the experimental accuracy of the tests. Furthermore, the IRA-ORA* oscillation tests (Fig. 45) quite obviously meet the same assumptions, and, having no command-frequency motion about the SRA, can be considered as predicted at zero rate by the same theory. Thus, about half the data are predicted by the new theory.

The data obtained with SRA-IRA* oscillations, shown in Fig. 49, demonstrate that the assumptions in Section 3.2.4.2 are necessary. With the large SRA rates applied in these tests, the assumptions for Eq. (3.14) to apply are not met, and the analysis fails to predict the results. Thus, contrasting both the widely differing oscillation amplitudes and the radically different results between Fig. 43 and Fig. 49, we find the assumptions in Section 3.2.4.2 both necessary and sufficient for the analysis therein to apply. It would now seem wise to test further to seek out the boundary where the value of Eq. (3.14) noticeably deteriorates.

3.6.3.2 SRA-ORA* Oscillations. When in-phase oscillations are applied about the SRA and ORA*, we lack any quantitative guidance of analysis. Qualitatively, one can best gain some understanding of this case by first considering the open-loop situation. If one forces the unit with

$$A_{SRA} = a \sin(\omega t) \qquad (3.15)$$

$$A_{ORA^*} = b \sin(\omega t + \epsilon), \tag{3.16}$$

the equivalent input rate open-loop is approximated by Schneider (ref. 4, pp 51, 64-5) as

$$W_D = \frac{a\,b\,\omega}{2(1 + \tau^2 \omega^2)} (\tau \omega \cos \epsilon - \sin \epsilon). \tag{3.17}$$

The term -(1/2) ab sin is, of course, the actual average coning rate which would be indicated by an ideal instrument. The term proportional to ω^2 is what we refer to as "rectified cross coupling." The frequency-sensitive denominator results from the float time constant. Notice that there is no anisoinertia effect. Rectification of cross coupling occurs when the float position has a component in phase with the oscillation about the SRA. Thus, insofar as closed-loop operation restricts the float from rotating within the case, one can expect less rectification for in-phase oscillation than is obtained open loop. This qualitative prediction is well supported as seen in Fig. 51 which shows the closed-loop data from Fig. 46 along with the open-loop rates which would be obtained at the same oscillation amplitudes.

One should be careful <u>not</u> to generalize the above result. It is not true that restraining the float always reduces undesired rates. In discussing the open-loop results in Section 3.6.2, we noted that the data with in-phase oscillation about the SRA and IRA results from the difference between cross-coupling and anisoinertia. Reduction of cross coupling in that case makes the apparent input rate <u>increase</u> toward the value caused by anisoinertia alone.

In considering the SRA-ORA* oscillation data, one should be aware of the limit on precision based on the ability to control phase angle. From Eq. (3.17), we observe that the open-loop relative size of the coning term and the cross-coupling term is proportional to

$$\tau \omega \cos(\epsilon) - \sin(\epsilon). \tag{3.18}$$

To test in phase, one attempts to set ϵ to zero, suppressing the coning, which is proportional to sin ϵ. Any coning which results is an error in the test. For small angle, the error, q, is

$$q = 100 \frac{\epsilon}{\tau \omega} \%. \tag{3.19}$$

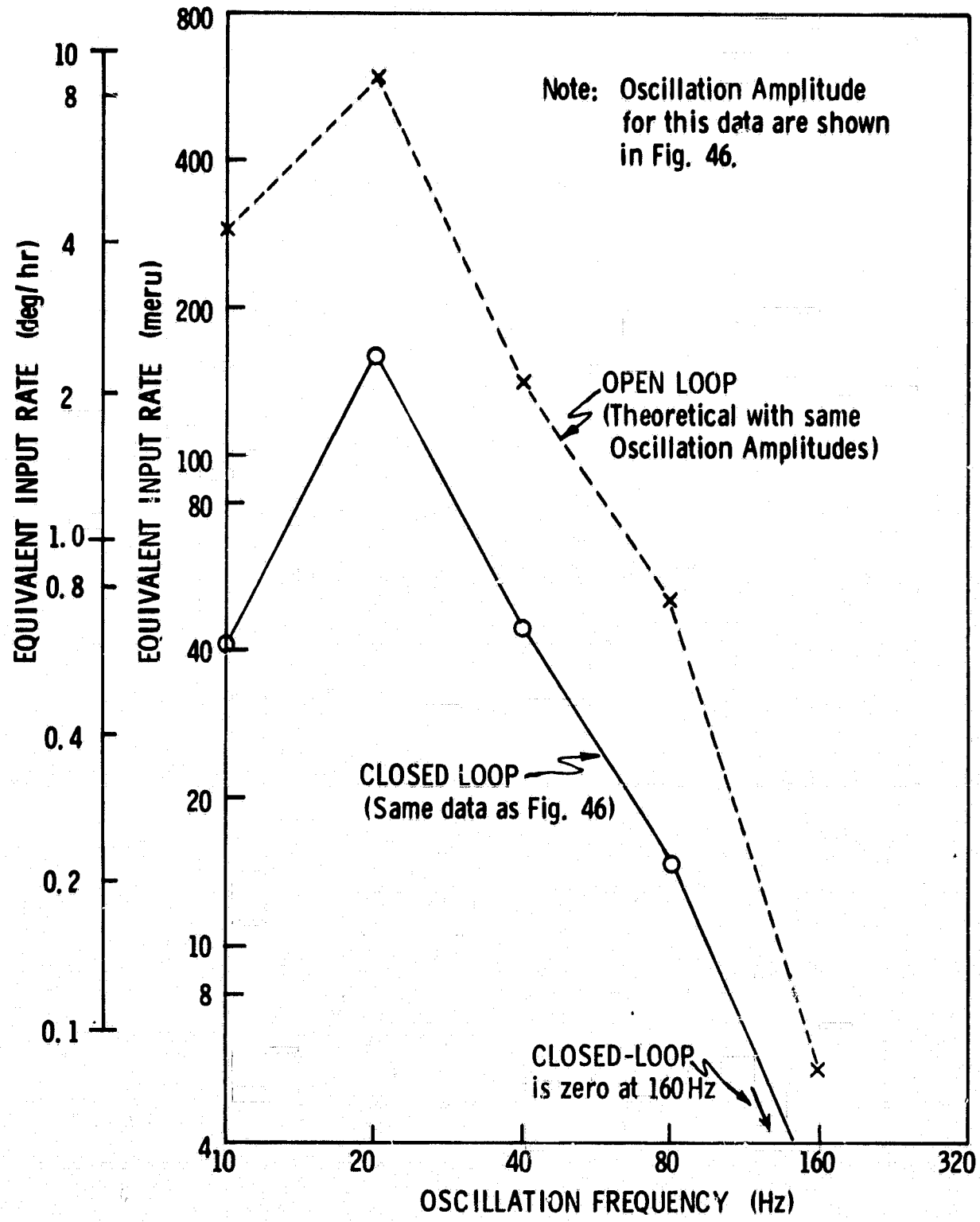

Fig. 51 Comparison of Open-Loop and Closed-Loop Rectified Cross Coupling

At 10 Hertz, this error is 55% per degree of phase angle. Since phase was held to one or two tenths of a degree in the tests, reasonable repeatability of the open-loop data was achieved. For the closed-loop data, however, the lowest frequency points may have large error despite extreme care in measuring. At 10 Hertz, for instance, Fig. 51 shows that the measured closed-loop rate is about one-seventh of the open-loop value. Thus the percentage error from inadvertent coning may be on the order of 50 to 70% for the same size phase error. One can conclude that rectification errors are small with the loop closed, but he cannot accurately measure just how small.

3.6.3.3 The "Lock-In" Phenomenon. In presenting the SRA-ORA* data in Section 3.5.3.4 above, a test point was described for which the two-axis oscillations produced a deadband in the response to superimposed dc rates. As stated above, the phase at which torque pulses occurred varied with small changes in dc IRA rate applied. This phase adjustment appears to change the net cross-coupling per cycle in a direction which opposes the applied IRA average rate. The occurrence of this condition at one of the selected test points was fortuitous. We might easily have overlooked it as being merely small or as being unimportant. But having grasped in some limited way the significance of this peculiar and unexpected phenomenon, we are compelled to study it further.

A brief search for other test conditions which would exhibit the "lock-in", or deadbanding or IRA rate, was performed. The phenomenon was produced at any frequencies from 10 to 160 Hertz by proper adjustment of the driving oscillation magnitudes and relative phase. It was clear that 10 Hertz was not a lower limit. The condition was obtained with both a compensated and an uncompensated loop. In obtaining these points, it appeared that the following are necessary conditions:

1) High SRA rates are required: There must be a substantial source of cross-coupled torque. (Peak SRA rates on the order of half a radian per second and above were used in our tests.)
2) The amplitude of A_{OA} motion at oscillation frequency (if the float were unrestrained) must be on the order of the distance between the thresholds or smaller.
3) The phase between the forcing oscillations must fall in a narrow range, depending on frequency.

Once these conditions were met, deadbands in IRA response up to three degrees per hour (200 meru) were observed.

Several thoughts about the so-called "lock-in" can be obtained from this limited data. We can note that the test oscillations at "lock-in" do not necessarily occur with in-phase oscillations as in the initial case observed. This means that a coning rate may exist, given by the sin ϵ term in Eq. (3.17), and the effect is seen to exist at conditions containing substantial average IRA rate. This suggests the hypothesis that nearby non-zero indicated rates may contain significant errors from the same process even though the output is not "locked-in" to zero. Another intuitive extension of this data is that IRA-SRA as well as ORA-SRA oscillations can achieve the lock-in circumstance. We also predict that a similar loop with binary logic can suffer the same as our ternary-logic controller. Finally, it is clear that the phenomenon in question extends to zero frequency; large dc SRA rates will quite obviously produce deadbanding of output to IRA rates over some range.

Observe that SRA cross-coupling appears to be the source of this disquieting phenomenon. It therefore varies with float angle. I have invented several schemes which control float angle to small values while still achieving accurate and high-resolution quantization: One must withhold estimating the impact of effects such as the lock-in on strapdown systems until these novel devices can be developed and evaluated in a two-axis angular vibration field.

Two important, comprehensive questions are extant. They should guide the long-term goals of further inquiry. The first question concerns our understanding of the "lock-in" phenomenon. Is it an isolated, singular happening, or is it closely related to the other anomalous data obtained at high SRA rates? For instance, how is it related to the reversal in sign of the data in Fig. 48? We shall be forced to start with narrower, myopic questions, but we should hope eventually to achieve some comprehensive analytic approach. The second major question is an inquiry into the importance of this phenomenon (and indeed of the other two-axis effects studies here) in the actual environment in which the strap-down gyro may be used. What is the relevance of large fixed-phase oscillations to the use of the gyro in some complex vibration environment? Are all the second-order statistics of oscillatory motions sufficient to evaluate use? Must we include also the statistics of linear vibrations? How well must one or can one estimate the necessary statistics of an aerospace vehicle prior to its actual design in order to describe the mission impact of the effects studied here? Shepard[11] has attempted to estimate the power spectral density of both translational and angular response of a vehicle which is intended to operate as an aircraft and as a spacecraft. For one-dimensional models, he discusses motions in three overlapping ranges:

1) Rigid-body maneuvering or control frequencies.
2) Large-scale flexural response frequencies.
3) Local or small-scale response frequencies.

A three-dimensional model becomes rapidly more complex. Even for rigid body motion, 6 x 6 matrices are required for the input and output power spectral densities and the system transfer function. Inclusion of bending raises the order. Shepard cites the application of normal mode analysis, which identifies the phugoid and short-period modes for longitudinal motion and identifies the spiral, rolling convergence, and dutch roll for lateral motion. Out of all this, one gathers that high-frequency vehicle response tends toward an uncorrelated, isotropic random process, which may not be a significant error source. The normal modes, however, may have enough synchronized response to cause concern. In summary, then, we have the motivation to understand the instrument response to dynamic input and, further, to participate in applying this understanding to the mission-success error analysis of proposed missions and equipment.

3.7 CONCLUSIONS AND RECOMMENDATIONS

3.7.1 Conclusions

A broad scan of pulse-rebalanced gyroscope two-axis angular oscillations has been obtained with sufficient confidence to be suggestive of new analytic methods. The principal researcher has deduced an approximate closed-form solution having excellent predictive value when input-axis rates dominate the independent forcing functions and thus determine the initiation of command torque. The data also include contrary cases for which nonlinear terms with time-varying coefficients comprise the major sources of independent torque. Several unexpected and perplexing phenomena were displayed in such data. In the discussion, it was noted that the relevance of the results to future aerospace vehicle environments cannot yet be assessed. The importance of random angular vibrations with known power spectral densities and cross spectra will become greater as progress is made toward the ultimate goal of mission impact evaluation.

The results so far seem to apply to any single-degree-of-freedom gyro with ternary-logic, pulse rebalancing. No effect observed has been associated with construction details peculiar to the Honeywell GG334A. One can conclude, therefore, that continued testing with the present instrument in the same test facility will best serve to evaluate any new analytic hypotheses.

3.7.2 Recommendations

We recommend that additional testing be conducted with the same instrument and electronics to examine the region of validity of the approximate solution, Eq. (3.14).

The new techniques available for reducing average float angle in pulse-rebalanced instruments should be developed into working prototype hardware. Since such devices can remove unwanted SRA-rate cross-coupling, several of the closed-loop tests above should be rerun to evaluate the new techniques.

Since the cross-coupling term for SRA rates is the apparent source of the difficult cases, it is recommended that a study by simulation, either analog or digital, be started. Results with only cross coupling can be compared to those with all nonlinear terms included. The effects of noise and test inaccuracies can be assessed. When agreement between test data and simulated results has been achieved, the simulation can be employed to generate larger fields of data at reduced cost. It will permit evaluation of new ideas even after the test equipment has been committed to other tests.

The testing to date has been difficult and time consuming. It is recommended that, if large amounts of similar test data are required in the future, the test equipment be redesigned to automate the procedures now achieved by laborious human control.

Fairly large harmonic distortion has been observed in oscillations commanded at frequencies below five hertz. When random vibration testing is contemplated, it is recommended that the gimbal-drive servo loops be redesigned to obtain higher fidelity prior to implementing tests with noise inputs.

REFERENCES

1. Lory, C.B., Compensation of Pulse-Rebalanced Inertial Instruments, M.S. Thesis, MIT Department of Aeronautics and Astronautics, Instrumentation Laboratory Report T-495, January 1968.
2. ———————, "GG334 Gas Bearing Gyro, Technical Description", Honeywell Aerospace Div. Minneapolis Report No. ASD-3, July 1967.
3. Salamin, E., "Interim Report on a Theoretical Analysis of the Impedance of the 18 IRIG Torquer", MIT Charles Stark Draper Laboratory Internal Memorandum ISS MEMO No. 559, July 1968.
4. Schneider, G.E., Studies of Dynamic Testing of a Single-Degree-of-Freedom Integrating Gyroscope Used in a Strapped-Down Environment, M.S. Thesis, MIT Department of Mechanical Engineering, Instrumentation Laboratory Report T-526, January 1970.
5. Weinstock, H., "Effect of Angular Vibration on Gyroscope Performance", MIT Department of Aeronautics and and Astronautics, Notes from Summer Program 16.395, 1963.
6. Weinstock, H. and V. Marchese, Frequency-Response Characteristics of a Typical Single-Degree-of-Freedom Integrating Gyroscope, MIT Instrumentation Laboratory Report E-1721, 1965.
7. Sher, L. and H. Weinstock, Performance Requirements for a High-Frequency Two-Axis Angular Vibrator, MIT Instrumentation Laboratory Report R-514, 1965.
8. Gelb, A. and A.A. Sutherland, Jr., Design of Strapdown Gyroscopes for a Dynamic Environment, The Analytic Sciences Corporation Report TR-101-1 (Semi-Annual Report under Contract NAS-12-508), July 1967.
9. Lory, C.B., Float Position of Inertial Instruments Having Torque Applied in Quantum Increments, MIT Charles Stark Draper Laboratory Report E-2622, to be published December 1971.
10. Fish, D.H., The MIT Inertial Measurement Unit Angular Vibrator, M.S. Thesis, MIT Department of Aeronautics and Astronautics, Charles Stark Draper Laboratory Report No. T-541, August 1970.
11. Shepard, G.D., "Progress Report — SSV Dynamic Environment," MIT Charles Stark Draper Laboratory Internal Memorandum ISS Memo No. 70-200 Rev. A, September 1970.